INVESTIGATIONS ON ENHANCED POWER FLOW CONTROLLER

by

Alekhya Vaddiraj

A thesis submitted to the faculty of
The University of North Carolina at Charlotte
in partial fulfillment of the requirements
for the degree of Master of Science in
Electrical Engineering

Charlotte

2014

Approved by:

_____
Dr. Madhav Manjrekar

_____
Dr. Sukumar Kamalasadan

_____
Dr. Zia Salami

ABSTRACT

ALEKHYA VADDIRAJ. Investigations on enhanced power flow controller. (Under the direction of Dr. MADHAV MANJREKAR)

Series Flexible AC Transmission Systems (FACTS) devices have been employed to increase power transfer capability of transmission networks and to provide direct control of power flow over designated transmission routes. However, high costs and reliability concerns associated with implementing one large FACTS device capable of altering the power flow in a wide transmission network have limited widespread deployment of FACTS solutions. Recently, concept of Distributed FACTS (D-FACTS) was proposed as an alternative approach to realize cost-effective power flow control through multiple, small, fixed series impedance injections. This thesis extends the functionality of D-FACTS concept by introducing variability in impedance injection of D-FACTS devices, thereby improving their controllability. Furthermore, this thesis presents a more detailed analytical treatment of such a topology termed enhanced Power Flow Controller (ePFC). It is shown that employing 1st order (assumes sinusoidal voltage across compensation capacitor) and 2nd order (assumes sinusoidal current in the transmission line) fundamental impedance model are inaccurate methods to analyze effective impedance inserted by ePFC. Instead, a new mathematical model that is based on sinusoidal voltage difference between two end buses is proposed. The efficacy of this approach and its advantages as compared to provide more accurate steady state impedance over existing models are presented.

Likewise, to analyze the stability of this system, Poincare mapping of entire bus-to-bus system is employed and the resultant dynamic model of an ePFC is systematically

derived in this paper. Finally, eigen values of this system are mapped as a function of conduction angle and regions of instability are identified for the enhanced Power Flow Controller.

ACKNOWLEDGEMENTS

Foremost, I wish to take this opportunity to express my gratitude to my guru Dr. Madhav Manjrekar for his patience, motivation, and encouragement. I could not have imagined having a better advisor and a mentor. He has always made himself available assuming various forms; as a respected teacher, a caring guardian and guiding brother in my hour of need.

I extend my gratitude to the committee members Dr. Sukumar Kamalasadan and Dr. Zia Salami for taking time to be on my committee and assess my work. My sincere and special thanks to Juanita Koilpillai and Waverley Labs., for giving me an opportunity to acquire hands on experience on through the Cybersecurity. This gave me a scope to improve my research abilities which helped during my thesis.

I also like thank Stephanie le Claire, Jerri Price, Yamilka Baez, Nathaniel Hatley, Reza Yousifian and Rohit Seshadri for their invaluable assistance and for keeping me motivated at all times.

Most importantly I would like to offer my gratitude to God for all the blessings. Acknowledge my grandparents, parents and friends & family for supporting me all the time.

TABLE OF CONTENTS

CHAPTER 1 : INTRODUCTION AND REVIEW

1.1. Introduction

The electricity transmission system is one of the greatest engineering achievements of the 20th century. It is an extensive system of interconnected networks in which high-voltage power lines transport electricity from generators to customers [1]. A critical early decision to rely on alternating current (AC) technologies for high-voltage transmission has led to the construction of three major interconnected power systems: the Eastern and Western Interconnections, and the Electric Reliability Council of Texas (ERCOT), as shown in FIGURE 1.1. This transmission system was built by vertically integrated utilities that produced electricity at large generation stations and this interdependence leads to reliability [1].

On the other hand, as power transfers grow the power system becomes increasingly more complex to operate and the system can become less secure for riding through the major outages [1]. Increasing demand of electricity has put unprecedented pressure on the US power-grid.

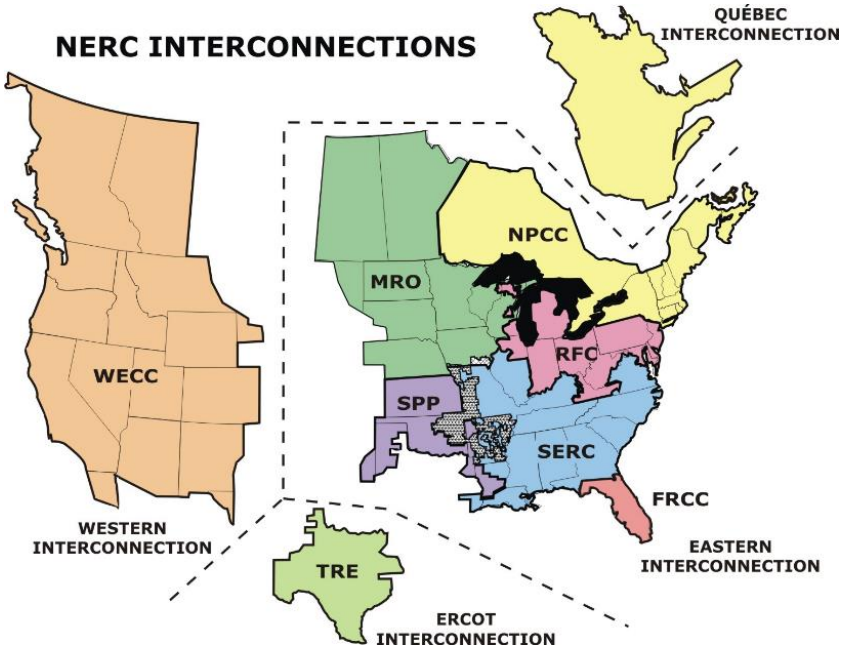

FIGURE 1.1: North American Electricity Transmission Systems [1]

The conventional method of reinforcing network capacity through building additional lines has become difficult to implement with long delays in siting and approval process. It may lead to large power flows with inadequate control, excessive reactive power in various parts of the system, large dynamic swings and bottlenecks, and thus the full potential of transmission interconnections cannot be utilized [1].

1.2. Power Delivery Infrastructure

Transmission bottlenecks and congestion have become a frequent sight for the network operators [2]. Substantial changes and capital investments are required to modify it for deregulated market needs. Thus it presents a major infrastructural obstacle for the continuing growth of the U.S. $ 224 billion U.S. electricity market [2]. Electricity demand has increased 25% over the last decade and continues to increase. Overall, adequate generation capacity now exists, or is planned to meet projected needs in the US. At the same time, annual investment in transmission facilities has declined over the last

decade [1]. As a result of load growth, deregulation, and limited investment in new facilities, transmission congestion has rapidly increased. Over 50 transmission corridors in the US are routinely congested, causing high economic impact. According to the New York Independent System Operator (NYISO), congestion on the T&D system cost over $1 billion per year [3].

Uncontrolled ‘loop flow’ causes congestion and reliability problems, and reduces the ability to fulfill energy contracts. Loop flows also impact the ability to fully utilize certain transmission lines, even as other lines suffer congestion, further limiting available transfer capacity under normal and contingency conditions. New transmission lines could relieve congestion, but are expensive to build (US$0.5–2 million/mile typically, but costs can exceed $10M/mile) and require several years for approval and construction [2]. Thus, one of the problems of smart grid is to have an ability to control power flow on transmission lines has been through the use of Flexible AC Transmission Systems (FACTS). FACTS devices allow control of power flows on ac power systems through the use of large power converters (10–300MW) [2]. While several FACTS installations are operating worldwide, wide scale deployment has not occurred. FACTS typically costs $120–$150 per kVAr, compared to $15–$20/kVAr for static capacitors.

1.3. Power Flow Control

As explained in the previous section, one of the desired objectives of smart power grids is to have precise control of power flow over a designated power route. In an emerging power ecosystem with multiple parallel paths between sources and loads, the actual route that carry real power can have an important impact on system operation during both steady-state and post-contingency conditions [2].

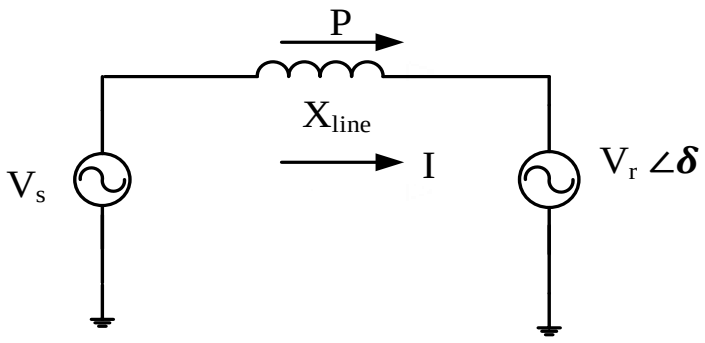

FIGURE 1.2: Real power flow in a fundamental two-bus system

FIGURE 1.2 shows two buses connected with a reactance X_{line}. Consider a two bus system consisting of sending voltage (V_s), line reactance (X_{line}), receiving voltage (V_r). Therefore,

$$V_s = V_s \cos(\omega t) \tag{1.1}$$

$$V_r \lfloor \delta = V_r \cos(\omega t + \delta) \tag{1.2}$$

Using Kirchhoff's Current Law (KCL), the current in the system is given by

$$I = \frac{V_s - V_r \lfloor \delta}{jX_{line}} \tag{1.3}$$

$$I = \frac{V_s \cos(\omega t) - V_r \cos(\omega t + \delta)}{jX_{line}} \tag{1.4}$$

$$= \frac{V_s \cos(\omega t)}{jX_{Line}} - \frac{V_r \cos(\omega t + \delta)}{jX_{line}} \tag{1.5}$$

Therefore, $$I = \frac{V_S}{jX_{line}} \sin(\omega t) - \frac{V_R}{jX_{line}} \sin(\omega t + \delta) \tag{1.6}$$

Now power in the circuit is given by,

$$\text{Power} = \text{Voltage} * \text{Current} \tag{1.7}$$

From (1.7) we have,

$$P = V_s \cos(\omega t) * I \tag{1.8}$$

$$P = V_s \cos(\omega t) * \left[\frac{V_s}{X_{line}} \sin(\omega t) - \frac{V_r}{X_{line}} \sin(\omega t + \delta)\right] \tag{1.9}$$

we get,

$$P = \frac{V_s^2}{X_{line}} \sin(\omega t) \cos(\omega t + \delta) - \frac{V_s V_r}{X_{line}} \sin(\omega t + \delta) \cos(\omega t) \tag{1.10}$$

Reducing equation (1.10),

$$P = \frac{V_{srms}^2}{X_{line}} \sin 2(\omega t) - \frac{V_{srms} V_{rrms}}{X_{line}} [\sin(2\omega t + \delta) + \sin(\delta)] \tag{1.11}$$

Now extending the power equation (1.11) from a single phase to a three phase system, we have

$$P_a = \frac{V_{srms}^2}{X_{line}} \sin 2(\omega t) - \frac{V_{srms} V_{rrms}}{X_{line}} [\sin(2\omega t + \delta) + \sin(\delta)] \tag{1.12}$$

$$P_b = \frac{V_{srms}^2}{X_{line}} \sin 2(\omega t + 120) - \frac{V_{srms} V_{rrms}}{X_{line}} [\sin(2\omega t + \delta + 240) + \sin(\delta)] \tag{1.13}$$

$$P_c = \frac{V_{srms}^2}{X_{line}} \sin 2(\omega t - 120) - \frac{V_{srms} V_{rrms}}{X_{line}} [\sin(2\omega t + \theta_R - 240) + \sin(\delta)] \tag{1.14}$$

Hence total power (P) is given by,

$$P = P_a + P_b + P_c \tag{1.15}$$

From equations (1.12), (1.13) and (1.14)

$$P = 3 \frac{V_{rrms} V_{srms}}{X_{line}} \sin(\delta) \tag{1.16}$$

$$P = \frac{\sqrt{3}V_{rrms}\sqrt{3}\,V_{srms}}{X_{line}}\sin(\delta) \tag{1.17}$$

The real power flow between these two buses is given by

$$P = \frac{V_{r(l-l)rms} * V_{s(l-l)rms}}{X_{line}}\sin(\delta) \tag{1.18}$$

As is evident from equation (1.18), real power can be controlled either by varying line-line voltages at sending (V_s,) or receiving (V_r) ends, or by varying the phase angle between these voltages (δ), or by varying impedance of the line (X_{line}) [4]. Power flow control has traditionally relied mostly on control of generators, network switching, and phase shifting transformers. Passive elements such as series reactors and capacitors have also been used to vary the effective line impedance, thereby altering the power flow through a given line [4]. Power electronic converters have been augmented with these passive methods to improve the controllability and to provide a faster response [5].

A Phase Shifting Transformer (PST) is a special form of three-phase regulating transformer and is realized by combining a series-connected transformer with a thyristor controlled tap-changing voltage transformer [5]. The windings of the voltage transformer are so connected that on its secondary side, phase-quadrature voltages are generated and fed into the secondary windings of the series transformer. Thus the addition of small, phase-quadrature voltage components to the phase voltages of the line creates phase-shifted output voltages without any appreciable change in magnitude. A phase shifting transformer is therefore able to introduce a phase shift in a transmission line. When a phase-shifting transformer employs an on load tap changer, controllable phase-shifting is

achieved. But this is an expensive solution and does not allow dynamic control capability [5], [6].

Another option is to decrease the total effective reactance, X, of the transmission line by adding series capacitors such that $jX = jX_L - jX_C$. This action increases the current flow through the line, and thus increases both the real and reactive power flow [5].

1.4. Thesis Motivation

On contrary to the increase in demand and generation on the grid, there has been a sustained decrease in transmission infrastructure investments. Increasing congestion and loop flows on the transmission have dramatically decreased the capacity of existing lines and are forced to operate under their thermal limits [7]. One of the accepted and technically proven approach for enabling the smart distribution grid in particular achieving control of active power flow on the grid, has been through the use of Flexible AC Transmission Systems or FACTS [2]–[4]. Even though FACTS technology is technically proven, it has not seen widespread commercial acceptance due to high cost. In this thesis, concept of Distributed FACTS (D-FACTS) was proposed as an alternative approach to realize cost-effective power flow control through multiple, small, fixed series impedance injections [2], [7]. The functionality of D-FACTS concept is extended by introducing variability in impedance injection of D-FACTS devices, thereby improving their controllability. Furthermore, a detailed analytical treatment of such a topology termed enhanced Power Flow Controller (ePFC) is presented [8]. It is shown that employing 1^{st} order (assumes sinusoidal voltage across compensation capacitor) and 2^{nd} order (assumes sinusoidal current in the transmission line) fundamental impedance model are inaccurate methods to analyze effective impedance inserted by ePFC. Instead, a new

mathematical model that is based on sinusoidal voltage difference between two end buses is proposed [8]. The efficacy of this approach and its advantages as compared to existing models and also its stability analysis are presented.

1.5. Organization of Thesis

This thesis is organized in the following format.

chapter 1: Introduction and Review

A brief introduction to the transmission system operation and interconnection and the power delivery infrastructure is provided in the first part. The later part describes the power flow control on the transmission grid and motivation for the thesis.

chapter 2: Flexible AC Transmission Systems (FACTS)

This chapter describes the concept of Flexible AC Transmission Systems (FACTS). The basic types of FACTS controllers are briefly outlined. The topologies of different types of FACTS controllers are explained. And a brief review on leading FACTS suppliers and installation of FACTS solutions are also presented.

chapter 3: Distributed FACTS (D- FACTS)

Limitations of the existing FACTS devices are documented. The Series Injected Transformer is explained using the equivalent impedance offered by a transformer. The concept of D-FACTS is introduced. DSR and DSI controllers are explained and analyzed.

chapter 4: Enhanced Power Flow Controller (ePFC)

The concept of D-FACTS in Chapter 3 is extended with conduction angle control. Three approximations are explained to determine the functionality of an ePFC system. A mathematical expression is derived to obtain the effective fundamental impedance

offered by the proposed controller. Detailed comparison of the effective fundamental impedance for three approximations is tabulated.

chapter 5: Modeling and Simulation Results

In this chapter DSR, DSI and ePFC devices are modeled in MATLAB Simulink. Simulation results of the controllers are compared with the calculated results from Chapter 3 and Chapter 4. The operations of the proposed ePFC system in transmission line are discussed with the help of control block schematic. A components of the controlled system are modeled in MATLAB Simulink and the results are presented.

chapter 6: Stability Analysis of ePFC

In this chapter the stability analysis of an ePFC system is presented. The dynamic state equations and projection matrix for the proposed system are explained. Poincare' mapping is used to determine the stability using the Eigen values of the Jacobian matrix.

chapter 67: Future Work and Conclusion

This chapter includes an overview of the thesis with conclusions are drawn and the assumptions are presented. The thesis concludes with a discussion on the future scope with regards to realizing an ePFC in hardware.

CHAPTER 2 : FLEXIBLE AC TRANSMISSION SYSTEMS (FACTS)

2.1. Introduction

The increase in demand on the power grid, a sustained decrease in transmission infrastructure investments over the last two decades, has increased the power flow congestion problem [1]. Many transmission facilities face inability to direct power flow at will, resulting in limited system reliability and constrained ability to provide interested customers with low-cost power [1]. There is general consensus that the future power grid will need to be smart and aware, fault tolerant and self-healing, dynamically and statically controllable, and asset and energy efficient [2]. The accepted and technically proven approach for realizing a smart grid, in particular achieving control of active power flow on the grid, has been through the use of Flexible AC Transmission Systems (FACTS).

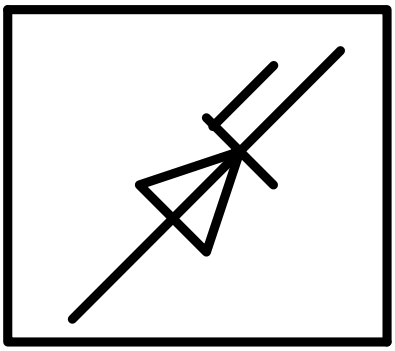

FIGURE 2.1: General symbol for FACTS Controller.

FIGURE 2.1 shows the general symbol for a FACTS controller [5]. Broadly, FACTS Controllers are divided into four categories:

- Shunt Controllers
- Series Controllers
- Combined Series-Series Controllers
- Combined Series-Shunt Controllers

2.2. Shunt Controllers

In principle, a shunt controller injects current into the system at the point of connection [5]. A simplified schematic of a shunt controller is shown in FIGURE 2.2. A shunt controller may be a variable impedance, variable source or a combination of these. As shunt controllers act like current source they can control voltage at, and around the point of connection through the injection of reactive current. Static Synchronous Compensator (STATCOM) and Static VAr Compensator (SVC) are the commonly used shunt controllers.

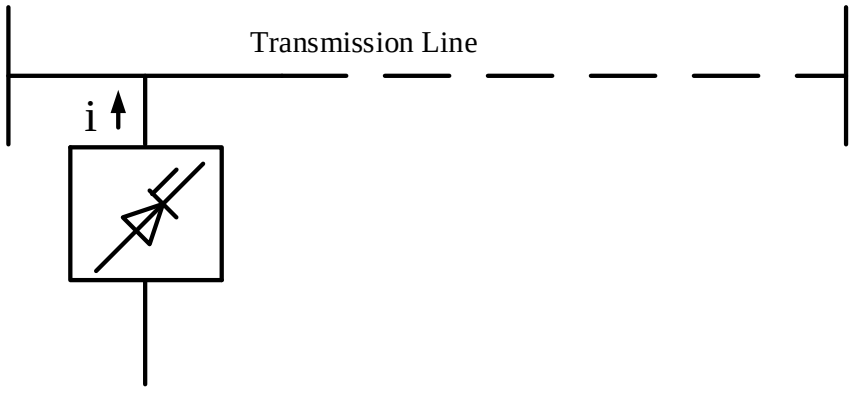

FIGURE 2.2: General symbol for shunt controller.

- Static Synchronous Compensator (STATCOM): A Static Synchronous Compensator (STATCOM) can be defined as a static synchronous generator operated as a shunt-

connected static VAr compensator whose capacitive or inductive output current can be controlled independent of the ac system voltage [4]. This is shown in FIGURE 2.3.

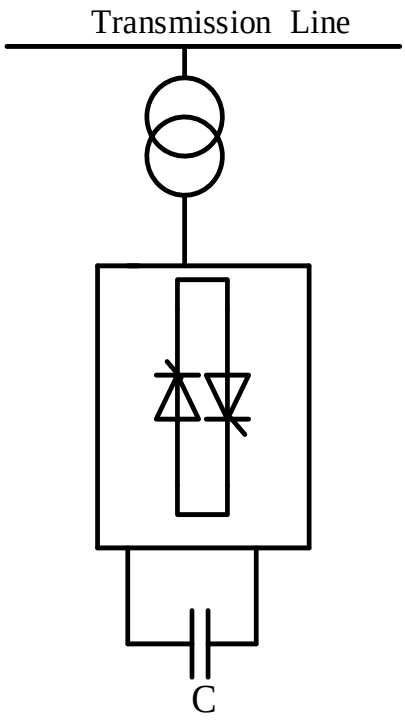

FIGURE 2.3: Simplified Schematic of Static Synchronous Compensator (STATCOM) based on voltage sourced converter

STATCOM instantly and continuously provides variable reactive power in response to voltage transients, supporting the stability of the grid voltage. The STATCOM acts as a stiff voltage source and is controlled by Pulse Width Modulation (PWM) control of power electronics devices. Installing a STATCOM in a grid increases power transfer capability by enhancing voltage stability and maintaining a smooth voltage profile under different network conditions [5]. STATCOM also enables improvement of power quality, when designed as an active filter to absorb system harmonics [4].

- Static VAr Compensator (SVC): An electrical device for providing fast-acting reactive power on high-voltage electricity transmission networks. The term "static" refers to

  the fact that the SVC has no moving parts (other than circuit breakers and disconnects, which do not move under normal SVC operation). Prior to the invention of the SVC, power factor compensation was the preserve of large rotating machines such as synchronous condensers [12]. FIGURE 2.4 shows the schematic of a SVC.

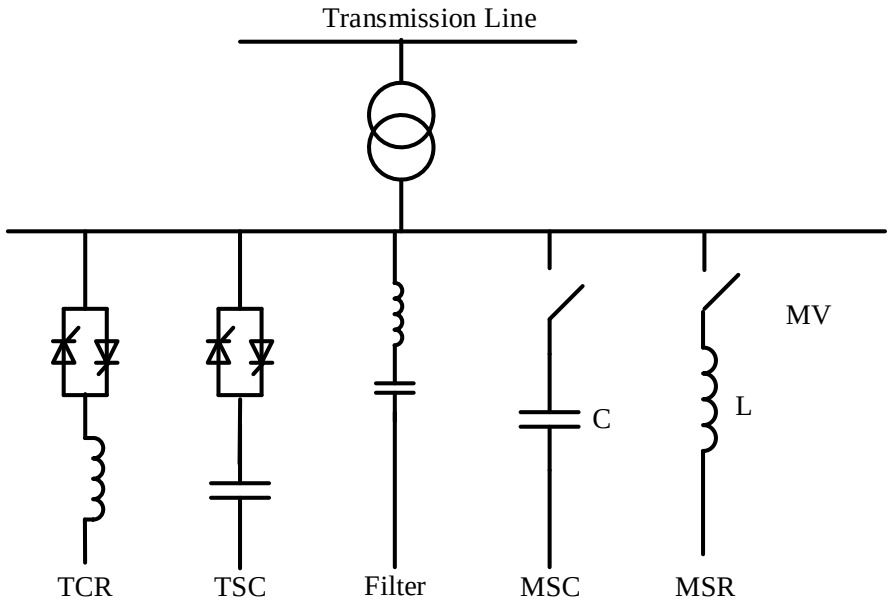

FIGURE 2.4: Schematic of Static Var Compensator.

SVC is an automated impedance matching device, designed to bring the system closer to unity power factor. If the power system's reactive load is capacitive (leading), the SVC will use reactors (usually in the form of Thyristor-Controlled Reactors) to consume VARs from the system, lowering the system voltage. Under inductive (lagging) conditions, the capacitor banks are automatically switched in, thus providing a higher system voltage. SVCs can control transmission line voltages and can also mitigate active

power oscillations because of their ability to modulate voltage amplitude [5]. They also may be placed near high and rapidly varying loads, such as arc furnaces, where they can smooth flicker voltage. Most common SVCs employee the following:

1. TCR (Thyristor Controlled Reactor) : A reactor connected in series with a bidirectional thyristor valve. The thyristor valve is phase-controlled. Equivalent reactance is varied continuously.
2. TSR (Thyristor Switched Reactor) : It is same as TCR but thyristor is either in zero- or full-conduction. Equivalent reactance is varied in stepwise manner.
3. TSC (Thyristor Switched Capacitor): A Capacitor is connected in series with a bidirectional thyristor valve. Thyristor is either in zero- or full- conduction. Equivalent reactance is varied in stepwise manner.
4. MSC (Mechanically Switched Capacitor) : A capacitor is switched by circuit-breaker. It aims at compensating steady state reactive power. It is switched only a few times a day.

- Mechanically Switched Capacitors with Damping Networks (MSCDN): A technology to provide a switchable source of reactive power to stabilize low frequency voltage variations [13]. It consists in large shunt capacitor banks, arranged as a C-type harmonic filter, connected to the high voltage system to provide reactive compensation and harmonic control and can be connected directly to the high voltage busbar system or via a coupling transformer as shown in FIGURE 2.5.

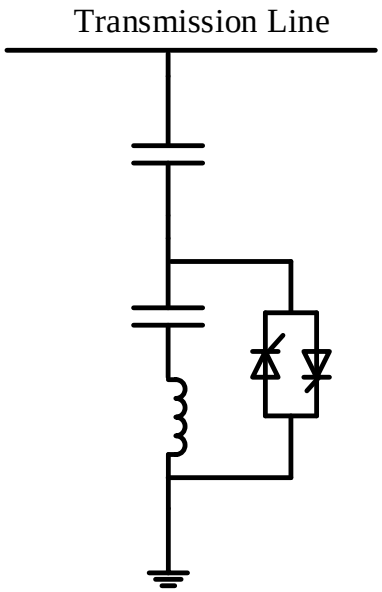

FIGURE 2.5: Schematic of Mechanically Switched Capacitors with Damping Networks.

MSCDNs are a simple and low-cost, but low-speed solution for voltage control and network stabilization under heavy load conditions. Their utilization has almost no effect on the short-circuit power but it supports the voltage at the point of connection. An advanced form of mechanically switched capacitor is the MSCDN (Mechanically Switched Capacitor with Damping Network) for avoidance of system resonances.

2.3. Series Controllers

The series controllers alter effective voltage in series with the transmission line. These controllers impact the driving voltage and hence vary the current and power flow. The series controller could be a variable impedance, such as capacitor, reactor etc., or a power electronics based variable source or both. This is shown in FIGURE 2.6.

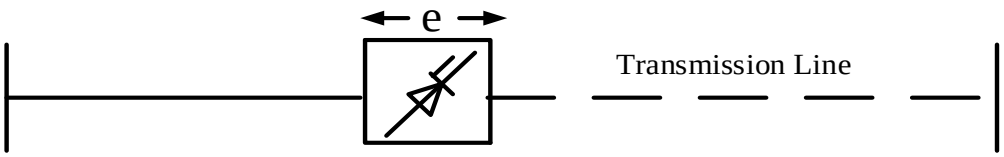

FIGURE 2.6: General symbol for series controller

As long as the voltage is in phase quadrature with the line current, the series controller only supplies or consumes variable reactive power [5]. They are designed to ride through contingency and dynamic overloads, and through or bypass short circuit currents. SSSC, TCSC and TCSR are commonly used series connected FACTS devices [5].

- Static Synchronous Series Compensator (SSSC): Static Synchronous Series Compensator (SSSC) is a type of series connected FACTS device. This is shown in FIGURE 2.7. A SSSC is a static synchronous generator operated without an external electrical energy source. As a series compensator the output voltage is controllable independently of, the line current to control the overall reactive voltage drop across the line, thereby controlling the transmitted power. SSSC has identical properties as STATCOM except for the output voltage is in series with the line.

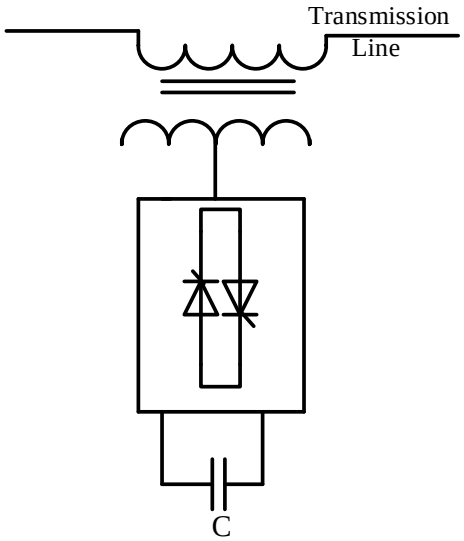

FIGURE 2.7: Simplified Schematic of Static Synchronous Series Compensator (SSSC).

- Thyristor Controlled Series Capacitor (TCSC): Thyristor Controlled Series Capacitor (TCSC) is composed of a variable reactor such as a Thyristor Controlled Reactor (TCR), which is connected across a series capacitor. This is shown in FIGURE 2.8.

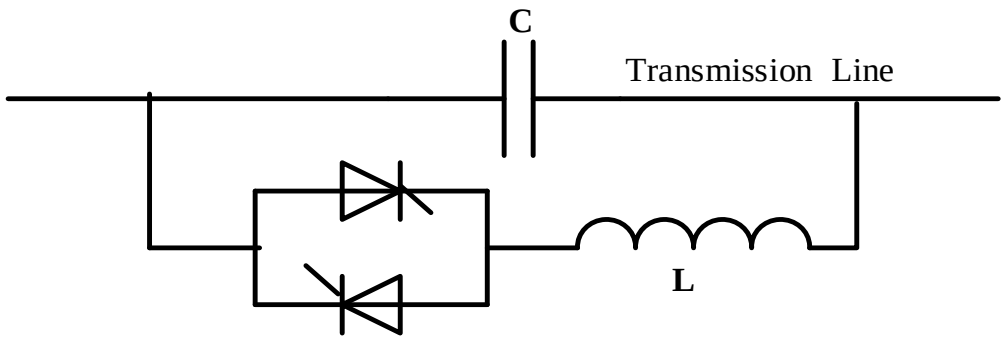

FIGURE 2.8: Simplified Schematic of Thyristor Controlled Switched Capacitor (TCSC).

Series compensation with TCSC enables rapid dynamic modulation of the inserted reactance. At interconnection points between transmission grids, this modulation will provide strong damping torque on inter-area electromechanical oscillations [11]. As a consequence, a TCSC rated at around 100 MVAr makes it possible to inteconnect grids having generating capacity in many thousands of megawatts. TCSC as expalined is combined with fixed series compensation to increase transient stability and also mitigate subsynchronous resonance (SSR). FIGURE 2.9 shows the circuit of a practical TCSC.

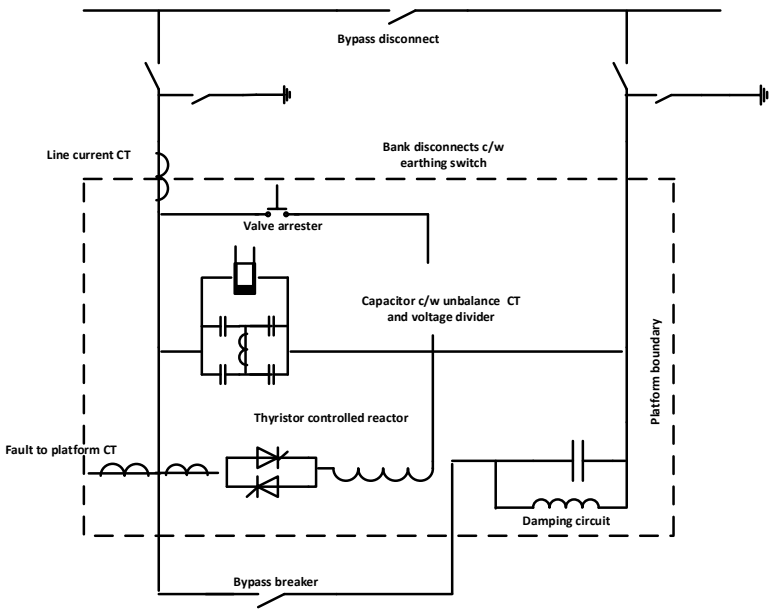

FIGURE 2.9: Schematic of Thyristor Controlled Switched Capacitor (TCSC).

Series compensation with TCSC enables rapid dynamic modulation of the inserted reactance [4]. At interconnection points between transmission grids, this modulation provides strong damping torque on inter-area electromechanical oscillations. As a consequence, a TCSC rated at around 100 MVAr makes it possible to interconnect grids having generating capacity in many thousands of megawatts [5].

- Fixed Series Compensation (FSC): The simplest, cost-effective and one of the preferred solution for optimizing performance in very large bulk transmission systems [11]. FSC comprise of a capacitor banks and parallel arresters metal oxide varistors, (MOVs) spark gaps and a bypass switch as shown in FIGURE 2.10. Installing a capacitive reactance in series in long (typically more than 200km) transmission line reduces both the angular deviation and the voltage drop, which increases the load ability and stability of the line.

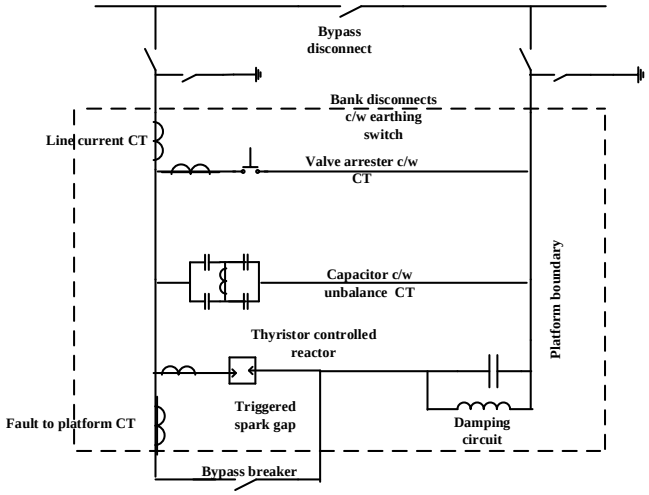

FIGURE 2.10: Schematic of Fixed Series Capacitor (FSC).

- Thyristor Protected Series Capacitor (TPSC): TPSCs are modified version of TCSCs with direct-light-triggered thyristors, instead of conventional spark gaps or surge arresters as shown in FIGURE 2.11. Due to the very short cooling times of the light-triggered thyristor valves, TPSCs return to service after a failure, allowing the transmission lines to operate at their maximum capacity [11].

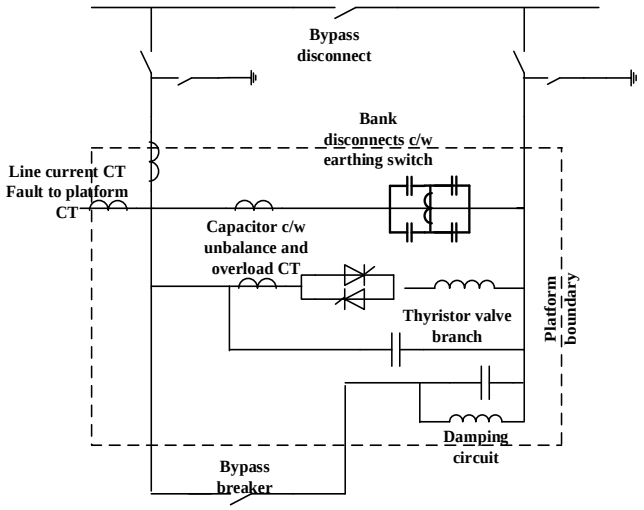

FIGURE 2.11: Schematic of Thyristor Protected Series Capacitor.

2.4. Combined Series-Shunt Controllers

Combined series-shunt controllers inject voltage in series in the line with the series part of the controller and current into the system with the shunt part of the controller. The general symbol of the combined shunt and series controller is shown in FIGURE 2.12.

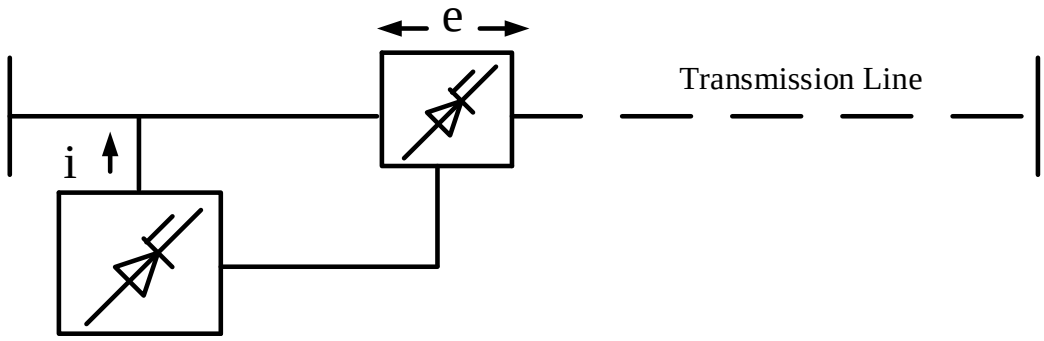

FIGURE 2.12: General symbol for unified series-shunt controller.

Unified Power Flow Control (UPFC) and Thyristor Controlled Phase shifting Transformer (TCPST) are the commonly used series-shunt controllers. When the shunt and series controllers are unified, there can be a real power exchange between the series and shunt controllers via the power link [5].

- Unified Power Flow Controller (UPFC): Unified Power Flow Controller (UPFC) is a combination of static synchronous compensator (STATCOM) and a static series compensator (SSSC) coupled via a common dc link, to allow bidirectional flow of real power between the series and shunt output terminals of SSSC and STATCOM respectively, and are controlled to provide real and reactive series line compensation without an external electric energy source [5]. This is shown in FIGURE 2.13. This is a complete controller for controlling active and reactive power control through the line, as well as line voltage control.

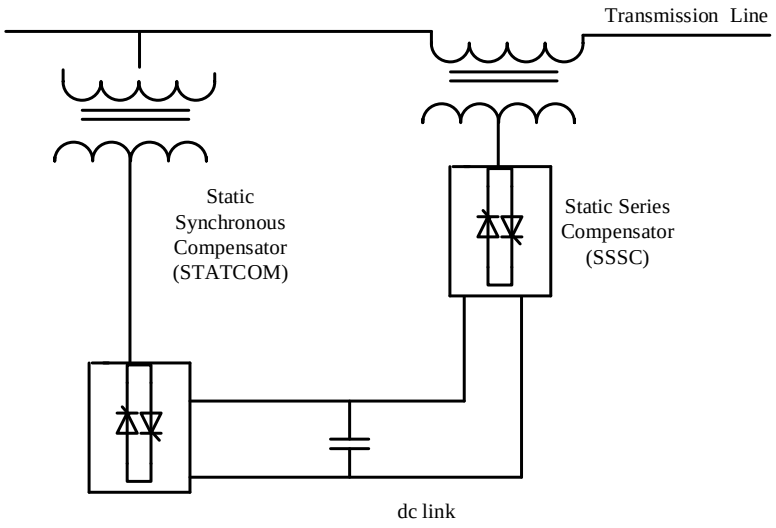

FIGURE 2.13: Simplified Schematic of Unified Power Flow Controller (UPFC)

- Thyristor-Controlled Phase Shifting Transformer (TCPST): *A* Thyristor-Controlled Phase Shifting Transformer (TCPST) is a phase-shifting transformer adjusted by thyristor switches to provide a rapidly variable phase angle [5]. This is shown in FIGURE 2.14. A perpendicular series voltage, (obtained by adding a perpendicular voltage vector in series with a phase voltage) is made variable using the conduction angle control of the power electronic topologies.

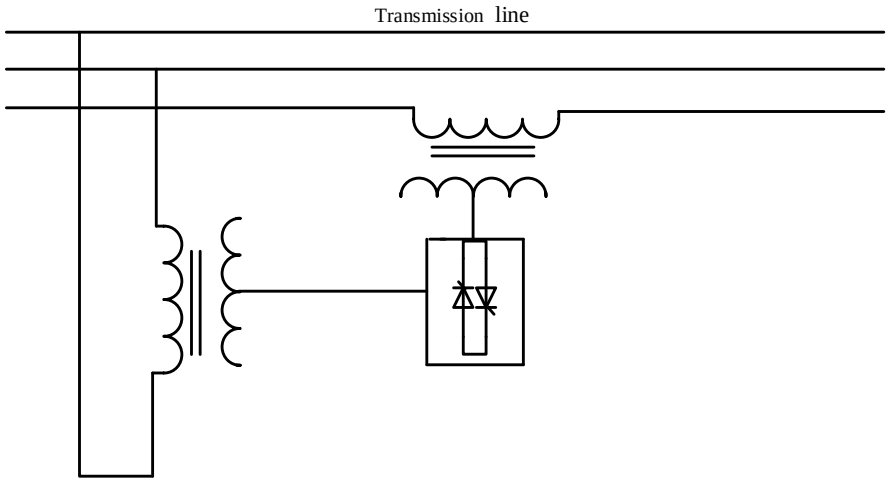

FIGURE 2.14: Simplified Schematic of Thyristor-Controlled Phase-Shifting Transformer (TCPST).

2.4.1. FACTS Benefits

IEEE defines FACTS as "a power electronic based system and other static equipment that provide control of one or more AC transmission system parameters to enhance controllability and increase power transfer capability [5]. The installation of FACTS started during mid-1970s with static VAr compensators (SVC). In 1986, Electric Power Research Institute (EPRI) introduced the concept, of FACTS based on then available power electronic devices. In 1990's General Electric (GE) in collaboration with EPRI, installed one of the first FACTS devices at the C.J. Slatt Substation in Northern Oregon which was a 500 kV, 3-phase 60 Hz substation [9]. FACTS controllers help mitigate stability and power congestion issues in interconnected systems. FACTS devices can also improve the synchronous operation and influence the load flow conditions [4]. Some of the benefits of FACTS devices are given as follows.

- Enhanced Static Performance - FACTS controllers provide increased loading, congestion management, reduced system losses and economic operation. They reduce transmission congestion costs from increased transmission transfer capability without building additional transmission capacity.
- Improved Dynamic Performance - FACTS controllers provide increased stability limits and damping of power system oscillation. They reduce or eliminate voltage violations on transmission lines. FACTS also provide reactive power support for transmission/distribution bus.
- Cost Savings – FACTS devices increases the amount of power that can be imported over existing transmission lines. They minimize cost of energy, kWh consumption at voltages beyond given voltage quality limit, and ensure standard voltages at customer

terminals. FACTS conserve energy via voltage reduction. They also reduce the need for construction of new capacitors, reactors, etc which mitigate environmental and regulatory concerns, and improves aesthetics by reducing the need for construction of new facilities.

- Dynamic Reactive Power Compensation- FACTS devices controls real and reactive power flow.
- Steady-State and Transient Stability Enhancement - FACTS devices mitigates potential Sub-Synchronous Resonance problems.

FACTS controllers also provide voltage regulation, power transfer capacity increase, three-phase voltage balancing, reduce transmission losses, flicker mitigation and oscillation damping [10]. Table 2.1 gives the steady state applications of FACTS devices and Table 2.2 gives dynamic applications of FACTS devices [5].

Table 2.1: List of Steady State Applications of FACTS.

Issues	**Problems**	**Corrective action**	**Conventional Solution**	**FACTS devices**
Voltage Limits	Low voltage at heavy load	Supply reactive power	Shunt capacitor, series capacitor	SVC, STATCOM
	High voltage at light load	Remove reactive power supply	Switch EHV and/or shunt capacitor	SVC, TCSC, STATCOM
	High voltage following outage	Absorb reactive power	Switch shunt capacitors, series capacitor	SVC, STATCOM
Thermal limits	Line or transformer over load	Reduce load	Add line or transformer	TCSC, UPSC, TCPAR
			Add series reactor	SVC, TCSC
	Tripping of parallel circuits	Limit line loading	Add series reactor, capacitor	UPSC, TCSC
Short Circuits	Excessive breaker Fault current	Limit short circuit breaker	Add series reactor, new circuit breaker	UPFC, TCSC

Issues	Problems	Corrective action	Conventional Solution	FACTS devices
Sub-synchronous resonance	Potential turbine/ generator shaft damage	Mitigate oscillations	Series compensation	NGH, TCSC
Loop flows	Post fault sharing	PAR, series capacitor/ reactor	PAR, series capacitor/ reactor	TCSC, UPSC, SVC, TCPAR
	Parallel line load sharing	Adjust series reactance/ phase reactance rearrange network or use thermal limit actions	Add series capacitor and PAR	TCSC, TCPAR
	Flow directional reversal	Adjust phase angle	PAR	TCPAR, UPFC

Table 2.2: List of Dynamic Applications of FACTS.

Issues	Problems	Corrective action	Conventional Solution	FACTS devices
Transient Stability	Remote generation/ Interconnected areas/ loosely meshed network	Increase synchronizing torque	High response exciter, series capacitor	TCSC, TSSC. UPFC
	Remote generation/ loosely meshed network	Absorb kinetic energy	Breaking resistor, Fast Valuing Turbine	TCBR, SMES, BESS
	Interconnected areas/ loosely meshed network/ tightly meshed network	Dynamic load flow control	HVDC	TCPAR. UPFC, TCSC
Dampening	Remote generation	Dampen 1Hz oscillations	Exciter, Power system stabilizer	SVC, UPFC, TCSC, STATCOM
	Interconnected areas/ loosely meshed network	Dampen low frequency oscillations	Power system stabilizer	SVC, UPFC, TCSC, STATCOM
Post contingency voltage control	Remote generation/ Interconnected areas/ loosely meshed network	Dynamic voltage support	-----	SVC, UPFC, STATCOM
Post contingency voltage control	Remote generation/ Interconnected areas/ loosely meshed network	Dynamic flow support	-----	SVC, UPFC
		Dynamic voltage support and flow control	-----	SVC, UPFC, TCSC

FACTS high-voltage AC transmission solutions are widely recognized by network suppliers and industrial energy managers. Grid operators can gain accurate control of reactive network power, maximize power flow along existing lines and improve steady-state and dynamic stability with the system.

Since AC transmission systems are prevalent in the transmission industry, the installation of FACTS solutions will continue, both to replace existing aging infrastructure and to support the trouble-free interconnection of wind and renewable generation. Thus, FACTS technologies can be used to creatively solve demanding problems in transmission all over the world. Table 2.3 gives the major Industry suppliers of FACTS in the market and Table 2.4 gives installions of key FACTS devices.

Table 2.3: List of major suppliers and FACTS in the market.

Supplier	**FSC**	**TCSC**	**SVC**	**STATCOM**	**MSCDN**	**TPSC**
SIEMENS	Yes	Yes	Yes	No	Yes	Yes
ABB	Yes	Yes	Yes	Yes	No	No
ALSTOM	Yes	Yes	Yes	Yes	Yes	No
GE	Yes	No	No	No	No	No
AMSC	No	No	Yes	Yes	No	No
S & C Electric	No	No	No	Yes	No	No

Table 2.4: List of key FACTS installations.

FACTS Device	Manufacture	Customer	Location	Rating
Fixed Series Capacitor/ Compensator (FSC)	SIEMENS	Powergrid Corporation of India, Ltd.	Lucknow - Bareilly- Unnao	2 x 189 Mvar 2 x 187 Mvar 2 x 311 Mvar
		Brazilian Electricity Regulatory Agency (ANEEL)	Colinas, Miracema and Gurupi	200 MVAr 2 x 194 MVAr 130 MVAr
		State Grid Corporation of China	Fengile County, Chongquing City	35.3 Ohm/2 x 610 MVAr
		Dominion Virginia Power	Rockbridge Bath, And near Weyers Cave, Virginia	13.1 Ohm / 355 MVAr at 3 kA 18.7 Ohm / 505 MVAr at 3 kA
	ABB	Transmission grid of Hydro-Québec	Des Hêtres - Canada	36 Ohm/ 108 MVAr
		Finnish transmission system operator, Fingrid	Asmunti, Finland	38 Ohm/ 369 MVAr
Fixed Series Capacitor/ Compensator (FSC)	GE	Cross Texas Transmission	Turkey, Texas – Cross Station 1,2	2 x 716 MVAr
		Electricity of Vietnam	DakNong 1 & 2, Di Linh 1 & 2, Pleiku 1 & 2	6 X 366 MVAr
		BPA (Bonneville Power Administration)	Bakeoven 1 &2, California-Oregon	2 X 675 MVAr
Static Var Compensator (SVC)	SIEMENS	Powerlink	Greenbank and South Pine	1 x TCR 2 xTSC 3 Filters
		SEAS-NVE, Denmark	Radsted, Denmark	12-pulse configuration 2 x TCR 2 x Filters
		SCE, USA	Palm Springs, California	2 x TCR 3 x TSC 2 x Filters
		Entergy, USA	Ninemile and Porter	3 x TSC
		ESKOM, South Africa	Impala and Illovo, SA	2 x TCR 3 x Filters
	ABB	Société Nationale d'Electricité	Karavia, Democratic Republic of Congo	75 Mvar inductive to 75 Mvar capacitive, continuously variable (-75/+75 Mvar)
		Chesf, a Brazilian transmission and generation utility	Rio Grande do Norte, NE Brazil	75Mvar induc-150Mvar cap continuous
FACTS Device	**Manufacture**	**Customer**	**Location**	**Rating**

Static Var Compensator (SVC)	ALSTOM	Saudi Electricity Company (SEC)	Quwayyah substation in Saudi Arabia	-50/+170 MVAr
		Energy Company of Minas Gerais	Minas Gerais in Brazil	-200/300 MVAr
Thyristor Controlled Switched Capacitor (TCSC)	SIEMENS	FURNAS – Centrais Elétricas S.A.	North of Brasilia, Brazil	Cap. rating: 13.27 Ohm (blocked valve) and 15.92 Ohm (TCSC)/107.46 MVAr at 1.5 kA, TCR rating : 23.9 kV nominal valve voltage at 3.55 kA
	ABB	Power Grid Corporation of India Ltd	Rourkela-Raipur	TCSC segment: 6.83 Ω/ 71 Mvar Fixed segment : 54.7 Ω/ 394 Mvar
Thyristor Controlled Switched Capacitor (TCSC)	SIEMENS	State Power South Company	PingGuo substation, Guangxi Province, P.R. China	Fixed segment: 29.2Ohm, 2000 A, 350 MVAr Controlled segment: 4.15 Ohm to 12.45 Ohm, 2000 A, operated at 4.57 Ohm, 55 MVAr TCR rating : Thyristor valve 10 kV, 2000 A
		WAPA (Western Area Power Administration)	north-eastern Arizona, USA	Cap. : 55 Ohm/165 MVAr 40 Ohm/120 MVAr 15 Ohm/45 MVAr (ASC) TCR : 100 mm thyristors 3.5kA, 5.5 kV blocking voltage
Thyristor Protected Series Capacitor (TPSC)	SIEMENS	Southern California Edison (SCE)	Near Boulder City, NV, USA	199 Mvar / segment[1] 162 Mvar / segment[2]
FACTS Device	**Manufacture**	**Customer**	**Location**	**Rating**
Thyristor Protected Series Capacitor (TPSC)	SIEMENS	Southern California Edison (SCE)	Near Buttonwillow, north of Los Angeles, CA, USA	23.23 Ohm/401 MVAr at 2.4 kA

Static Compensator (STATCOM)	ABB	Austin Energy	Holly, Austin	Dynamic Var : 80 Mvar inductive to 110 Mvar capacitive VSC: 95 MVA, 3-level, neutral point clamping converter, IGBT based, PWM. MSCs, each rated at 138 kV, 31 Mvar.
	S&C	Single-turbine wind farm	Dounby, Scotland	±1.25 MVAR Continuous into 11-kV bus,
Mechanical Switched Capacitor (MSC)	SIEMENS	TNB (Tenaga National Berhard)	Kuala Lumpur North	3 x 60 MVAr
Mechanical Switched Capacitor (MSC)	SIEMENS	SEC Saudi Electric Company	Baish, Saudi Arabia	2 x 20 MVAr
	ALSTOM	TransnetBW, subsidiary of EnBW	Engstlatt (Baden-Württemberg), Germany	250 MVAr
Mechanically Switched Capacitor Damping Network (MSCDN)	SIEMENS	RTE	Five stations, France	4x80 MVAr + 1x8 MVAr
		RED Electrica de Espana	Benejama and Saladas near the Costa Blanca in Spain	2x100 MVAr
		National Grid Company, U.K.	Beddington, U.K.	45 MVAr
	ALSTOM	German transmission grid operator TenneT TSO GmbH	Frankfurt, Germany	300 MVAr
		TransnetBW, subsidiary of EnBW	Engstlatt (Baden-Württemberg), Germany	250 MVAr

CHAPTER 3 : DISTRIBUTED FACTS (D-FACTS)

3.1. Introduction

FACTS devices have proved to increase the transfer capacity and the utilization of the power-system [2]. However, their commercial success has been limited due to the following difficulties in convincing the utilities for making investments in FACTS technology [14].

1. High Cost: Converter complexity and semiconductor ratings make FACTS devices an expensive solution. Moreover, the maintenance and repair calls for skilled labor, which further increase the cost.

2. Low Reliability: A single component failure can lead to reduced overall performance of the module.

3. Custom Engineering: Most FACTS devices are custom-designed and have long build times. They further require additional infrastructure such as mounting platforms and isolation transformers.

The limitations listed can be attributed to the lumped nature of FACTS devices [14]. The reliability of the technology can be increased and the cost can be decreased, if the same control objective is served by replicating a lumped controller into smaller controllers and distributing them over the grid. Thus, the concept of Distributed FACTS (D-FACTS) has been proposed by Divan, et al. [2].

D-FACTS consist of single phase devices that can clamp onto existing conductors, providing easy installation procedure and the possibility for on-site repairs. The cost of D-FACTS is lower, as off-the-shelf components can be used to meet the rating of the individual controllers/devices and can be further scaled down with volume production [7]. The reliability of the solution is also improved as the failure of a single component or even a complete device is seen to have limited impact on the overall functionality of the solution [14].

3.2. Equivalent Impedance Offered by Transformer

Towards understanding the principle of D-FACTS devices, let us analyze, the equivalent impedance offered by a basic transformer shown in FIGURE 3.1. Let the source voltage applied to the primary side of the transformer be V_1, and the primary: secondary turns ratio be N_1:N_2 [24]. Let there be a switch S_M connected across the secondary side and V_2 be the voltage across the switch.

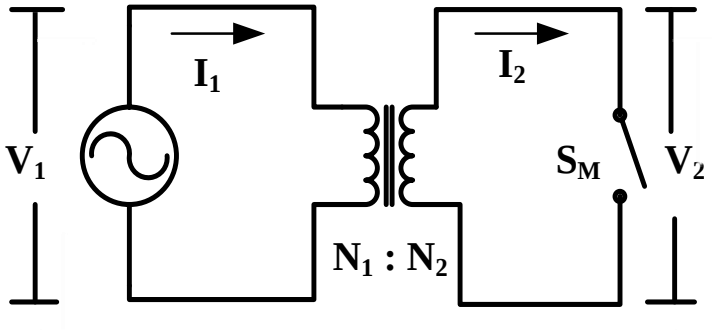

FIGURE 3.1: Basic circuit of an Ideal Transformer.

Under ideal conditions, 1) winding losses and leakage flux are neglected and 2) permeability of the core is assumed to infinity. Therefore, when the switch S_M is closed, current I_1 flows through the turns of the primary coil, producing flux Φ_m which links with

secondary coils and induces voltage in the secondary side, by Faraday's law of electromagnetic induction. This gives

$$V_1 = N_1 \frac{d\Phi_m}{dt} \tag{3.1}$$

$$\text{where } \Phi_m = \Phi_{max} \sin \omega t \tag{3.2}$$

we get, $$V_1 = N_1 \omega \Phi_{max} \cos \omega t \tag{3.3}$$

Similarly

for secondary turns N_2 , we get

$$V_2 = N_2 \omega \Phi_{max} \cos \omega t \tag{3.4}$$

From (3.3) and (3.4), we get $$\frac{V_1}{V_2} = \frac{N_1}{N_2} \tag{3.5}$$

Let us consider a load Z_L across the secondary terminal, current I_2 flows in the circuit, produces flux Φ_2 , which acts in opposition to the flux produced by primary turns Φ_1 (where $\Phi_m = \Phi_1 - \Phi_2$). Hence, the relation between I_1 and I_2 is given by

$$I_1 = \frac{N_1}{N_2} I_2 \tag{3.5}$$

Now, consider that the transformer windings have losses. Let R_1 and R_2 be resistances of the primary windings and secondary windings. Secondly, let us consider that the core of the transformer is no longer infinitely permeable. Therefore, there is some leakage flux Φ_{L1} and Φ_{L2} which does not link the secondary and primary turns. Hence, let L_1 and L_2 be the leakage reactance of primary and secondary coils respectively. Also, at no load condition, the transformer draws a magnetizing current I_m. Thus, a magnetizing inductance L_m is introduced across the primary winding. Finally, due to core losses

(hysteresis and eddy current losses), a resistance R_0 is introduced across the primary windings. Therefore, such a non-ideal transformer with losses is shown in FIGURE 3.2.

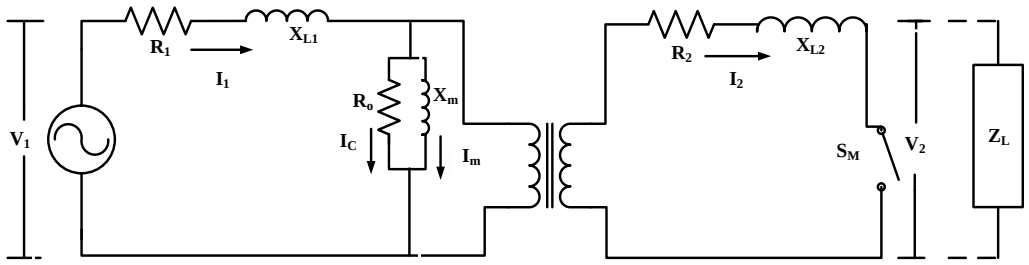

FIGURE 3.2: Equivalent circuit of transformer with leakage, winding, core and magnetizing losses.

From FIGURE 3.2, applying Kirchhoff's Voltage law on the primary side, we get,

$$V_1 = R_1 I_1 + jX_{L1} I_1 + E_1 \tag{3.6}$$

Similarly, applying KVL on the secondary side, we get,

$$E_2 = R_2 I_2 + jX_{L2} + V_2 \tag{3.7}$$

Also, V_2 can be expressed as

$$V_2 = Z_L I_2 \tag{3.8}$$

Finally, applying Kirchhoff's Current Law, we get,

$$I_1 = I_2' + I_m + I_c \tag{3.9}$$

Referring the secondary side of the transformer with reference to primary side, results in transformer the equivalent parameters as

$$R_2' = \left(\frac{N_1}{N_2}\right)^2 R_2 \tag{3.10}$$

$$X_{L2}' = \left(\frac{N_1}{N_2}\right)^2 X_{L2} \tag{3.11}$$

$$Z_L' = \left(\frac{N_1}{N_2}\right)^2 Z_L \tag{3.12}$$

Therefore, the approximate equivalent parameters of the transformer, can be given as shown in the FIGURE 3.3.

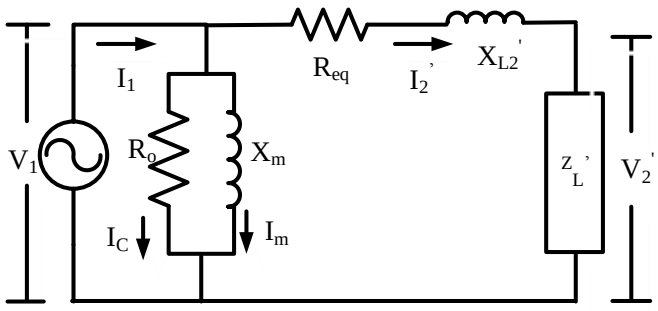

FIGURE 3.3: Equivalent circuit of transformer

where $R_{eq} = R_1 + R'_2$ (3.13)

$X_{eq} = X_1 + X'_2$ (3.14)

3.3. Series Injected Transformer

The transformer analyzed in previous section can be used to control the power flow by introducing it in series in the transmission system. This technique is termed as Single Turn Transformer (STT). STT uses the line conductor itself as the primary winding of the transformer. A single turn transformer is used to magnetically couple and mechanically attach the module to the line. It is designed with a large number of secondary turns, say 1:50. This unit enables, the controller to be used with line voltages ranging from 13kV to 500kV and line current varying from 500 A to 1500 A [14], [7]. The transmission line representation with a STT is shown in FIGURE 3.4.

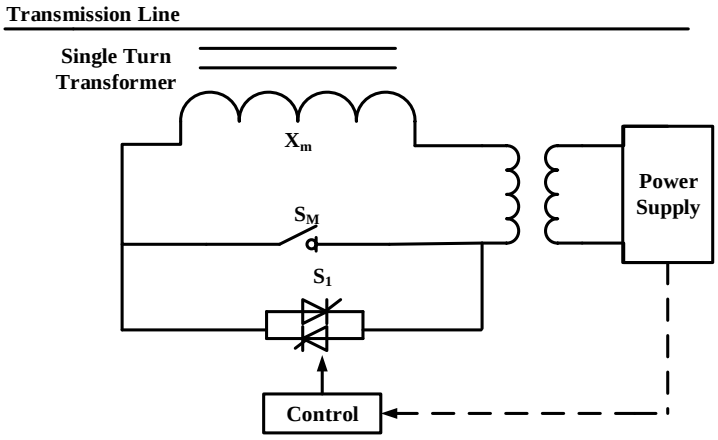

FIGURE 3.4: Transmission line with Single Turn Transformer (STT)

3.3.1. Distributed Series Reactance

The concept of D-FACTS, introducing a variable equivalent reactance into the transmission line by means of a series connected transformer is termed as Distributed Series Reactance (DSR) [7]. A DSR consists of a Single Turn Transformer (STT) where the transmission line itself acts as the primary winding. The secondary winding is connected to back-to-back thyristors, which when closed creates a short circuit across the secondary winding thereby varying the effective reactance introduced into the power line.

A simplified schematic of the DSR is shown in FIGURE 3.4. An equivalent circuit of DSR consists of sending voltage (V_s), line reactance (X_{line}), receiving voltage (V_r), leakage reactance (X_{leak}) and magnetizing reactance (X_{mag}) as shown in FIGURE 3.5.

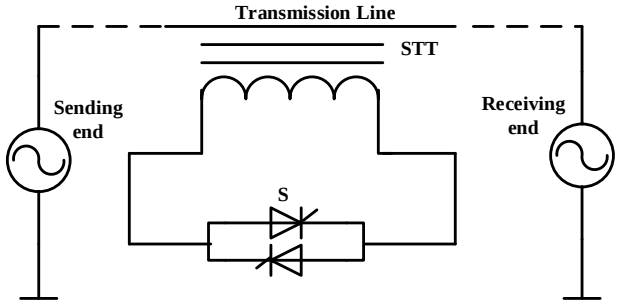

FIGURE 3.5: Simplified Schematic of a Distributed Series Reactance (DSR)

Analysis of the DSR circuit

When switch S is open across the secondary winding, magnetizing reactance of the STT is injected into the circuit. The equivalent circuit of DSR with switch S open [7], [8] is shown FIGURE 3.6.

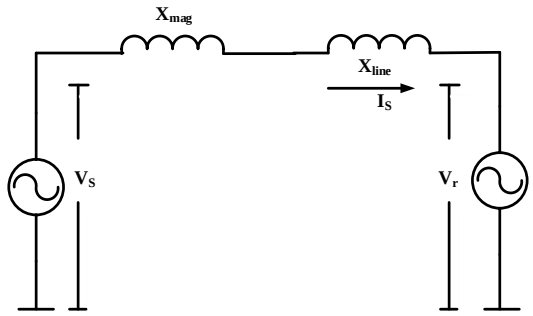

FIGURE 3.6: Equivalent circuit of DSR when switch S is open

Therefore the equivalent impedance on the line is given by

$$jX_{eq} \approx jX_{mag} + jX_{line} \tag{3.16}$$

Similarly, when switch S is closed across the secondary winding, leakage reactance of the STT is connected in shunt with magnetizing reactance. But because leakage reactance (X_{leak}) << magnetizing reactance (X_{mag}), the effective reactance that gets injected is more closer leakage reactance [24], [7]. The equivalent circuit of DSR with switch S closed is shown FIGURE 3.7.

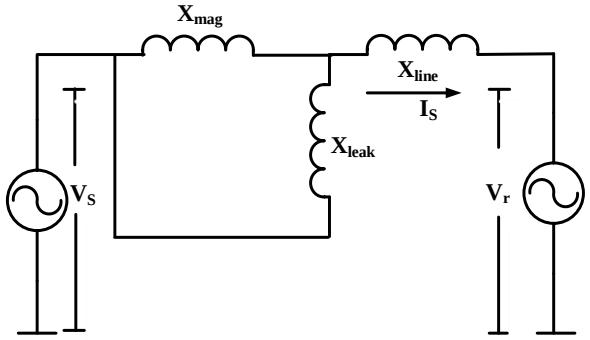

FIGURE 3.7: Equivalent circuit of DSR when switch S is closed

Therefore, the equivalent impedance is given by

$$jX_{eq} \approx jX_{leak} + jX_{line} \tag{3.17}$$

A DSR circuit is designed with following transmission system parameters: $V_r = V_s =$ $230kV_{L\text{-}L}$, S = 100 MVA, $\boldsymbol{\delta}$ = 30° lag, X_{line}= 8.46 Ω, X_{leak}= 0.033 Ω, X_{mag} = 162.11 Ω

$$V_{ph} = \frac{V_{L-L}}{\sqrt{3}} \tag{3.18}$$

$$V_{ph} = \frac{230\ \text{kV}}{\sqrt{3}} = 132.791\ \text{kV}$$

$$V_{peak} = \sqrt{2}\, V_{ph} \tag{3.19}$$

$$V_{peak} = \sqrt{2} * 132.791\ \text{kV} = 187.794\ \text{kV}$$

When switch S is open, from equation (3.16), we get

$$jX_{eq} = j162.11 + j0.03 + j8.46$$

$$= j170.6\ \Omega$$

Using Ohms law, we get current I in the circuit

$$I = \frac{V_s - V_r}{jX_{eq}} \tag{3.20}$$

$$I = \frac{187794(1 - 1\angle 30)}{j170.6} = 550.40\text{A}$$

When switch S is closed, from equation (3.17), we get

$$jX_{eq} = j8.46 + \left(jX_{mag} \| jX_{leak}\right)$$

$$= j8.46 + j0.033\ \Omega = j8.49\ \Omega$$

Using Ohms law, we get current I in the circuit

$$I = \frac{V_s - V_r}{jX_{eq}} \tag{3.20}$$

Therefore the current in the system is

$$I = \frac{187794(1-1\angle 30)}{j8.49} = 11055.58A$$

Table 3.1 presents analytical results. Simulation results for these scenarios are presented FIGUREs 7.1 and 7.2

Table 3.1: Calculated Currents of DSR system

S	**X_{eff}**	**Calculated Current**
Open	170.6 Ω	550.40 A
Closed	8.49 Ω	$1.11e^4$ A

3.3.2. Distributed Series Impedance

The power flow control can be improved by extending the principle of DSR by adding an L-C impedance network to the secondary side of the transformer. This topology is called Distributed Series Impedance (DSI) [7], [8], [14]. A simplified schematic of the DSI is shown in FIGURE 3.8.

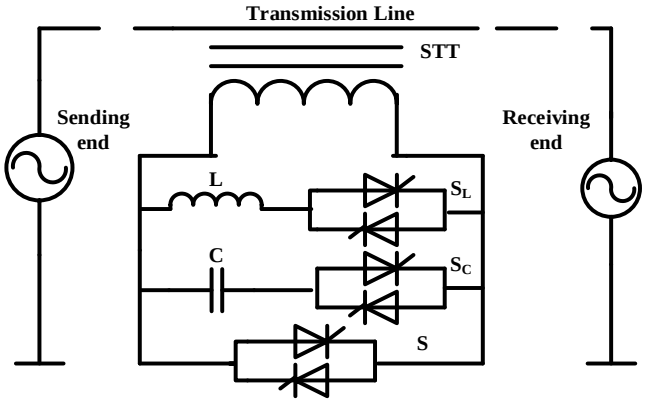

FIGURE 3.8: Simplified schematic of a Distributed Series Impedance (DSI)

A Distributed Series Impedance (DSI) can control active power flow by realizing variable line impedance. The transfer capacity and consequently the grid utilization can be improved by routing the power flow from overloaded lines to underutilized parts of the network [7]. Capacitive compensation on under-utilized lines makes them more receptive to the inflow of current, while inductive compensation on over-loaded lines makes them less attractive to current flow [14]. In both the cases, the throughput of the system is increased by diverting additional power flow from the congested parts of the network to the lines with available capacity.

In addition to the series connected STT and its switch S on the secondary side, inductor L and capacitor C are inserted along with their switches S_L and S_C respectively. The equivalent circuit now consists of source voltage (V_s), line reactance (X_{line}), receiving voltage (V_r), leakage reactance (X_{leak}), magnetizing reactance (X_{mag}), and additional compensation reactances X_L and X_C as shown in FIGURE 3.9.

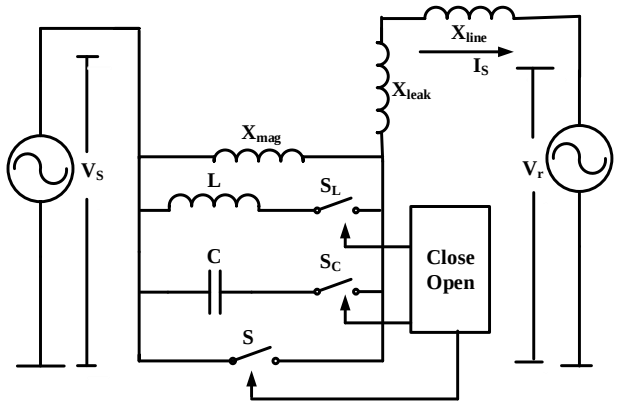

FIGURE 3.9: Equivalent circuit of a Distributed Series Impedance (DSI)

As may be seen from FIGURE 3.10, when the switch S is closed, leakage impedance of the STT is injected, whereas when all switches S, S_L and S_C are open, magnetizing reactance is inserted into the line. These two modes are similar to that of DSR and the effective line reactance [8] is given by equations (3.16) and (3.17).

Analysis of the DSI circuit

When switch S is open and switch S_L is closed, the DSI injects inductance L and operates into "inductance (L) mode" [8]. The equivalent circuit of DSI in inductance mode is shown FIGURE 3.10.

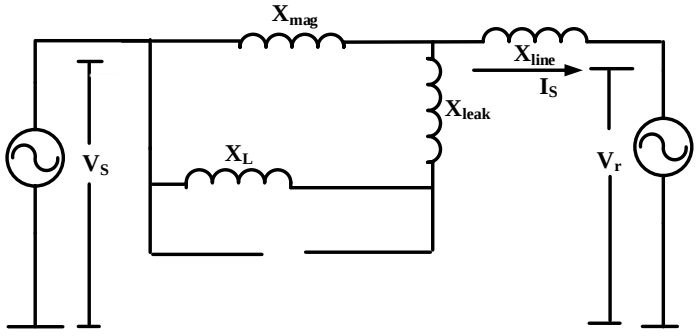

FIGURE 3.10: Equivalent circuit of DSI in inductance mode

The effective line reactance in this mode is given by

$$X_{eff(inductance\ mode)} \cong jX_{line} + jX_{leak} + jX_L \quad (3.21)$$

where $$X_L = \omega L \quad (3.22)$$

When switch S is open and switch S_C is closed, the DSI injects capacitance C and operates into "capacitance (C) mode" [8]. The equivalent circuit of DSI in inductance mode is shown FIGURE 3.11.

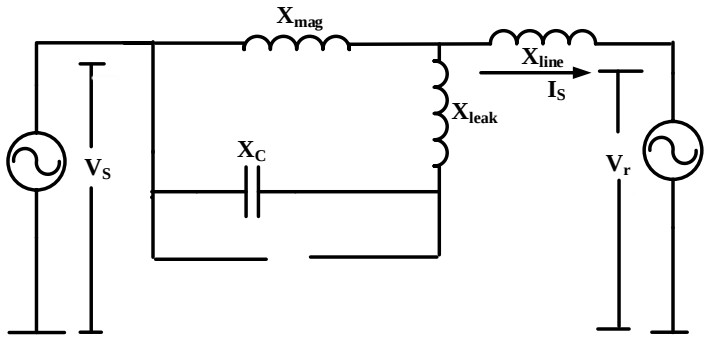

FIGURE 3.11: Equivalent circuit of DSI in capacitance mode

The effective line reactance in this mode is given by

$$jX_{eff(capacitance\ mode)} \cong jX_{line} + jX_{leak} - jX_C \quad (3.23)$$

where $$X_C = \frac{1}{\omega C} \quad (3.24)$$

When switch S is open and both switches S_L and S_C are closed, the DSI injects impedance and operates into "impedance (Z) mode" [8]. The equivalent circuit of DSI in inductance mode is shown FIGURE 3.13.

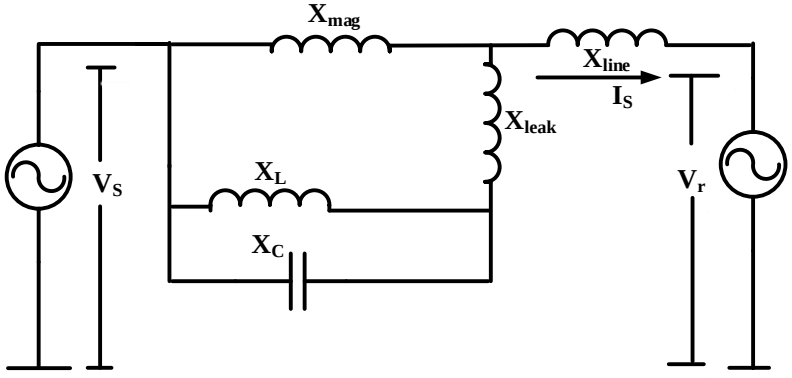

FIGURE 3.12: Equivalent circuit of DSI in impedance mode

The effective line reactance in this mode is given by

$$jX_{eff(impedance\ mode)} \cong jX_{line} + jX_{leak} + jX_L||(-jX_C) \quad (3.25)$$

A DSI circuit is designed with following transmission system parameters: $V_r = V_s = 230kV_{L\text{-}L}$, S = 100 MVA, $\boldsymbol{\delta} = 30^\circ$ lag, $X_{line} = 8.46\ \Omega$, $X_{leak} = 0.033\ \Omega$, $X_{mag} = 162.11\ \Omega$, $X_L = 152.3\ \Omega$, $X_C = 566\ \Omega$

$$V_{ph} = \frac{V_{L-L}}{\sqrt{3}} \quad (3.26)$$

$$V_{ph} = \frac{230\ kV}{\sqrt{3}} = 132.791\ kV$$

$$V_{peak} = \sqrt{2}\, V_{ph} \quad (3.27)$$

$$V_{peak} = \sqrt{2} * 132.791\ kV = 187.794\ kV$$

When switch S_L is closed and S_C is open, i.e., in inductance mode, as shown in FIGURE 3.11. The equivalent impedance offered by DSI is

$$jX_{eff(inductance\ mode)} \cong jX_{line} + jX_{leak} + jX_L \quad (3.28)$$

$$= j8.46 + j0.03 + j152.3 = j160.79\ \Omega$$

Using Ohms law, we get current I in the circuit

$$I = \frac{V_s - V_r}{X_{eq}} \quad (3.29)$$

$$I = \frac{187794(1 - 1\angle 30)}{j160.79} = 583.96\ A$$

When switch S_L is open and S_C is closed i.e., in capacitance mode, as shown in FIGURE 3.12. The equivalent impedance offered by DSI is

$$jX_{eff(capacitance\ mode)} \cong jX_{line} + jX_{leak} - jX_C \quad (3.30)$$

$$= j8.46 + j0.033 - 566 = -j557.50\ \Omega$$

Using Ohms law, we get current I in the circuit

$$I = \frac{V_s - V_r}{X_{eq}} \tag{3.31}$$

$$I = \frac{187794(1-1\angle 30)}{-j5574.50} = -168.42 \text{ A}$$

When switch S is open and both switches S_L and S_C are closed i.e., in impedance mode, as shown in FIGURE 3.13. The equivalent impedance offered by DSI is

$$jX_{eff(\text{impedance mode})} \cong jX_{line} + jX_{leak} + jX_L||(-jX_C) \tag{3.32}$$

$$= j8.46 + j0.033 + \left(\frac{-j566 * j152.3}{j152.3 - j566}\right) = j216.45\ \Omega$$

Using Ohms law, we get current I in the circuit

$$I = \frac{V_s - V_r}{X_{eq}} \tag{3.33}$$

$$I = \frac{187794(1-1\angle 30)}{j128.50} = 433.79 \text{ A}$$

Table 3.2 presents analytical results. FIGUREs 7.1 and 7.2 illustrate the waveforms for the cases when switch S is open and closed respectively.

Table 3.2: Calculated Currents of DSI system

Mode	**X_{eff}**	**Calculated Current**
Inductance	160.79 Ω	583.96 A
Capacitance	-557.50 Ω	168.42 A
Impedance	216.45 Ω	433.79 A

CHAPTER 4 : ENHANCED POWER FLOW CONTROLLER (EPFC)

4.1. Introduction

Due to increased demands of power, ability to control power flow in the transmission system can be improved by Flexible AC Transmission Systems (FACTS) devices such as Thyristor Controlled Switched Capacitor (TCSC) and Unified Power Flow Controller (UPFC). However, such devices require a break in the line and a high volatges platform, thus adding to the cost and complexity. The solution to this problem is proposed to be as Distributed FACTS (D-FACTS) [2], explained in chapter 3. D-FACTS are deployed without breaking the existing transmission line. But, D-FACTS provide only on/off control limiting the variable effective impedance on the line, therefore the controllability of power flow. Hence a concept of conduction angle (σ) control is proposed in this chapter [8]. Conduction angle (σ) control can provide continuous variation of impedance offered by inductor (L) and Capacitor (C) in combination with the line inductance (L_{Line}). In this Chapter 4, the concept of enhanced Power Flow Controller (ePFC) is explained in detail with its mathematical model. The effective fundamental impedance of ePFC for the following three approximations is presented in sections 4.1 through 4.3.

4.2. Principle of operation of ePFC

A simplified schematic of the proposed enhanced Power Flow Controller (ePFC) with conduction angle control is shown in FIGURE 4.1. As may be seen, the circuit schematic

of ePFC closely resembles that of a Distributed Series Impedance (DSI). However, the control mechanisms are significantly different in these two approaches. In a DSI, inductance L is either injected entirely, or not injected at all (switch S_L is either closed or open). Thus $X_{Linjected} = X_L$ or $X_{Linjected} = 0$. Whereas in an ePFC, the amount of inductance injection is controlled continuously by varying the conduction angle (σ) of thyristors (switch S_L is operated under conduction angle control) [8].

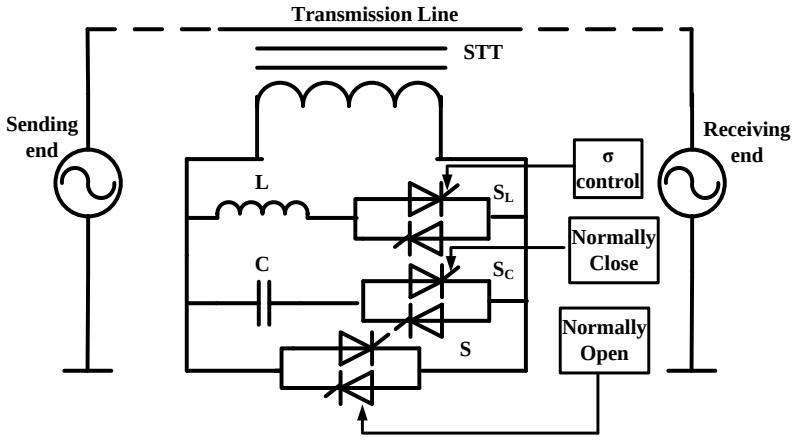

FIGURE 4.1: Simplified schematic of the proposed enhanced Power Flow Controller (ePFC)

Thus $X_{Linjected} = X_L(\sigma)$. Also in an ePFC, capacitance C is injected entirely in a normal operating mode (switch S_C is normally closed). Thus $X_{Cinjected} = X_C$. However, this capacitance is so sized in an ePFC that, X_C combined with $X_L(\sigma)$ offers a continuously variable effective impedance $X_{LC}(\sigma)$ injected into the transmission line which results in a precise power flow control. This is illustrated in Table 4.1.

To derive a mathematical expression for $X(X_{line}, X_L, X_C)_{|\sigma}$, three approaches are considered. The first approach adopts a 1st order approximation method [5] by assuming that the voltage across the capacitor is sinusoidal, as explained in section 4.3. The second approach adopts a 2nd order approximation method [5], [15] by assuming that the current

in the transmission line is sinusoidal and devoid of any harmonic components, given in section 4.4.

Table 4.1: Modes of Operation in the Proposed Enhanced Power Flow Controller

S	S_L	S_C	**Effective transmission line impedance (neglecting effects of X_{mag} and X_{leak} in STT)**
Closed	-	-	$jX_{\text{eff no compensation}} = jX_{\text{line}}$
Open	σ control	Close	$jX_{\text{eff compensation}} = jX(X_{\text{line}}, X_L, X_C)_{\|\sigma}$ Note: for $\sigma = \pi$ $jX_{\text{eff min comp}} = jX_{\text{line}} + (jX_L \| \| (-jX_C))$ Note: for $\sigma = 0$ $jX_{\text{eff max comp}} = jX_{\text{line}} - jX_C$

Finally, the proposed approach is based on the principle that only the end bus voltages are sinusoidal and all associated harmonics generated by series injection of ePFC are absorbed in the transmission line itself, derived in section 4.5.

4.3. 1st Order Approximation

The 1st order approximation method assumes that the voltage across the capacitor is sinusoidal. The voltage and current waveforms of such a system is shown in FIGURE 4.2.

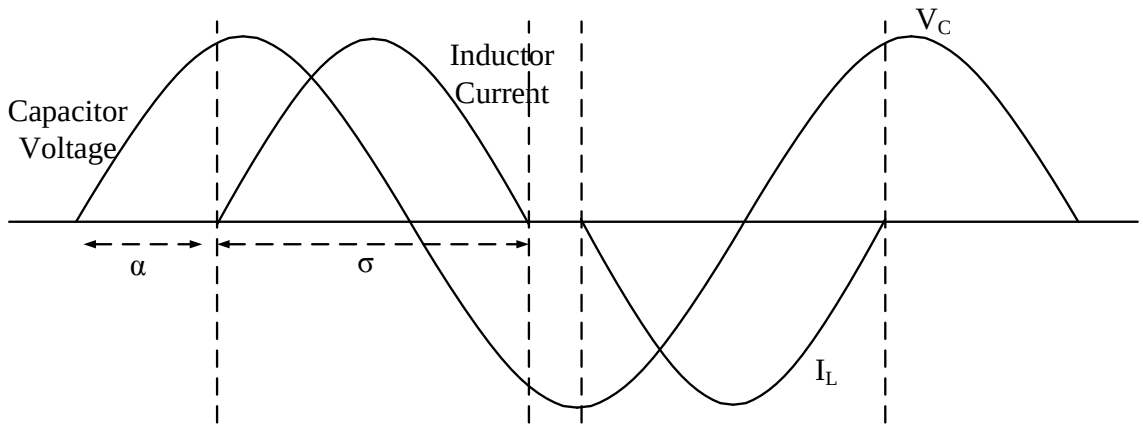

FIGURE 4.2: Operating waveforms for 1st order approximation towards derivation of fundamental impedance of enhanced Power Flow Controller.

An equivalent circuit is shown in FIGURE 4.3. As shown, this reduces $X(X_{line}, X_L, X_C)_{|\sigma}$ to a simple parallel combination of X_C and $X_L(\sigma)$ that is connected in series with line reactance X

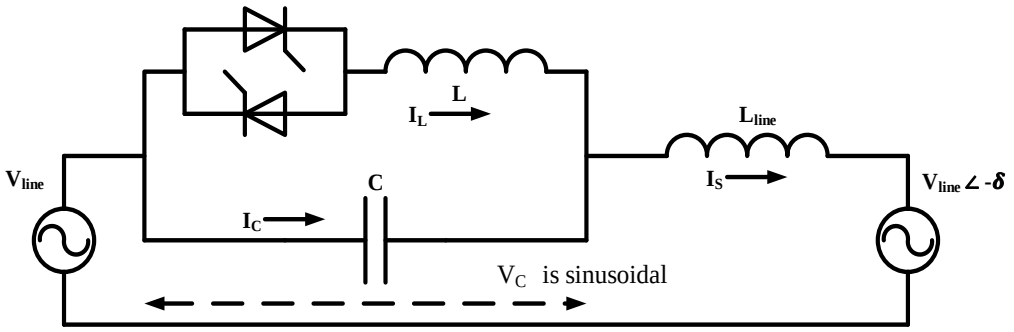

FIGURE 4.3: Equivalent circuit of ePFC using 1st order approximation.

Analytical expression for $X_L(\sigma)$ has been amply documented in literature [4], [5], [8] as "equivalent average inductance model" and derived as follows:

Let V_S be the voltage across the capacitor

$$V_S = V_m \cos \omega t = V_m \cos \theta \tag{4.1}$$

$$V_S - L\frac{dI_L}{dt} = 0 \tag{4.2}$$

$$i_L(t) = \frac{1}{\omega L}\int V_S \tag{4.3}$$

$$= \frac{1}{\omega L}\int V_S \cos\theta \, d\theta \tag{4.4}$$

$$i_L(t) = \frac{1}{\omega L}(V_S \sin\theta) + C \tag{4.5}$$

Since at $\theta = \alpha$ and $i(\alpha) = 0$, where α is firing angle

$$i_L(\alpha) = \frac{1}{\omega L}(V_S \sin\alpha) + C = 0 \tag{4.6}$$

$$C = -\frac{1}{\omega L}(V_S \sin\alpha) \tag{4.7}$$

Therefore,

$$i_L(t) = \frac{V_m}{\omega L}(\sin\theta - \sin\alpha) \tag{4.8}$$

Fundamental component of i_L is given by

$$i_{Lfunda} = \frac{2}{\pi}\int i_L \sin\theta \, d\theta \tag{4.9}$$

$$i_{L\,funda} = \frac{2}{\pi}\int_0^{\pi} \frac{V_m}{\omega L}(\sin\theta - \sin\alpha)\sin\theta \; d\theta \tag{4.10}$$

$$i_{L\,funda} = \frac{2}{\pi}\int_{\alpha}^{\pi-\alpha} \frac{V_m}{\omega L}(\sin\theta - \sin\alpha)\sin\theta \; d\theta \tag{4.11}$$

$$i_{L\,funda} = \frac{2}{\pi}\frac{V_m}{\omega L}\left[\int_{\alpha}^{\pi-\alpha}(\sin\theta - \sin\alpha)\sin\theta \; d\theta\right] \tag{4.12}$$

$$i_{L\,funda} = \frac{2}{\pi}\frac{V_m}{\omega L}\left[\int_{\alpha}^{\pi-\alpha}(\sin\theta \sin\theta d\theta - \sin\theta \sin\alpha d\theta)\right] \tag{4.13}$$

$$i_{L\,funda} = \frac{2}{\pi}\frac{V_m}{\omega L}\left[\int_{\alpha}^{\pi-\alpha}\left(\frac{(1-\cos 2\theta)}{2}\, d\theta - \sin\theta \sin\alpha d\theta\right)\right] \tag{4.14}$$

$$i_{L\,funda} = \frac{2}{\pi}\frac{V_m}{\omega L}\left[\frac{\theta}{2} - \frac{\sin 2\theta}{4} + \sin\alpha\cos\theta\right]_{\alpha}^{\pi-\alpha} \tag{4.15}$$

$$i_{L\,funda} = \frac{2}{\pi}\frac{V_m}{\omega L}\left[\frac{\pi-\alpha}{2} - \frac{\alpha}{2} - \frac{\sin 2(\pi-\alpha)}{4} + \frac{\sin 2\alpha}{4}\right. \tag{4.16}$$

$$\left. + \sin\alpha\cos(\pi-\alpha) - \sin\alpha\cos(\alpha)\right]$$

$$i_{L\,funda} = \frac{2}{\pi}\frac{V_m}{\omega L}\left[\frac{\pi}{2} - \alpha - \frac{\sin(2\pi-2\alpha)}{4} + \frac{\sin 2\alpha}{4} - 2\sin\alpha\cos(\alpha)\right] \tag{4.17}$$

$$i_{L\,funda} = \frac{2}{\pi}\frac{V_m}{\omega L}\left[\frac{\pi}{2} - \alpha + \frac{\sin 2\alpha}{2} - \sin 2\alpha\right] \tag{4.18}$$

Therefore,

$$i_{L\,funda} = \frac{V_m}{\omega L}\left[1 - \frac{2\alpha}{\pi} - \frac{\sin 2\alpha}{\pi}\right] \tag{4.19}$$

Let ‘σ’ be the conduction angle,

$$\text{where} \qquad 2\pi - 2\alpha = \sigma \tag{4.20}$$

$$\Longrightarrow \left(\frac{2\pi-\sigma}{2}\right) = \alpha \tag{4.21}$$

Substituting equation (4.21) in equation (4.19). We get,

$$i_{L\,funda} = \frac{V_m}{\omega L}\left[1 - \frac{2\,\frac{(\pi-\sigma)}{2}}{\pi} - \frac{\sin 2\,\frac{(\pi-\sigma)}{2}}{\pi}\right] \tag{4.20}$$

$$i_{L\,funda} = \frac{V_m}{\omega L}\left[1 - \frac{(\pi-\sigma)}{\pi} - \frac{\sin(\pi-\sigma)}{\pi}\right] \tag{4.21}$$

$$i_{L\,funda} = \frac{V_m}{\omega L}\left[1 - 1 + \frac{\sigma}{\pi} - \frac{\sin\sigma}{\pi}\right] \tag{4.22}$$

$$i_{L\,funda} = \frac{V_m}{\omega L}\left[\frac{\sigma - \sin\sigma}{\pi}\right] \tag{4.23}$$

Hence effective fundamental impedance is

$$X_L(\sigma) = \frac{|V_S|}{|i_{L\,funda}|} = \frac{|V_m|}{\left|\frac{V_m}{\omega L}\right|\left[\frac{\sigma - \sin\sigma}{\pi}\right]} \tag{4.24}$$

$$X_L(\sigma) = X_L \frac{\pi}{\sigma - \sin\sigma} \tag{4.25}$$

Because the effective fundamental impedance ($X_{L(\sigma)}$) is in parallel with the capacitor impedance (X_C) and in series with the line inductance (X_{line}), the effective fundamental impedance assuming the 1st order approximation, X(sigma-1) or $X(X_{line}, X_L, X_C)_{|\sigma}$ is given by

$$jX_{(sigma-1)} = jX(X_{line}, X_L, X_C)_{|\sigma-1} = (jX_L \frac{\pi}{\sigma - \sin\sigma} || (-jX_C)) + jX_{line} \tag{4.26}$$

It may be verified that, when $\sigma = \pi$,

$$jX(X_{line}, X_L, X_C)_{|\sigma-1} \cong jX_L || (-jX_C) + jX_{line} \tag{4.27}$$

and when $\sigma = 0$,

$$jX(X_{line}, X_L, X_C)_{|\sigma-1} \cong -jX_C + jX_{line} \tag{4.28}$$

4.4. 2nd Order Approximation

Although the expression (4.26) accurately confirms with the boundary conditions (4.27) and (4.28), it has been shown in [10] that the capacitor voltage does indeed contain harmonic content, specifically during the conduction period of thyristors as shown in FIGURE 4.4.

This phenomenon introduces an error in calculating fundamental effective impedance $X(X_{line}, X_L, X_C)_{|\sigma}$ of this circuit over the operating range of conduction angle (σ). Furthermore, this also leads to anomalies in determining the region of resonance for the L-C parallel circuit. To resolve these issues, a 2nd order approximation has been presented

[10], [11] by assuming that the current in the transmission line is sinusoidal and devoid of any harmonic components. This leads to construction of a second order cross-coupled differential equation [11], the solution for which has been derived as follows:

Let the fundamental current in the power line be given by,

$$I_s = I_m \sin \omega t \tag{4.30}$$

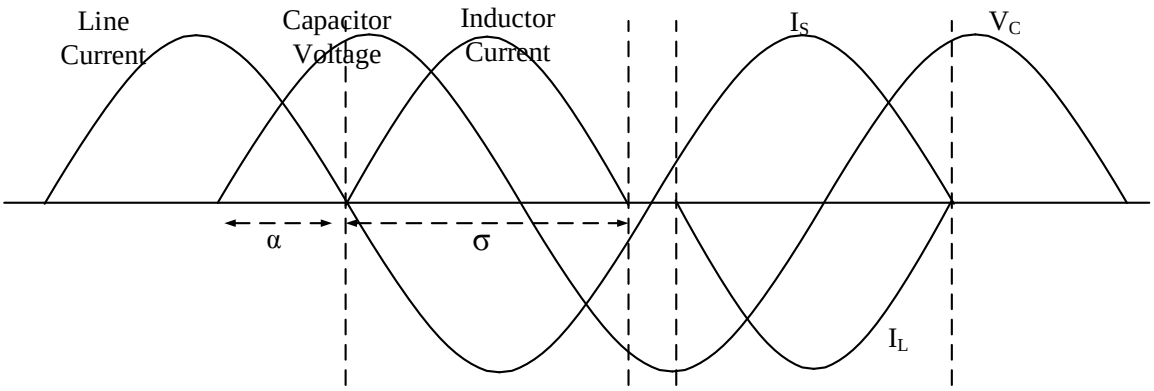

FIGURE 4.4: Operating waveforms for 2nd order approximation towards derivation of fundamental impedance of ePFC

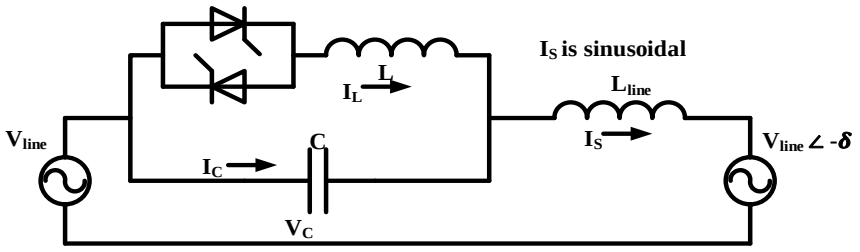

FIGURE 4.5: Equivalent circuit of ePFC using 2nd order approximation

When thyristor switches are open, entire line current flows through the capacitor. Hence

$$C\frac{dV_C}{dt} = I_s \tag{4.31}$$

$$\frac{dV_C}{dt} = \frac{1}{C} I_s \tag{4.32}$$

$$V_C = \frac{1}{C}\int I_m \sin \omega t \, dt \tag{4.33}$$

$$V_C = -\frac{1}{\omega C} I_m \cos \omega t \tag{4.34}$$

Thus V_C can be expressed as

$$V_C = -\frac{1}{\omega C} I_m \cos \omega t \tag{4.35}$$

where

$$K = -\frac{1}{\omega C} I_m \tag{4.36}$$

This is the expression for V_C during the interval $\omega t = (0, \frac{\pi}{2} - \frac{\sigma}{2})$

To find V_C at $\omega t = \frac{\pi}{2} - \frac{\sigma}{2}$

$$V_C(\frac{\pi}{2} - \frac{\sigma}{2}) = \frac{1}{C}\int_0^{\frac{\pi}{2}-\frac{\sigma}{2}} I_m \sin \omega t \, dt \tag{4.37}$$

$$V_C(\frac{\pi}{2} - \frac{\sigma}{2}) = \frac{1}{\omega C} I_m (1 - \sin \frac{\sigma}{2}) \tag{4.38}$$

When thyristor switches are closed, current is distributed between inductor and capacitor.

Hence,

$$I_s = C\frac{dV_C}{dt} + I_L \tag{4.39}$$

$$C\frac{dV_C}{dt} = I_s - I_L \tag{4.40}$$

$$C\frac{d^2V_C}{dt^2} = \frac{dI_s}{dt} - \frac{dI_L}{dt} \tag{4.41}$$

$$C\frac{d^2V_C}{dt^2} = \frac{dI_s}{dt} - \frac{V_C}{L} \tag{4.42}$$

$$\frac{d^2V_C}{dt^2} + \frac{1}{LC}V_C = \frac{1}{C}\frac{dI_s}{dt} \tag{4.45}$$

$$\frac{d^2V_C}{dt^2} + \frac{1}{LC}V_C = \frac{1}{C}\omega I_m \cos \omega t \tag{4.46}$$

rewriting,

$$\frac{d^2V_C}{dt^2} + \omega_0{}^2 V_C = \frac{1}{C}\omega I_m \cos \omega t \tag{4.47}$$

where

$$\omega_0 = \frac{1}{\sqrt{LC}} \tag{4.48}$$

Let the solution of this differential equation be,

$$V_C = C_1 \sin \omega_0 t + C_2 \cos \omega_0 t + A \cos \omega t \tag{4.49}$$

$$\omega_0{}^2 V_C = C_1 \omega_0{}^2 \sin \omega_0 t + C_2 \omega_0{}^2 \cos \omega_0 t + A\omega_0{}^2 \cos \omega t \tag{4.50}$$

$$\frac{dV_C}{dt} = C_1 \omega_0 \cos \omega_0 t - C_2 \omega_0 \sin \omega_0 t - A\omega \sin \omega t \tag{4.51}$$

$$\frac{d^2V_C}{dt^2} = -C_1 \omega_0{}^2 \sin \omega_0 t - C_2 \omega_0{}^2 \cos \omega_0 t - A\omega^2 \cos \omega t \tag{4.52}$$

$$\frac{d^2V_C}{dt^2} + \omega_0{}^2 V_C = A(\omega_0{}^2 - \omega^2) \cos \omega t \tag{4.53}$$

Hence,

$$A(\omega_0{}^2 - \omega^2) \cos \omega t = \frac{1}{C}\omega I_m \cos \omega t \tag{4.54}$$

Therefore

$$A = \frac{1}{C}\frac{\omega}{\omega_0{}^2 - \omega^2} I_m \tag{4.55}$$

Thus the solution for V_c is,

$$V_C = C_1 \sin \omega_0 t + C_2 \cos \omega_0 t + \frac{1}{C}\frac{\omega}{\omega_0{}^2 - \omega^2} I_m \cos \omega t \tag{4.56}$$

As determined earlier, at $\omega t = \frac{\pi}{2} - \frac{\sigma}{2}$

$$V_C(\frac{\pi}{2}-\frac{\sigma}{2}) = \frac{1}{\omega C} I_m(1-\sin\frac{\sigma}{2}) \tag{4.57}$$

and at $\omega t = \frac{\pi}{2}$

$$V_C(\frac{\pi}{2}) = 0 \tag{4.58}$$

So now, at $\omega t = \frac{\pi}{2}-\frac{\sigma}{2}$

$$V_C(\frac{\pi}{2}-\frac{\sigma}{2}) = C_1 \sin\frac{\omega_0}{\omega}(\frac{\pi}{2}-\frac{\sigma}{2}) + C_2 \cos\frac{\omega_0}{\omega}(\frac{\pi}{2}-\frac{\sigma}{2}) \tag{4.59}$$

$$+\frac{1}{C}\frac{\omega}{{\omega_0}^2-\omega^2} I_m \cos(\frac{\pi}{2}-\frac{\sigma}{2})$$

$$V_C\left(\frac{\pi}{2}-\frac{\sigma}{2}\right) = C_1 \sin\frac{\omega_0}{\omega}\left(\frac{\pi}{2}-\frac{\sigma}{2}\right) + C_2 \cos\frac{\omega_0}{\omega}\left(\frac{\pi}{2}-\frac{\sigma}{2}\right) \tag{4.60}$$

$$+\frac{1}{C}\frac{\omega}{{\omega_0}^2-\omega^2} I_m \sin\frac{\sigma}{2} = \frac{1}{\omega C} I_m(1-\sin\frac{\sigma}{2})$$

Thus

$$C_1 \sin\frac{\omega_0}{\omega}\left(\frac{\pi}{2}-\frac{\sigma}{2}\right) + C_2 \cos\frac{\omega_0}{\omega}\left(\frac{\pi}{2}-\frac{\sigma}{2}\right) = \frac{1}{\omega C} I_m(1-\frac{{\omega_0}^2}{{\omega_0}^2-\omega^2}\sin\frac{\sigma}{2}) \tag{4.61}$$

Also, at $\omega t = \frac{\pi}{2}$

$$V_c\left(\frac{\pi}{2}\right) = C_1 \sin\frac{\omega_0}{\omega}\frac{\pi}{2} + C_2 \cos\frac{\omega_0}{\omega}\frac{\pi}{2} = 0 \tag{4.62}$$

Thus

$$C_1 = -C_2 \frac{\cos\frac{\omega_0}{\omega}\frac{\pi}{2}}{\sin\frac{\omega_0}{\omega}\frac{\pi}{2}} \tag{4.63}$$

Substituting,

$$-C_2 \frac{\cos\frac{\omega_0 \pi}{\omega\ 2}}{\sin\frac{\omega_0 \pi}{\omega\ 2}} \sin\frac{\omega_0}{\omega}\left(\frac{\pi}{2}-\frac{\sigma}{2}\right) + C_2 \cos\frac{\omega_0}{\omega}\left(\frac{\pi}{2}-\frac{\sigma}{2}\right) = \frac{1}{\omega C} I_m(1-\frac{{\omega_0}^2}{{\omega_0}^2-\omega^2}\sin\frac{\sigma}{2}) \tag{4.64}$$

$$C_2 = \frac{1}{\omega C} I_m \left(1 - \frac{{\omega_0}^2}{{\omega_0}^2 - \omega^2} \sin\frac{\sigma}{2}\right) \frac{\sin\frac{\omega_0 \pi}{\omega\ 2}}{\sin\frac{\omega_0 \sigma}{\omega\ 2}} \tag{4.65}$$

$$C_1 = -\frac{1}{\omega C} I_m \left(1 - \frac{{\omega_0}^2}{{\omega_0}^2 - \omega^2} \sin\frac{\sigma}{2}\right) \frac{\cos\frac{\omega_0}{\omega}\frac{\pi}{2}}{\sin\frac{\omega_0}{\omega}\frac{\sigma}{2}} \tag{4.66}$$

Therefore,

$$V_C = -\frac{1}{\omega C} I_m \left(1 - \frac{{\omega_0}^2}{{\omega_0}^2 - \omega^2} \sin\frac{\sigma}{2}\right) \frac{\cos\frac{\omega_0 \pi}{\omega\ 2}}{\sin\frac{\omega_0 \sigma}{\omega\ 2}} \sin\omega_0 t + \frac{1}{\omega C} I_m \left(1 - \frac{{\omega_0}^2}{{\omega_0}^2 - \omega^2} \sin\frac{\sigma}{2}\right) \frac{\sin\frac{\omega_0 \pi}{\omega\ 2}}{\sin\frac{\omega_0 \sigma}{\omega\ 2}} \cos\omega_0 t + \frac{1}{C} \frac{\omega}{{\omega_0}^2 - \omega^2} I_m \cos\omega t \tag{4.67}$$

This is the expression for V_C during the interval $\omega t = \left(\frac{\pi}{2} - \frac{\sigma}{2}, \frac{\pi}{2}\right)$

To find fundamental component of V_C, which is

$$V_C = K\cos\omega t \text{ during } \omega t = \left(0, \frac{\pi}{2} - \frac{\sigma}{2}\right), \text{ and}$$

$$V_C = C_1 \sin\omega_0 t + C_2 \cos\omega_0 t + A\cos\omega t \text{ during, } \omega t = \left(\frac{\pi}{2} - \frac{\sigma}{2}, \frac{\pi}{2}\right),$$

Let
$$V_C = M\cos\omega t \tag{4.68}$$

where
$$V_C = M\cos\omega t \tag{4.69}$$

$$M = \frac{4}{\pi}\int_0^{\frac{\pi}{2}-\frac{\sigma}{2}} V_C \cos\omega t\, dt + \frac{4}{\pi}\int_{\frac{\pi}{2}-\frac{\sigma}{2}}^{\frac{\pi}{2}} V_C \cos\omega t\, dt$$

$$M = \frac{4}{\pi}\int_0^{\frac{\pi}{2}-\frac{\sigma}{2}} K\cos\omega t \cos\omega t\, dt + \frac{4}{\pi}\int_{\frac{\pi}{2}-\frac{\sigma}{2}}^{\frac{\pi}{2}} [C_1 \sin\omega_0 t + C_2 \cos\omega_0 t + A\cos\omega t]\cos\omega t\, dt \tag{4.70}$$

$$M = \frac{4}{\pi} K \int_0^{\frac{\pi}{2}-\frac{\sigma}{2}} \cos\omega t \cos\omega t\, dt + \frac{4}{\pi} C_1 \int_{\frac{\pi}{2}-\frac{\sigma}{2}}^{\frac{\pi}{2}} \sin\omega_0 t \cos\omega t\, dt + \tag{4.71}$$

$$\frac{4}{\pi}C_2\int_{\frac{\pi}{2}-\frac{\sigma}{2}}^{\frac{\pi}{2}}\cos\omega_0 t\cos\omega t\,dt+\frac{4}{\pi}A\int_{\frac{\pi}{2}-\frac{\sigma}{2}}^{\frac{\pi}{2}}\cos\omega t\cos\omega t\,dt$$

$$M=\frac{2}{\pi}K\int_0^{\frac{\pi}{2}-\frac{\sigma}{2}}[1+\cos 2\omega t]dt+\frac{2}{\pi}C_1\int_{\frac{\pi}{2}-\frac{\sigma}{2}}^{\frac{\pi}{2}}[\sin(\omega_0+\omega)t+\sin(\omega_0-\omega)t]dt+$$

$$\frac{2}{\pi}C_2\int_{\frac{\pi}{2}-\frac{\sigma}{2}}^{\frac{\pi}{2}}[\cos(\omega_0+\omega)t+\cos(\omega_0-\omega)t]\,dt+\frac{2}{\pi}A\int_{\frac{\pi}{2}-\frac{\sigma}{2}}^{\frac{\pi}{2}}[1+\cos 2\omega t]dt \tag{4.72}$$

$$\begin{aligned}M=\frac{1}{\omega\pi}K[\pi-\sigma+\sin\sigma]&+\frac{2}{\pi}C_1\int_{\frac{\pi}{2}-\frac{\sigma}{2}}^{\frac{\pi}{2}}[\sin(\omega_0+\omega)t]dt\\&+\frac{2}{\pi}C_1\int_{\frac{\pi}{2}-\frac{\sigma}{2}}^{\frac{\pi}{2}}[\sin(\omega_0-\omega)t]dt+\frac{2}{\pi}C_2\int_{\frac{\pi}{2}-\frac{\sigma}{2}}^{\frac{\pi}{2}}[\cos(\omega_0+\omega)t]dt\\&+\frac{2}{\pi}C_2\int_{\frac{\pi}{2}-\frac{\sigma}{2}}^{\frac{\pi}{2}}[\cos(\omega_0-\omega)t]\,dt+\frac{1}{\omega\pi}A[\sigma-\sin\sigma]\end{aligned} \tag{4.73}$$

$$\begin{aligned}M=\frac{1}{\omega\pi}\{K[\pi-\sigma+\sin\sigma]+A[\sigma-\sin\sigma]\}&+\frac{2}{\pi}C_1\int_{\frac{\pi}{2}-\frac{\sigma}{2}}^{\frac{\pi}{2}}[\sin(\omega_0+\omega)t]dt\\&+\frac{2}{\pi}C_2\int_{\frac{\pi}{2}-\frac{\sigma}{2}}^{\frac{\pi}{2}}[\cos(\omega_0+\omega)t]dt+\frac{2}{\pi}C_1\int_{\frac{\pi}{2}-\frac{\sigma}{2}}^{\frac{\pi}{2}}[\sin(\omega_0-\omega)t]dt\\&+\frac{2}{\pi}C_2\int_{\frac{\pi}{2}-\frac{\sigma}{2}}^{\frac{\pi}{2}}[\cos(\omega_0-\omega)t]\,dt\end{aligned} \tag{4.74}$$

$$\begin{aligned}M=\frac{1}{\omega\pi}\{K[\pi-\sigma+\sin\sigma]+A[\sigma-\sin\sigma]\}&+\frac{2}{(\omega_0+\omega)\pi}\{-C_1\cos\frac{\omega_0+\omega}{\omega}\frac{\pi}{2}\\&+C_1\cos\frac{\omega_0+\omega}{\omega}\frac{\pi-\sigma}{2}+C_2\sin\frac{\omega_0+\omega}{\omega}\frac{\pi}{2}\\&-C_2\sin\frac{\omega_0+\omega}{\omega}\frac{\pi-\sigma}{2}\}+\frac{2}{(\omega_0-\omega)\pi}\{-C_1\cos\frac{\omega_0-\omega}{\omega}\frac{\pi}{2}\\&+C_1\cos\frac{\omega_0-\omega}{\omega}\frac{\pi-\sigma}{2}+C_2\sin\frac{\omega_0-\omega}{\omega}\frac{\pi}{2}\\&-C_2\sin\frac{\omega_0-\omega}{\omega}\frac{\pi-\sigma}{2}\}\end{aligned} \tag{4.75}$$

$$M = \frac{1}{\omega\pi}\{K[\pi - \sigma + \sin\sigma] + A[\sigma - \sin\sigma]\} - \frac{2}{\omega_p\pi}\{C_1 \cos\frac{\omega_p}{\omega}\frac{\pi}{2} - C_1 \cos\frac{\omega_p}{\omega}\frac{\pi-\sigma}{2} - C_2 \sin\frac{\omega_p}{\omega}\frac{\pi}{2} + C_2 \sin\frac{\omega_p}{\omega}\frac{\pi-\sigma}{2}\} - \frac{2}{\omega_n\pi}[C_1 \cos\frac{\omega_n}{\omega}\frac{\pi}{2} - C_1 \cos\frac{\omega_n}{\omega}\frac{\pi-\sigma}{2} - C_2 \sin\frac{\omega_n}{\omega}\frac{\pi}{2} + C_2 \sin\frac{\omega_n}{\omega}\frac{\pi-\sigma}{2}] \quad (4.76)$$

where $\omega_p = \omega_0 + \omega$ and $\omega_n = \omega_0 - \omega$

$$M = \frac{1}{\omega\pi}\{K[\pi - \sigma + \sin\sigma] + A[\sigma - \sin\sigma]\} + \frac{4}{\omega_p\pi}\sin\frac{\omega_p}{\omega}\frac{\sigma}{4}\left\{C_1 \sin\frac{\omega_p}{\omega}\frac{2\pi-\sigma}{4} + C_2 \cos\frac{\omega_p}{\omega}\frac{2\pi-\sigma}{4}\right\} + \frac{4}{\omega_n\pi}\sin\frac{\omega_n}{\omega}\frac{\sigma}{4}[C_1 \sin\frac{\omega_n}{\omega}\frac{2\pi-\sigma}{4} + C_2 \cos\frac{\omega_n}{\omega}\frac{2\pi-\sigma}{4}] \quad (4.77)$$

$$C_2 = \frac{1}{\omega C} I_m\left(1 - \frac{{\omega_0}^2}{{\omega_0}^2 - \omega^2}\sin\frac{\sigma}{2}\right)\frac{\sin\frac{\omega_0}{\omega}\frac{\pi}{2}}{\sin\frac{\omega_0}{\omega}\frac{\sigma}{2}} = D\frac{\sin\frac{\omega_0}{\omega}\frac{\pi}{2}}{\sin\frac{\omega_0}{\omega}\frac{\sigma}{2}} \quad (4.78)$$

$$C_1 = -\frac{1}{\omega C} I_m\left(1 - \frac{{\omega_0}^2}{{\omega_0}^2 - \omega^2}\sin\frac{\sigma}{2}\right)\frac{\cos\frac{\omega_0}{\omega}\frac{\pi}{2}}{\sin\frac{\omega_0}{\omega}\frac{\sigma}{2}} = -D\frac{\cos\frac{\omega_0}{\omega}\frac{\pi}{2}}{\sin\frac{\omega_0}{\omega}\frac{\sigma}{2}} \quad (4.79)$$

$$M = \frac{1}{\omega\pi}\{K[\pi - \sigma + \sin\sigma] + A[\sigma - \sin\sigma]\} + \frac{4}{\omega_p\pi} D \frac{\sin\frac{\omega_p\sigma}{\omega\ 4}}{\sin\frac{\omega_0\sigma}{\omega\ 2}}\left\{-\cos\frac{\omega_0}{\omega}\frac{\pi}{2}\sin\frac{\omega_p}{\omega}\frac{2\pi-\sigma}{4} + \sin\frac{\omega_0}{\omega}\frac{\pi}{2}\cos\frac{\omega_p}{\omega}\frac{2\pi-\sigma}{4}\right\} + \frac{4}{\omega_n\pi} D \frac{\sin\frac{\omega_n\sigma}{\omega\ 4}}{\sin\frac{\omega_0\sigma}{\omega\ 2}}\left\{-\cos\frac{\omega_0}{\omega}\frac{\pi}{2}\sin\frac{\omega_n}{\omega}\frac{2\pi-\sigma}{4} + \sin\frac{\omega_0}{\omega}\frac{\pi}{2}\cos\frac{\omega_n}{\omega}\frac{2\pi-\sigma}{4}\right\} \quad (4.80)$$

$$M = \frac{1}{\omega\pi}\{K[\pi - \sigma + \sin\sigma] + A[\sigma - \sin\sigma]\} + \frac{4}{\omega_p\pi} D \frac{\sin\frac{\omega_p\sigma}{\omega\ 4}}{\sin\frac{\omega_0\sigma}{\omega\ 2}}\left\{\sin\frac{\omega_0}{\omega}\frac{\pi}{2} - \frac{\omega_p}{\omega}\frac{2\pi-\sigma}{4}\right\} + \frac{4}{\omega_n\pi} D \frac{\sin\frac{\omega_n\sigma}{\omega\ 4}}{\sin\frac{\omega_0\sigma}{\omega\ 2}}\left\{\sin\frac{\omega_0}{\omega}\frac{\pi}{2} - \frac{\omega_n}{\omega}\frac{2\pi-\sigma}{4}\right\} \quad (4.81)$$

$$M = \frac{1}{\omega\pi}\{K[\pi - \sigma + \sin\sigma] + A[\sigma - \sin\sigma]\} - \frac{4}{\omega_p\pi} D \frac{\sin\frac{\omega_p}{\omega}\frac{\sigma}{4}}{\sin\frac{\omega_0}{\omega}\frac{\sigma}{2}}\cos\frac{\omega_p}{\omega}\frac{\sigma}{4} + \frac{4}{\omega_n\pi} D \frac{\sin\frac{\omega_n}{\omega}\frac{\sigma}{4}}{\sin\frac{\omega_0}{\omega}\frac{\sigma}{2}}\cos\frac{\omega_n}{\omega}\frac{\sigma}{4} \quad (4.82)$$

$$M = \frac{1}{\omega\pi}\{K[\pi - \sigma + \sin\sigma] + A[\sigma - \sin\sigma]\} - \frac{2}{\omega_p\pi} D \frac{\sin\frac{\omega_p}{\omega}\frac{\sigma}{2}}{\sin\frac{\omega_0}{\omega}\frac{\sigma}{2}} + \frac{2}{\omega_n\pi} D \frac{\sin\frac{\omega_n}{\omega}\frac{\sigma}{2}}{\sin\frac{\omega_0}{\omega}\frac{\sigma}{2}} \quad (4.83)$$

$$M = \frac{1}{\omega\pi}\{K[\pi - \sigma + \sin\sigma] + A[\sigma - \sin\sigma]\} - \frac{2}{\pi\sin\frac{\omega_0\sigma}{\omega\ 2}} D\left[\frac{\sin\frac{\omega_p\sigma}{\omega\ 2}}{\omega_p} - \frac{\sin\frac{\omega_n\sigma}{\omega\ 2}}{\omega_n}\right] \quad (4.84)$$

$$M = \frac{1}{\omega\pi}\{K[\pi - \sigma + \sin\sigma] + A[\sigma - \sin\sigma]\} - \frac{2}{\pi\sin\frac{\omega_0\sigma}{\omega\ 2}} D\left[\frac{\omega_n\sin\frac{\omega_p\sigma}{\omega\ 2} - \omega_p\sin\frac{\omega_n\sigma}{\omega\ 2}}{{\omega_0}^2 - \omega^2}\right] \quad (4.85)$$

$$M = \frac{1}{\omega\pi}\{K[\pi - \sigma + \sin\sigma] + A[\sigma - \sin\sigma]\} - \frac{2}{\pi\sin\frac{\omega_0\sigma}{\omega\ 2}}\frac{1}{\omega C} I_m\left(1 - \frac{{\omega_0}^2}{{\omega_0}^2 - \omega^2}\sin\frac{\sigma}{2}\right)\left(\frac{\omega_n\sin\frac{\omega_p\sigma}{\omega\ 2} - \omega_p\sin\frac{\omega_n\sigma}{\omega\ 2}}{{\omega_0}^2 - \omega^2}\right) \quad (4.86)$$

$$M = \frac{1}{\omega\pi}\{K[\pi - \sigma + \sin\sigma] + A[\sigma - \sin\sigma]\} - \frac{2}{\pi \sin\frac{\omega_0\sigma}{\omega\ 2}}\frac{1}{\omega C} I_m \frac{(\omega_0{}^2 - \omega^2 - \omega_0{}^2 \sin\frac{\sigma}{2})(\omega_n \sin\frac{\omega_p\sigma}{\omega\ 2} - \omega_p \sin\frac{\omega_n\sigma}{\omega\ 2})}{(\omega_0{}^2 - \omega^2)^2} \quad (4.87)$$

$$M = \frac{1}{\omega\pi}\left\{-\frac{1}{\omega C} I_m[\pi - \sigma + \sin\sigma] + \frac{1}{C}\frac{\omega}{\omega_0{}^2 - \omega^2} I_m[\sigma - \sin\sigma]\right\} - \frac{2}{\pi \sin\frac{\omega_0\sigma}{\omega\ 2}}\frac{1}{\omega C} I_m \frac{(\omega_0{}^2 - \omega^2 - \omega_0{}^2 \sin\frac{\sigma}{2})(\omega_n \sin\frac{\omega_p\sigma}{\omega\ 2} - \omega_p \sin\frac{\omega_n\sigma}{\omega\ 2})}{(\omega_0{}^2 - \omega^2)^2} \quad (4.88)$$

$$M = \frac{I_m}{\pi\omega C}\left\{-\frac{1}{\omega}[\pi - \sigma + \sin\sigma] + \frac{\omega}{\omega_0{}^2 - \omega^2}[\sigma - \sin\sigma] - \frac{2}{\sin\frac{\omega_0\sigma}{\omega\ 2}} \frac{(\omega_0{}^2 - \omega^2 - \omega_0{}^2 \sin\frac{\sigma}{2})(\omega_n \sin\frac{\omega_p\sigma}{\omega\ 2} - \omega_p \sin\frac{\omega_n\sigma}{\omega\ 2})}{(\omega_0{}^2 - \omega^2)^2}\right\} \quad (4.89)$$

$$M = \frac{I_m}{\pi\omega C}\left\{-\frac{\pi}{\omega} + \frac{\omega_0{}^2}{\omega_0{}^2 - \omega^2}[\sigma - \sin\sigma] - \frac{2}{\sin\frac{\omega_0\sigma}{\omega\ 2}} \frac{\left(\omega_0{}^2 - \omega^2 - \omega_0{}^2 \sin\frac{\sigma}{2}\right)\left(\omega_n \sin\frac{\omega_p\sigma}{\omega\ 2} - \omega_p \sin\frac{\omega_n\sigma}{\omega\ 2}\right)}{(\omega_0{}^2 - \omega^2)^2}\right\} \quad (4.90)$$

Thus, fundamental component of voltage V_C is

$$V_{Cfunda} = \frac{I_m}{\pi\omega C}\left\{-\frac{\pi}{\omega} + \frac{\omega_0{}^2}{\omega_0{}^2 - \omega^2}[\sigma - \sin\sigma] - \frac{2}{\sin\frac{\omega_0\sigma}{\omega\ 2}} \frac{(\omega_0{}^2 - \omega^2 - \omega_0{}^2 \sin\frac{\sigma}{2})(\omega_n \sin\frac{\omega_p\sigma}{\omega\ 2} - \omega_p \sin\frac{\omega_n\sigma}{\omega\ 2})}{(\omega_0{}^2 - \omega^2)^2}\right\} \cos\omega t \quad (4.91)$$

As stated, line current is

$$I_s = I_m \sin \omega t \tag{4.92}$$

Therefore, fundamental effective reactance of this circuit is

$$jX_{(sigma-2)} = jX(X_{line}, X_L, X_C)_{|\sigma-2} = jX_C \left[1 + \frac{2}{\pi} \frac{k^2}{k^2-1} \left[\frac{2\cos\left(\frac{\sigma}{2}\right)\cos\left(\frac{\sigma}{2}\right)}{(k^2-1)} \left(k\left(\tan\left(k\frac{\sigma}{2}\right)\right) - \tan\frac{\sigma}{2}\right) - \frac{[\sin\sigma+\sigma]}{2} \right] \right] + jX_{line} \tag{4.94}$$

where

$$k = \frac{\omega_0}{\omega} \tag{4.95}$$

and

$$\omega_0{}^2 = \frac{1}{LC} \tag{4.96}$$

It may again be verified that, when $\sigma = \pi$,

$$jX(X_{line}, X_L, X_C)_{|\sigma-2} \cong jX_L||(-jX_C) + jX_{line} \tag{4.97}$$

and when $\sigma = 0$,

$$jX(X_{line}, X_L, X_C)_{|\sigma-2} \cong -jX_C + jX_{line} \tag{4.98}$$

However, it may be observed that series insertion of ePFC affects the transmission line current as well. Thus, once an ePFC is inserted, this current is no longer sinusoidal, and contains elements of resonant components caused by switching of the thyristors. Hence, although expression (4.5) also confirms with the boundary conditions (4.8) and (4.9), this calls for a further extension of the analysis, where one can no longer assume the transmission line current to be sinusoidal.

4.5. Equivalent Fundamental Impedance of ePFC

To construct this mathematical problem, let us consider an equivalent circuit of the ePFC in compensation mode which now consists of sending voltage (V_{line}), line reactance (L_{line}), receiving voltage ($V_{line}\angle\text{-}\boldsymbol{\delta}$), compensation reactances L and C. The schematic waveform as shown in FIGURE 4.6 and the equivalent circuit is shown in FIGURE 4.7. From the main diagram, under all conditions, we observe,

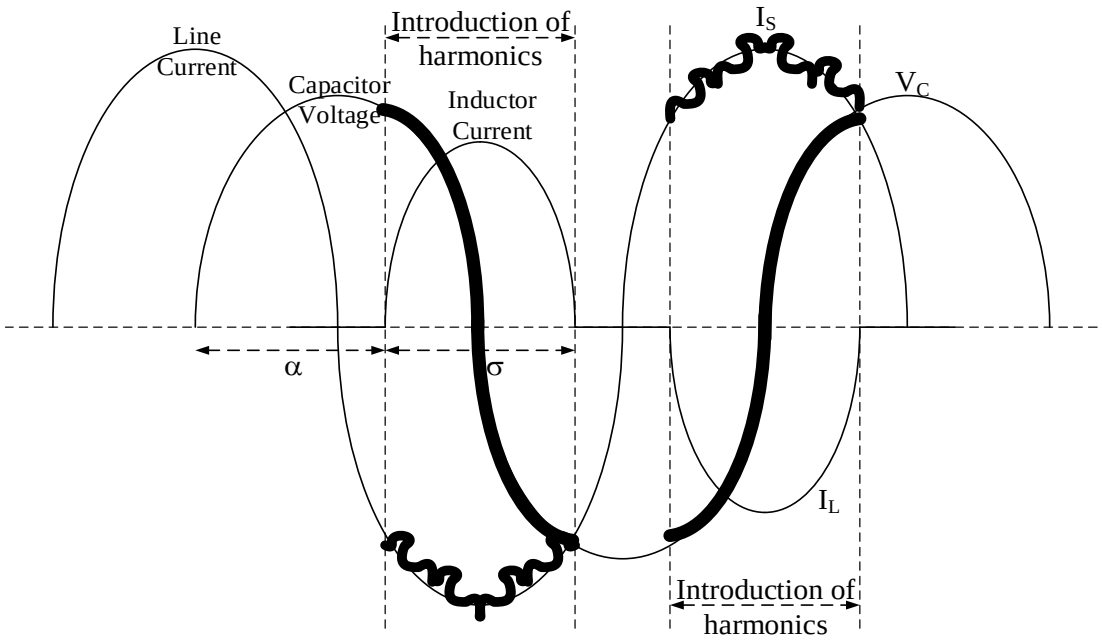

FIGURE 4.6: Operating waveforms for 3rd order approximation towards derivation of fundamental impedance of ePFC

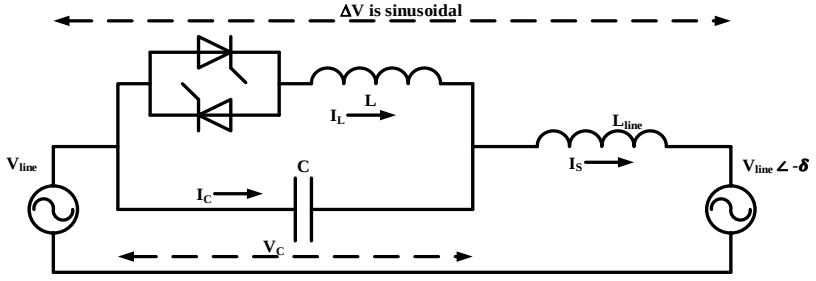

FIGURE 4.7: Equivalent circuit of the proposed enhanced Power Flow Controller (ePFC)

Under all conditions

$$\Delta V = V_{line}\cos\omega T - V_{line}\cos(\omega T - \delta) \tag{4.99}$$

$$\Delta V = -2V_{line} \sin\frac{\delta}{2} \sin(\omega T - \frac{\delta}{2}) \quad (4.100)$$

$$\Delta V = -A \sin \omega t \quad (4.101)$$

where $$A = 2V_{line} \sin\frac{\delta}{2} \quad (4.102)$$

and $$\omega t = \omega T - \frac{\delta}{2} \quad (4.103)$$

For the circuit shown in FIGURE 4.2,

$$\Delta V = L_{line} \frac{dI_s}{dt} + V_C \quad (4.104)$$

This gives $$-A \sin \omega t = L_{line} \frac{dI_s}{dt} + V_C \quad (4.105)$$

When thyristors are open

$$C \frac{dV_c}{dt} = I_s \quad (4.106)$$

Differentiating, $$C \frac{d^2V_c}{dt^2} = \frac{dI_s}{dt} \quad (4.107)$$

From (4.16) $$C \frac{d^2V_c}{dt^2} = -\frac{A}{L_{line}} \sin \omega t - \frac{V_c}{L_{line}} \quad (4.108)$$

Rearranging, $$\frac{d^2V_c}{dt^2} + \frac{1}{L_{line}C} V_c = -\frac{A}{L_{line}C} \sin \omega t \quad (4.109)$$

Solution for (4.20) is $$V_c = F \sin \omega_1 t + G \cos \omega_1 t + H \sin \omega t \quad (4.110)$$

where $$\omega_1{}^2 = \frac{1}{L_{line}C} \quad (4.110)$$

Differentiating (4.21) twice

$$\frac{d^2V_c}{dt^2} = -\omega^2{}_1 F \sin \omega_1 t - \omega^2{}_1 G \cos \omega_1 t - \omega^2 H \sin \omega t \quad (4.111)$$

Multiplying (4.21) by

$$\omega^2{}_1 V_c = \omega^2{}_1 F \sin \omega_1 t + \omega^2{}_1 G \cos \omega_1 t + \omega^2{}_1 H \sin \omega t \quad (4.112)$$

From (4.20), (4.23), (4.24)

$$(\omega^2{}_1 - \omega^2) H \sin \omega t = -\frac{A}{L_{line} C} \sin \omega t \quad (4.113)$$

So $$H = -\frac{A}{L_{line} C} \frac{1}{(\omega^2{}_1 - \omega^2)} \quad (4.114)$$

Thus $$V_c = F \sin \omega_1 t + G \cos \omega_1 t - \frac{A}{L_{line} C} \frac{1}{(\omega^2{}_1 - \omega^2)} \sin \omega t \quad (4.115)$$

Now, because of symmetry $$V_c\left(\frac{-\theta}{\omega}\right) = -V_c\left(\frac{\theta}{\omega}\right) \quad (4.116)$$

Thus

$$F \sin\left(-\frac{\omega_1}{\omega}\theta\right) + G \cos\left(-\frac{\omega_1}{\omega}\theta\right) - \frac{A}{L_{line} C} \frac{1}{(\omega^2{}_1 - \omega^2)} \sin(-\theta) = -F \sin \frac{\omega_1}{\omega}\theta - G \cos \frac{\omega_1}{\omega}\theta + \frac{A}{L_{line} C} \frac{1}{(\omega^2{}_1 - \omega^2)} \sin \theta \quad (4.117)$$

This gives $$G = 0 \quad (4.118)$$

Hence $$V_c = F \sin \omega_1 t - \frac{A}{L_{line} C} \frac{1}{(\omega^2{}_1 - \omega^2)} \sin \omega t \quad (4.119)$$

Now $$I_C = C \frac{dV_C}{dt} \quad (4.120)$$

From (4.30) and (4.31)

$$I_C = \omega_1 CF \cos \omega_1 t - \frac{\omega A}{L_{line}} \frac{1}{(\omega^2{}_1 - \omega^2)} \cos \omega t \quad (4.121)$$

However, because thyristors are open

$$I_S = I_C \quad (4.122)$$

This leads to $$I_S = \omega_1 CF \cos \omega_1 t - \frac{\omega A}{L_{line}} \frac{1}{(\omega^2{}_1 - \omega^2)} \cos \omega t \quad (4.123)$$

Hence state equations are $$V_c = F \sin \omega_1 t + H \sin \omega t \quad (4.124)$$

and $$I_S = \omega_1 CF \cos \omega_1 t + \omega CH \cos \omega t \quad (4.125)$$

where $$H = -\frac{A}{L_{line} C} \frac{1}{(\omega^2{}_1 - \omega^2)} \quad (4.126)$$

When thyristors are closed

$$C\frac{dV_c}{dt} = I_s - I_L \tag{4.127}$$

Differentiating,

$$C\frac{d^2V_c}{dt^2} = \frac{dI_s}{dt} - \frac{dI_L}{dt} \tag{4.128}$$

From (4.16)

$$C\frac{d^2V_c}{dt^2} = -\frac{A}{L_{line}}\sin\omega t - \frac{V_c}{L_{line}} - \frac{dI_L}{dt} \tag{4.129}$$

$$C\frac{d^2V_c}{dt^2} = -\frac{A}{L_{line}}\sin\omega t - \frac{V_c}{L_{line}} - \frac{V_c}{L} \tag{4.130}$$

Rearranging,

$$\frac{d^2V_c}{dt^2} + \frac{1}{C}\left(\frac{1}{L_{line}} + \frac{1}{L}\right)V_c = -\frac{A}{L_{line}C}\sin\omega t \tag{4.131}$$

Solution for (4.42) is

$$V_c = P\sin\omega_2 t + Q\cos\omega_2 t - R\sin\omega t \tag{4.132}$$

where $$\omega_2{}^2 = \frac{1}{C}\left(\frac{1}{L_{line}} + \frac{1}{L}\right) \tag{4.133}$$

Differentiating (4.43) twice

$$\frac{d^2V_c}{dt^2} = -\omega^2{}_2 P\sin\omega_2 t - \omega^2{}_2 Q\cos\omega_1 t + \omega^2 R\sin\omega t \tag{4.134}$$

Multiplying (4.46) by $\omega^2{}_2$

$$\omega^2{}_2 V_c = \omega^2{}_2 P\sin\omega_2 t + \omega^2{}_2 Q\cos\omega_2 t - \omega^2{}_2 R\sin\omega t \tag{4.135}$$

From (4.45), (4.48), (4.49)

$$(-\omega^2{}_2 + \omega^2)R\sin\omega t = -\frac{A}{L_{line}C}\sin\omega t \tag{4.136}$$

So $$R = +\frac{A}{L_{line}C}\frac{1}{(\omega^2{}_2 - \omega^2)} \tag{4.137}$$

Thus $$V_c = P\sin\omega_2 t + Q\cos\omega_2 t - \frac{A}{L_{line}C}\frac{1}{(\omega^2{}_2 - \omega^2)}\sin\omega t \tag{4.138}$$

Inductor current (I_L)

$$I_L = \frac{1}{L}\int_{\frac{-\sigma}{2\omega}}^{t} V_C dt \quad (4.139)$$

From (4.52)

$$I_L = \frac{1}{L}\int_{\frac{-\sigma}{2\omega}}^{t}(P\sin\omega_2 t + Q\cos\omega_2 t - \frac{A}{L_s C}\frac{1}{(\omega^2{}_2 - \omega^2)}\sin\omega t)dt \quad (4.140)$$

Solving the integral

$$I_L = \frac{1}{L}(-\frac{P}{\omega_2}\cos\omega_2 t + \frac{Q}{\omega_2}\sin\omega_2 t + \frac{A}{\omega L_s C}\frac{1}{(\omega^2{}_2 - \omega^2)}\cos\omega t + \frac{P}{\omega_2}\cos\frac{\omega_2}{\omega}\frac{\sigma}{2} + \frac{Q}{\omega_2}\sin\frac{\omega_2}{\omega}\frac{\sigma}{2} -$$

$$\frac{A}{\omega L_s C}\frac{1}{(\omega^2{}_2 - \omega^2)}\cos\frac{\sigma}{2}) \quad (4.141)$$

Now $$I_L\left(\frac{\sigma}{2\omega}\right) = 0 \quad (4.142)$$

Hence

$$I_L\left(\frac{\sigma}{2\omega}\right) = \frac{1}{L}\left(-\frac{P}{\omega_2}\cos\frac{\omega_2}{\omega}\frac{\sigma}{2} + \frac{Q}{\omega_2}\sin\frac{\omega_2}{\omega}\frac{\sigma}{2} + \frac{A}{\omega L_s C}\frac{1}{(\omega^2{}_2 - \omega^2)}\cos\frac{\sigma}{2} + \frac{P}{\omega_2}\cos\frac{\omega_2}{\omega}\frac{\sigma}{2} +\right.$$

$$\left.\frac{Q}{\omega_2}\sin\frac{\omega_2}{\omega}\frac{\sigma}{2} - \frac{A}{\omega L_s C}\frac{1}{(\omega^2{}_2 - \omega^2)}\cos\frac{\sigma}{2}\right) = 0 \quad (4.143)$$

This gives $$Q = 0 \quad (4.144)$$

Thus, from (4.52) $$V_c = P\sin\omega_2 t - \frac{A}{L_s C}\frac{1}{(\omega^2{}_2 - \omega^2)}\sin\omega t \quad (4.145)$$

And, from (4.55)

$$I_L = \frac{1}{L}(-\frac{P}{\omega_2}\cos\omega_2 t + \frac{A}{\omega L_s C}\frac{1}{(\omega^2{}_2 - \omega^2)}\cos\omega t + \frac{P}{\omega_2}\cos\frac{\omega_2}{\omega}\frac{\sigma}{2} - \frac{A}{\omega L_s C}\frac{1}{(\omega^2{}_2 - \omega^2)}\cos\frac{\sigma}{2}) \quad (4.146)$$

Now $$I_C = C\frac{dV_C}{dt} \quad (4.147)$$

From (4.59) and (4.61) $$I_C = \omega_2 CP\cos\omega_2 t - \frac{\omega A}{L_s}\frac{1}{(\omega^2{}_2 - \omega^2)}\cos\omega t \quad (4.148)$$

However, because thyristors are closed

$$I_S = I_C + I_L \tag{4.149}$$

Thus, from (4.60), (4.62), and (4.63)

$$I_S = \omega_2 CP\cos\omega_2 t - \frac{\omega A}{L_s}\frac{1}{(\omega^2{}_2-\omega^2)}\cos\omega t + \frac{1}{L}\left(-\frac{P}{\omega_2}\cos\omega_2 t + \frac{A}{\omega L_s C}\frac{1}{(\omega^2{}_2-\omega^2)}\cos\omega t + \right.$$

$$\left.\frac{P}{\omega_2}\cos\frac{\omega_2}{\omega}\frac{\sigma}{2} - \frac{A}{\omega L_s C}\frac{1}{(\omega^2{}_2-\omega^2)}\cos\frac{\sigma}{2}\right) \tag{4.150}$$

Simplifying

$$I_S = \omega_2 CP\cos\omega_2 t - \frac{\omega A}{L_s}\frac{1}{(\omega^2{}_2-\omega^2)}\cos\omega t - \frac{P}{\omega_2}\frac{1}{L}\cos\omega_2 t + \frac{A}{\omega L L_s C}\frac{1}{(\omega^2{}_2-\omega^2)}\cos\omega t +$$

$$\frac{P}{\omega_2}\frac{1}{L}\cos\frac{\omega_2}{\omega}\frac{\sigma}{2} - \frac{A}{\omega L L_s C}\frac{1}{(\omega^2{}_2-\omega^2)}\cos\frac{\sigma}{2} \tag{4.151}$$

$$I_S = -\left(\frac{1}{\omega_2 L} - \omega_2 C\right)P\cos\omega_2 t + \left(-\omega + \frac{1}{\omega LC}\right)\frac{1}{(\omega^2{}_2-\omega^2)}\frac{A}{L_s}\cos\omega t + \frac{P}{\omega_2}\frac{1}{L}\cos\frac{\omega_2}{\omega}\frac{\sigma}{2} -$$

$$\frac{A}{\omega L L_s C}\frac{1}{(\omega^2{}_2-\omega^2)}\cos\frac{\sigma}{2} \tag{4.152}$$

$$I_S = -(1-\omega^2{}_2 LC)\frac{P}{\omega_2 L}\cos\omega_2 t + (1-\omega^2 LC)\frac{1}{(\omega^2{}_2-\omega^2)}\frac{A}{\omega L L_s C}\cos\omega t + \frac{P}{\omega_2}\frac{1}{L}\cos\frac{\omega_2}{\omega}\frac{\sigma}{2} -$$

$$\frac{A}{\omega L L_s C}\frac{1}{(\omega^2{}_2-\omega^2)}\cos\frac{\sigma}{2} \tag{4.153}$$

$$I_S = -(1-\omega^2{}_2 LC)\frac{P}{\omega_2 L}\cos\omega_2 t + (1-\omega^2 LC)\frac{R}{\omega L}\cos\omega t + \frac{P}{\omega_2}\frac{1}{L}\cos\frac{\omega_2}{\omega}\frac{\sigma}{2} - \frac{R}{\omega L}\cos\frac{\sigma}{2} \tag{4.154}$$

$$I_S = -\left((1-\omega^2{}_2 LC)\cos\omega_2 t - \cos\frac{\omega_2}{\omega}\frac{\sigma}{2}\right)\frac{P}{\omega_2 L} + \left((1-\omega^2 LC)\cos\omega t - \cos\frac{\sigma}{2}\right)\frac{R}{\omega L} \tag{4.155}$$

Hence state equations are

$$V_c = P\sin\omega_2 t - R\sin\omega t \tag{4.156}$$

and

$$I_S = -\left((1-\omega^2{}_2 LC)\cos\omega_2 t - \cos\frac{\omega_2}{\omega}\frac{\sigma}{2}\right)\frac{P}{\omega_2 L} + \left((1-\omega^2 LC)\cos\omega t - \cos\frac{\sigma}{2}\right)\frac{R}{\omega L} \quad (4.157)$$

where $$R = \frac{A}{L_{line}C}\frac{1}{(\omega^2{}_2-\omega^2)} \quad (4.156)$$

Equating capacitor voltages from (22) and (48) at $t = \frac{\sigma}{2\omega}$

$$F\sin\frac{\omega_1}{\omega}\frac{\sigma}{2} + H\sin\frac{\sigma}{2} = P\sin\frac{\omega_2}{\omega}\frac{\sigma}{2} - R\sin\frac{\sigma}{2} \quad (4.158)$$

Similarly, equating line currents from (4.37) and (4.71) at $t = \frac{\sigma}{2\omega}$

$$\omega_1 CF\cos\frac{\omega_1}{\omega}\frac{\sigma}{2} + \omega CH\cos\frac{\sigma}{2} = -\frac{P}{\omega_2 L}\left((1-\omega^2{}_2 LC)\cos\frac{\omega_2}{\omega}\frac{\sigma}{2} - \cos\frac{\omega_2}{\omega}\frac{\sigma}{2}\right) + \frac{R}{\omega L}\left((1-\omega^2 LC)\cos\frac{\sigma}{2} - \cos\frac{\sigma}{2}\right) \quad (4.159)$$

$$\omega_1 CF\cos\frac{\omega_1}{\omega}\frac{\sigma}{2} + \omega CH\cos\frac{\sigma}{2} = \omega_2 CP\cos\frac{\omega_2}{\omega}\frac{\sigma}{2} - \omega CR\cos\frac{\sigma}{2} \quad (4.160)$$

$$\omega_1 F\cos\frac{\omega_1}{\omega}\frac{\sigma}{2} + \omega H\cos\frac{\sigma}{2} = \omega_2 P\cos\frac{\omega_2}{\omega}\frac{\sigma}{2} - \omega R\cos\frac{\sigma}{2} \quad (4.161)$$

Rearranging (4.73), $$F\sin\frac{\omega_1}{\omega}\frac{\sigma}{2} - P\sin\frac{\omega_2}{\omega}\frac{\sigma}{2} = (-H-R)\sin\frac{\sigma}{2} \quad (4.162)$$

Rearranging (4.76), $$\omega_1 F\cos\frac{\omega_1}{\omega}\frac{\sigma}{2} - \omega_2 P\cos\frac{\omega_2}{\omega}\frac{\sigma}{2} = (-H-R)\omega\cos\frac{\sigma}{2} \quad (4.163)$$

This is of the form

$$\begin{bmatrix} K & L \\ M & N \end{bmatrix}\begin{bmatrix} F \\ P \end{bmatrix} = \begin{bmatrix} (-H-R)\sin\frac{\sigma}{2} \\ (-H-R)\omega\cos\frac{\sigma}{2} \end{bmatrix} \quad (4.164)$$

where $$K = \sin\frac{\omega_1}{\omega}\frac{\sigma}{2} \quad (4.165)$$

$$L = -\sin\frac{\omega_2}{\omega}\frac{\sigma}{2} \quad (4.166)$$

$$M = \omega_1\cos\frac{\omega_1}{\omega}\frac{\sigma}{2} \quad (4.167)$$

$$N = -\omega_2\cos\frac{\omega_2}{\omega}\frac{\sigma}{2} \quad (4.168)$$

Solution of (4.78) is $$\begin{bmatrix} F \\ P \end{bmatrix} = \frac{1}{KN-ML}\begin{bmatrix} N & -L \\ -M & K \end{bmatrix}\begin{bmatrix} (-H-R)\sin\frac{\sigma}{2} \\ (-H-R)\omega\cos\frac{\sigma}{2} \end{bmatrix} \quad (4.169)$$

Hence

$$F = \frac{1}{-\omega_2 \sin\frac{\omega_1\sigma}{\omega\ 2}\cos\frac{\omega_2\sigma}{\omega\ 2}+\omega_1 \sin\frac{\omega_2\sigma}{\omega\ 2}\cos\frac{\omega_1\sigma}{\omega\ 2}}(H+R)\left(\omega_2 \sin\frac{\sigma}{2}\cos\frac{\omega_2}{\omega}\frac{\sigma}{2} - \omega\cos\frac{\sigma}{2}\sin\frac{\omega_2}{\omega}\frac{\sigma}{2}\right)$$

(4.170)

and $P = -\frac{1}{-\omega_2 \sin\frac{\omega_1\sigma}{\omega\ 2}\cos\frac{\omega_2\sigma}{\omega\ 2}+\omega_1 \sin\frac{\omega_2\sigma}{\omega\ 2}\cos\frac{\omega_1\sigma}{\omega\ 2}}(H+R)\left(\omega_1 \sin\frac{\sigma}{2}\cos\frac{\omega_1}{\omega}\frac{\sigma}{2} + \omega\cos\frac{\sigma}{2}\sin\frac{\omega_1}{\omega}\frac{\sigma}{2}\right)$ (4.171)

Thus, when thyristors are closed, $0 \le t \le \frac{\sigma}{2\omega}$

$$V_c = P\sin\omega_2 t - R\sin\omega t \quad (4.172)$$

and $I_S = -\left((1-\omega^2{}_2 LC)\cos\omega_2 t - \cos\frac{\omega_2}{\omega}\frac{\sigma}{2}\right)\frac{P}{\omega_2 L} + \left((1-\omega^2 LC)\cos\omega t - \cos\frac{\sigma}{2}\right)\frac{R}{\omega L}$

(4.173)

where $$R = -\frac{A}{L_{line}C}\frac{1}{(\omega^2{}_2-\omega^2)} \quad (4.174)$$

and $P = -\frac{1}{-\omega_2 \sin\frac{\omega_1\sigma}{\omega\ 2}\cos\frac{\omega_2\sigma}{\omega\ 2}+\omega_1 \sin\frac{\omega_2\sigma}{\omega\ 2}\cos\frac{\omega_1\sigma}{\omega\ 2}}(H+R)\left(\omega_1 \sin\frac{\sigma}{2}\cos\frac{\omega_1}{\omega}\frac{\sigma}{2} + \omega\cos\frac{\sigma}{2}\sin\frac{\omega_1}{\omega}\frac{\sigma}{2}\right)$ (4.175)

And when thyristors are open, i.e. $\frac{\sigma}{2\omega} \le t \le \frac{\pi}{2\omega}$

$$V_c = F\sin\omega_1 t + H\sin\omega t \quad (4.176)$$

and $$I_S = \omega_1 CF\cos\omega_1 t + \omega CH\cos\omega t \quad (4.177)$$

where $$H = -\frac{A}{L_{line}C}\frac{1}{(\omega^2{}_1-\omega^2)} \quad (4.178)$$

and $F = \frac{1}{-\omega_2 \sin\frac{\omega_1\sigma}{\omega\ 2}\cos\frac{\omega_2\sigma}{\omega\ 2}+\omega_1 \sin\frac{\omega_2\sigma}{\omega\ 2}\cos\frac{\omega_1\sigma}{\omega\ 2}}(H+R)\left(\omega_2 \sin\frac{\sigma}{2}\cos\frac{\omega_2}{\omega}\frac{\sigma}{2} - \omega\cos\frac{\sigma}{2}\sin\frac{\omega_2}{\omega}\frac{\sigma}{2}\right)$

(4.179)

Fundamental component of capacitor voltage is

$$V_{Cfunda} = \frac{4}{\pi}\int_0^{\frac{\pi}{2}} V_C \sin\theta \, d\theta \tag{4.180}$$

$$V_{Cfunda} = \frac{4}{\pi}\int_0^{\frac{\sigma}{2}} V_C \sin\theta \, d\theta + \frac{4}{\pi}\int_{\frac{\sigma}{2}}^{\frac{\pi}{2}} V_C \sin\theta \, d\theta \tag{4.181}$$

$$V_{Cfunda} = \frac{4}{\pi}\int_0^{\frac{\sigma}{2}} (P\sin\frac{\omega_2}{\omega}\theta - R\sin\theta)\sin\theta \, d\theta + \frac{4}{\pi}\int_{\frac{\sigma}{2}}^{\frac{\pi}{2}} (F\sin\frac{\omega_1}{\omega}\theta + H\sin\theta)\sin\theta \, d\theta \tag{4.182}$$

$$V_{Cfunda} = \frac{4}{\pi}\int_0^{\frac{\sigma}{2}} P\sin\frac{\omega_2}{\omega}\theta\sin\theta \, d\theta - \frac{4}{\pi}\int_0^{\frac{\sigma}{2}} R(\sin\theta)^2 d\theta + \frac{4}{\pi}\int_{\frac{\sigma}{2}}^{\frac{\pi}{2}} F\sin\frac{\omega_1}{\omega}\theta\sin\theta \, d\theta +$$

$$\frac{4}{\pi}\int_{\frac{\sigma}{2}}^{\frac{\pi}{2}} H(\sin\theta)^2 d\theta \tag{4.183}$$

$$V_{Cfunda} = \frac{2}{\pi}\int_0^{\frac{\sigma}{2}} P\cos(\frac{\omega_2}{\omega} - 1)\theta \, d\theta - \frac{2}{\pi}\int_0^{\frac{\sigma}{2}} P\cos\left(\frac{\omega_2}{\omega} + 1\right)\theta \, d\theta - \frac{2}{\pi}\int_0^{\frac{\sigma}{2}} R d\theta +$$

$$\frac{2}{\pi}\int_0^{\frac{\sigma}{2}} R\cos 2\theta \, d\theta + \frac{2}{\pi}\int_{\frac{\sigma}{2}}^{\frac{\pi}{2}} F\cos(\frac{\omega_1}{\omega} - 1)\theta \, d\theta - \frac{2}{\pi}\int_{\frac{\sigma}{2}}^{\frac{\pi}{2}} F\cos(\frac{\omega_1}{\omega} + 1)\theta \, d\theta + \frac{2}{\pi}\int_{\frac{\sigma}{2}}^{\frac{\pi}{2}} H d\theta -$$

$$\frac{2}{\pi}\int_{\frac{\sigma}{2}}^{\frac{\pi}{2}} H\cos 2\theta \, d\theta \tag{4.184}$$

$$V_{Cfunda} = \frac{2}{\pi}\frac{P}{\frac{\omega_2}{\omega}-1}\sin(\frac{\omega_2}{\omega} - 1)\frac{\sigma}{2} - \frac{2}{\pi}\frac{P}{\frac{\omega_2}{\omega}+1}\sin\left(\frac{\omega_2}{\omega} + 1\right)\frac{\sigma}{2} - \frac{2}{\pi}R\frac{\sigma}{2} + \frac{2}{\pi}\frac{R}{2}\sin\sigma +$$

$$\frac{2}{\pi}\frac{F}{\frac{\omega_1}{\omega}-1}\left(\sin\left(\frac{\omega_1}{\omega} - 1\right)\frac{\pi}{2} - \sin\left(\frac{\omega_1}{\omega} - 1\right)\frac{\sigma}{2}\right) - \frac{2}{\pi}\frac{F}{\frac{\omega_1}{\omega}+1}\left(\sin\left(\frac{\omega_1}{\omega} + 1\right)\frac{\pi}{2} - \sin\left(\frac{\omega_1}{\omega} + 1\right)\frac{\sigma}{2}\right) +$$

$$\frac{2}{\pi}H\frac{\pi-\sigma}{2} + \frac{2}{\pi}\frac{H}{2}\sin\sigma \tag{4.185}$$

Fundamental component of line current is

$$I_{Sfunda} = \frac{4}{\pi}\int_0^{\frac{\pi}{2}} I_S \cos\theta \, d\theta \tag{4.186}$$

$$I_{Sfunda} = \frac{4}{\pi}\int_0^{\frac{\sigma}{2}} I_S \cos\theta \, d\theta + \frac{4}{\pi}\int_{\frac{\sigma}{2}}^{\frac{\pi}{2}} I_S \cos\theta \, d\theta \tag{4.187}$$

$$I_{Sfunda} = \frac{4}{\pi}\int_0^{\frac{\sigma}{2}} (-\left((1 - \omega^2{}_2 LC)\cos\frac{\omega_2}{\omega}\theta - \cos\frac{\omega_2}{\omega}\frac{\sigma}{2}\right)\frac{P}{\omega_2 L} + \left((1 - \omega^2 LC)\cos\theta -$$

$$\cos\frac{\sigma}{2}\right)\frac{R}{\omega L})\cos\theta \, d\theta + \frac{4}{\pi}\int_{\frac{\sigma}{2}}^{\frac{\pi}{2}} (\omega_1 CF\cos\frac{\omega_1}{\omega}\theta + \omega CH\cos\theta)\cos\theta \, d\theta \tag{4.188}$$

$$I_{Sfunda} = \frac{4}{\pi}\int_0^{\frac{\sigma}{2}}\left(-\left((1-\omega^2{}_2LC)\cos\frac{\omega_2}{\omega}\theta - \cos\frac{\omega_2}{\omega}\frac{\sigma}{2}\right)\frac{P}{\omega_2 L}\cos\theta\,d\theta + \frac{4}{\pi}\int_0^{\frac{\sigma}{2}}\left((1-\omega^2LC)\cos\theta - \cos\frac{\sigma}{2}\right)\frac{R}{\omega L}\cos\theta\,d\theta + \frac{4}{\pi}\int_{\frac{\sigma}{2}}^{\frac{\pi}{2}}\omega_1 CF\cos\frac{\omega_1}{\omega}\theta\cos\theta\,d\theta + \frac{4}{\pi}\int_{\frac{\sigma}{2}}^{\frac{\pi}{2}}\omega CH(\cos\theta)^2 d\theta \quad (4.189)$$

$$I_{Sfunda} = -\frac{4}{\pi}\frac{P}{\omega_2 L}(1-\omega^2{}_2LC)\int_0^{\frac{\sigma}{2}}\cos\frac{\omega_2}{\omega}\theta\cos\theta\,d\theta + \frac{4}{\pi}\frac{P}{\omega_2 L}\cos\frac{\omega_2}{\omega}\frac{\sigma}{2}\int_0^{\frac{\sigma}{2}}\cos\theta\,d\theta + \frac{4}{\pi}\frac{R}{\omega L}(1-\omega^2LC)\int_0^{\frac{\sigma}{2}}(\cos\theta)^2 d\theta - \frac{4}{\pi}\frac{R}{\omega L}\cos\frac{\sigma}{2}\int_0^{\frac{\sigma}{2}}\cos\theta\,d\theta + \frac{4}{\pi}\omega_1 CF\int_{\frac{\sigma}{2}}^{\frac{\pi}{2}}\cos\frac{\omega_1}{\omega}\theta\cos\theta\,d\theta + \frac{4}{\pi}\omega CH\int_{\frac{\sigma}{2}}^{\frac{\pi}{2}}(\cos\theta)^2 d\theta \quad (4.190)$$

$$I_{Sfunda} = -\frac{2}{\pi}\frac{P}{\omega_2 L}(1-\omega^2{}_2LC)\int_0^{\frac{\sigma}{2}}\cos\left(\frac{\omega_2}{\omega}+1\right)\theta\,d\theta - \frac{2}{\pi}\frac{P}{\omega_2 L}(1-\omega^2{}_2LC)\int_0^{\frac{\sigma}{2}}\cos\left(\frac{\omega_2}{\omega}-1\right)\theta\,d\theta + \frac{4}{\pi}\frac{P}{\omega_2 L}\cos\frac{\omega_2}{\omega}\frac{\sigma}{2}\sin\frac{\sigma}{2} + \frac{2}{\pi}\frac{R}{\omega L}(1-\omega^2LC)\int_0^{\frac{\sigma}{2}}(1+\cos 2\theta)d\theta - \frac{4}{\pi}\frac{R}{\omega L}\cos\frac{\sigma}{2}\sin\frac{\sigma}{2} + \frac{2}{\pi}\omega_1 CF\int_{\frac{\sigma}{2}}^{\frac{\pi}{2}}\cos\left(\frac{\omega_1}{\omega}+1\right)\theta\,d\theta + \frac{2}{\pi}\omega_1 CF\int_{\frac{\sigma}{2}}^{\frac{\pi}{2}}\cos\left(\frac{\omega_1}{\omega}-1\right)\theta\,d\theta + \frac{2}{\pi}\omega CH\int_{\frac{\sigma}{2}}^{\frac{\pi}{2}}(1+\cos 2\theta)d\theta \quad (4.191)$$

$$I_{Sfunda} = -\frac{2}{\pi}\frac{P}{\omega_2 L}(1-\omega^2{}_2LC)\frac{1}{\frac{\omega_2}{\omega}+1}\sin\left(\frac{\omega_2}{\omega}+1\right)\frac{\sigma}{2} - \frac{2}{\pi}\frac{P}{\omega_2 L}(1-\omega^2{}_2LC)\frac{1}{\frac{\omega_2}{\omega}-1}\sin\left(\frac{\omega_2}{\omega}-1\right)\frac{\sigma}{2} + \frac{4}{\pi}\frac{P}{\omega_2 L}\cos\frac{\omega_2}{\omega}\frac{\sigma}{2}\sin\frac{\sigma}{2} + \frac{2}{\pi}\frac{R}{\omega L}(1-\omega^2LC)\frac{\sigma}{2} + \frac{2}{\pi}\frac{R}{\omega L}(1-\omega^2LC)\frac{\sin\sigma}{2} - \frac{4}{\pi}\frac{R}{\omega L}\cos\frac{\sigma}{2}\sin\frac{\sigma}{2} + \frac{2}{\pi}\omega_1 CF\frac{1}{\frac{\omega_1}{\omega}+1}\sin\left(\frac{\omega_1}{\omega}+1\right)\frac{\pi}{2} - \frac{2}{\pi}\omega_1 CF\frac{1}{\frac{\omega_1}{\omega}+1}\sin\left(\frac{\omega_1}{\omega}+1\right)\frac{\sigma}{2} + \frac{2}{\pi}\omega_1 CF\frac{1}{\frac{\omega_1}{\omega}-1}\sin\left(\frac{\omega_1}{\omega}-1\right)\frac{\pi}{2} - \frac{2}{\pi}\omega_1 CF\frac{1}{\frac{\omega_1}{\omega}-1}\sin\left(\frac{\omega_1}{\omega}-1\right)\frac{\sigma}{2} + \frac{2}{\pi}\omega CH\frac{\pi-\sigma}{2} - \frac{2}{\pi}\omega CH\frac{\sin\sigma}{2} \quad (4.192)$$

Finally, the equivalent fundamental impedance of enhanced Power Flow Controller (ePFC) is,

$$jX_{ePFC} = \frac{V_{Cfunda}}{I_{Sfunda}} \quad (4.193)$$

Therefore, the equation (4.193) gives a more generalized and complete expression of the effective fundamental impedance inserted by an ePFC. Furthermore, it may also be noted that, this same mathematical expressions is equally applicable in determining the fundamental impedance of other series FACTS devices such as Thyristor Controlled Switched Capacitor (TCSC).

4.6. Comparison of Methods of Impedance Calculation

The proposed ePFC circuit is modeled with transmission system and compensation L and C parameters, V_{line} = 230kV, δ =30^o, X_{line} = 8.46Ω, X_L = 152.3Ω, X_C = 566Ω taken from [17]. FIGURE 4.8 presents comparison of analytical results for the effective equivalent impedance obtained by 1st order approximation, i.e. X(sigma-1) from equation (4.27), 2nd order approximation, i.e. X(sigma-2) from equation (4.94), and proposed approach, i.e. X_{ePFC} from equation (4.193).

Table 4.2. Comparison between the effective fundamental impedance

Conduction angle	X(sigma-1)	X(sigma-2)	XePFC
1	574.46	10.0	-50.0529
20	579.22	590.35	618.3387
40	614.14	596.7	565.5254
60	729.00	845.96	973.9234
80	1111.96	1002.546	918.9605
100	5683.94	5483.96	-5325.49
120	-1238.20	-1637.58	-1938.53
140	-491.85	-394.04	-496.717
160	-289.40	-226.19	-301.588
180	-199.79	-208.68	-208.258

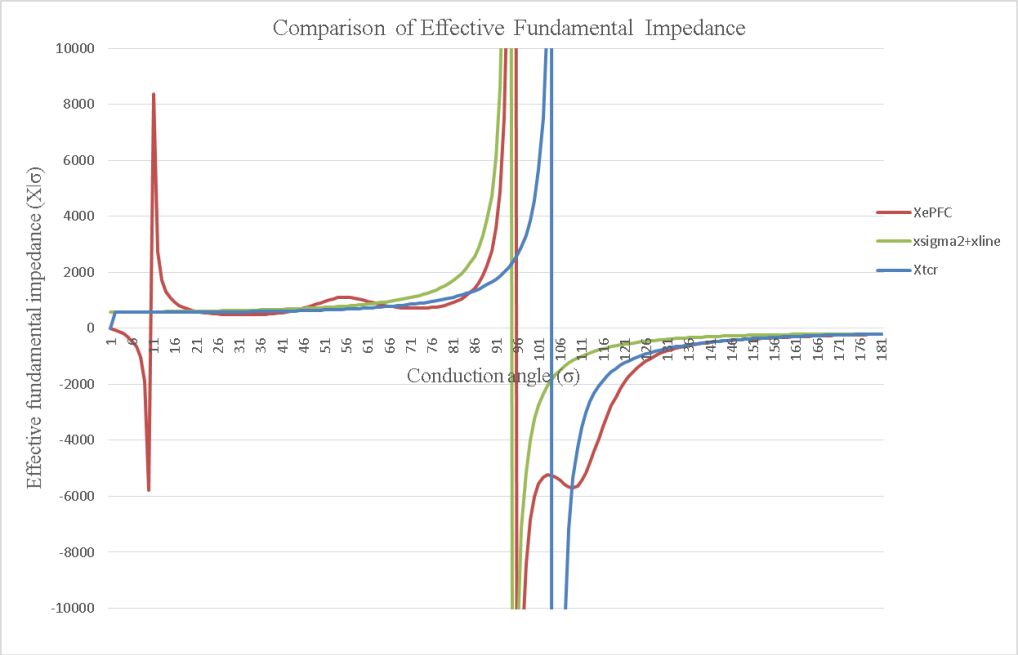

FIGURE 4.8: Comparison of effective fundamental impedance versus conduction angle, i.e. $X_{l\sigma}$ v/s σ, obtained by three approaches

As may be seen, not only the fundamental impedance is different over the operating range of conduction angle (σ), but also there is a difference in the resonance zone determined by three approaches. As shown in [17], resonance zone obtained by fundamental current model (2^{nd} order approximation) is different from the fundamental voltage model (1^{st} order approximation). The proposed model is close to this 2^{nd} order approximation, however introduces a further correction in calculated impedance, accounting for line reactance as well.

Furthermore, one may also note that the proposed analysis method reveals that such systems exhibit two resonance zones. The first one (Resonance 1 in FIGURE 4.8) is similar to the two approaches documented in literature [17], [18] where the compensating capacitance has been known to resonate with compensating reactance. However, there is also an additional resonance (Resonance 2) between compensating capacitance and line reactance as illustrated in FIGURE 4.8.

The proposed ePFC circuit equations are also modeled using Matlab. The effective fundamental impedance with conduction angle (σ) control is calculated for two sets of line inductance (X_{line}), compensation inductance (X_L), and compensation capacitance (X_C). Parameters for ePFC on transmission line:

a. S_{3phase} =100 MVA, V_{line} =230kV, $\boldsymbol{\delta}$ =30º, X_{line} =8.46Ω, X_L =152.3Ω, X_C =566Ω.

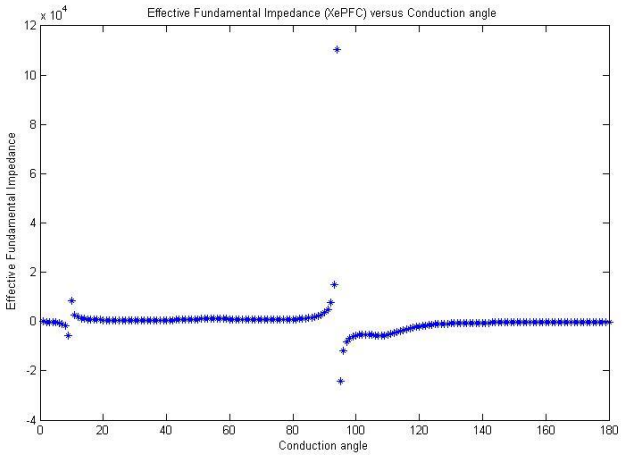

FIGURE 4.9: Effective fundamental impedance offered by X_{line} =8.46Ω, X_L =152.3Ω, X_C =566Ω System

b. S_{3phase} =100 MVA, V_{line} =230kV, $\boldsymbol{\delta}$ =30º, X_{line} =0.0735Ω, X_L =0.0735Ω, X_C = 1.77Ω [19].

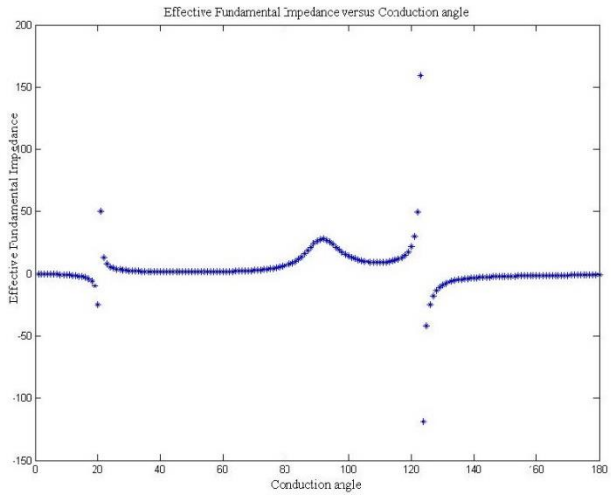

FIGURE 4.10: Effective fundamental impedance offered by X_{line} =0.0735Ω, X_L =0.0735Ω, X_C =

1.77Ω system

FIGURE 4.9 and FIGURE 4.10 exhibit an additional resonance between compensating capacitance and line reactance. Thus, the proposed treatment based on the principle that only the end bus voltages are sinusoidal illustrates all associated harmonics generated by series injection of ePFC are absorbed in the transmission line itself. To further explain, the majority of the harmonic voltage drop occurs in the line and that the source impedance behind the bus is very small compared to the line impedance and thus has small harmonic voltage drops. This approach further generalizes the state of the art (2^{nd} order approximation) model that has been employed to analyze series FACTS devices such as TCSC. The proposed ePFC analytical model is superior to the 2^{nd} order approximation in terms of predicting an additional resonance zone.

CHAPTER 5 : MODELING AND SIMULATION RESULTS

5.1. Introduction

This chapter describes the modeling of Distributed Series Reactance (DSR), Distributed Series Impedance (DSI) and proposed enhanced Power Flow Controller (ePFC) using MATLAB-Simulink. And also the simulation results of Distributed Series Reactance (DSR), Distributed Series Impedance (DSI) and enhanced Power Flow Controller (ePFC) are shown. The simulations are conducted for different modes of operation of DSR and DSI and also for various conduction angles (σ) of ePFC. The simulation results demonstrate the desired operation of the system, through different modes of operation. The obtained simulation results are compared with the mathematical calculations, presented in chapter 3. Finally, an overview of the model and the functional block diagram of the system is discussed in section 5.8.

5.2. Modeling of Distributed Series Reactance

The Distributed Series Reactance (DSR) system is modelled in MATLAB-Simulink software [20]. The schematic of the DSR model is shown in FIGURE 5.1. As explained in the earlier chapter, DSR consists of a Single Turn Transformer (STT) where the transmission line itself acts as the primary winding. The secondary winding is connected

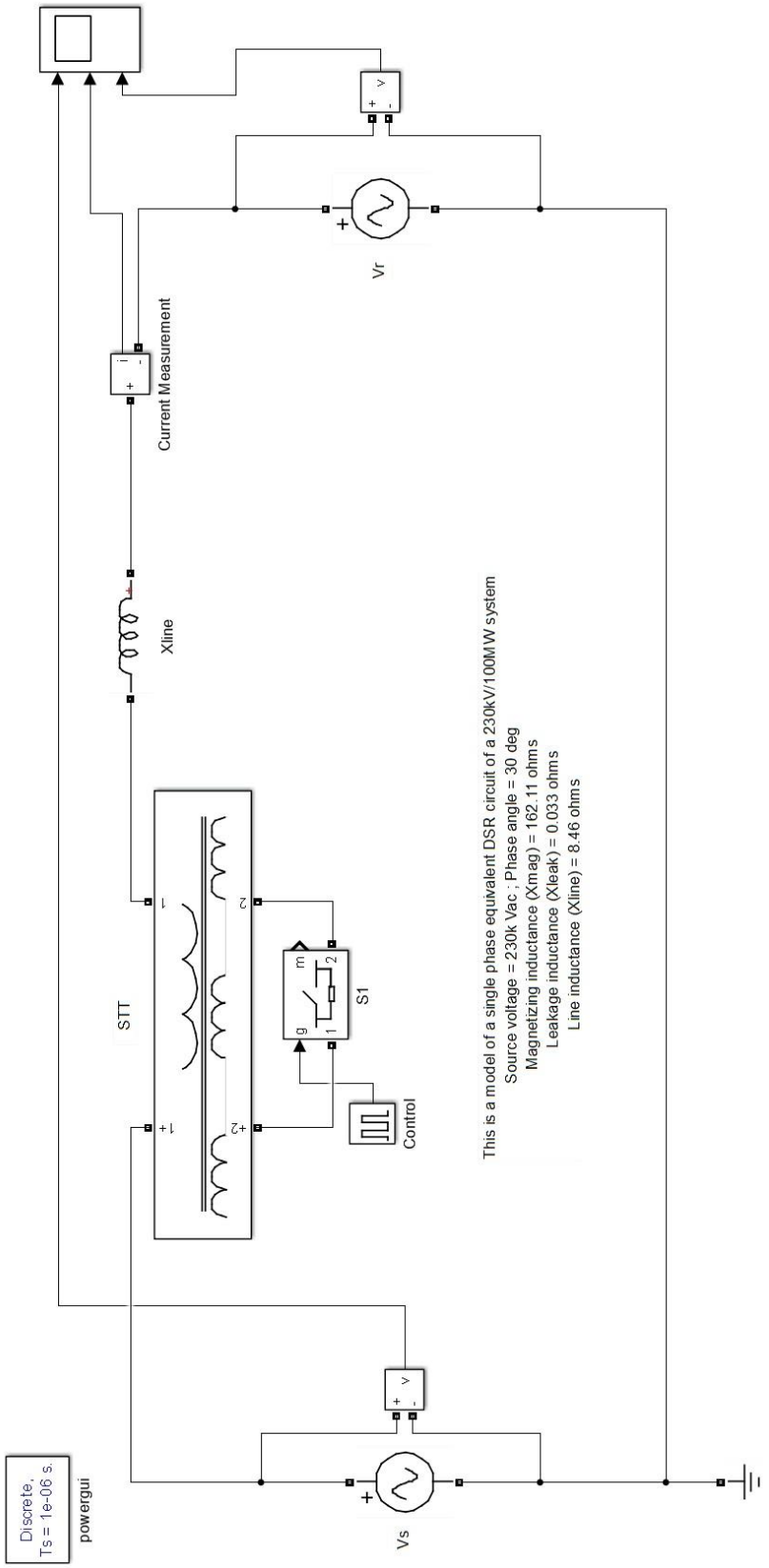

FIGURE 5.1: Simulation model of Distributed Series Reactance (DSR)

to back-to-back thyristors, which when closed creates a short circuit across the secondary winding thereby varying the effective reactance introduced into the power line.

When switch S is open across the secondary winding, magnetizing reactance (X_{mag}) of the STT is injected into the circuit. Similarly, when switch S is closed across the secondary winding, leakage reactance (X_{leak}) of the STT is injected into the circuit. Thus, controlling the effective impedance on the line.

The simulation is performed in the MATLAB-Simulink software. The results obtained for different positions of the switch S are presented in the following Section 5.3.

5.3. Simulated Results of Distributed Series Reactance

A single phase Distributed Series Reactor (DSR) circuit is modeled using Matlab-Simulink. The transmission system parameters: $V_r = V_s = 230kV_{L-L}$, S = 100 MVA, $\boldsymbol{\delta}$ = 30° lag, X_{line}= 8.46 Ω, X_{leak}= 0.033 Ω, X_{mag} = 162.11 Ω. From chapter 3 and FIGURE 3.5, it can be seen that DSR operates in two modes, depending upon the position of the switch S.

When switch S is open across the secondary winding, magnetizing reactance of the STT is injected into the circuit. This mode of operation is modelled in MATLAB-SIMULINK and the current I_S in the system is determine. FIGURE 5.2 shows the simulation results of a DSR when switch S is open.

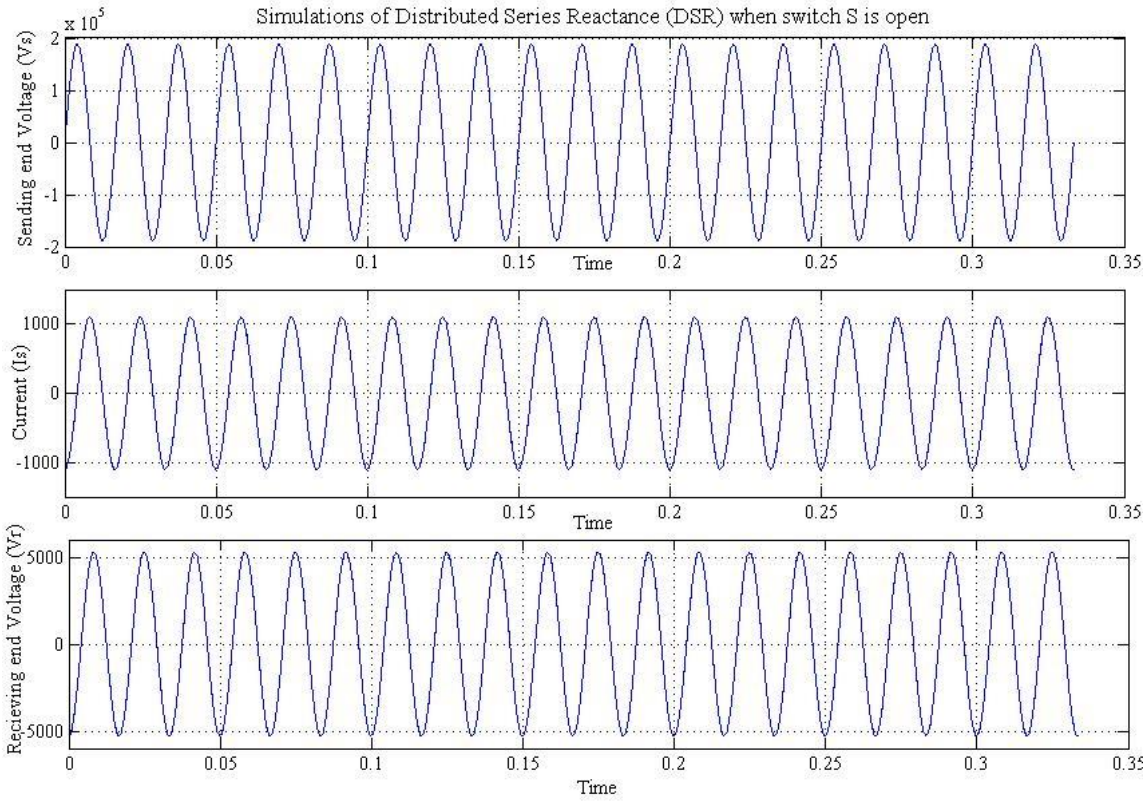

FIGURE 5.2: Sending Voltage (V_s), Line Current (I_s) and Receiving Voltage (V_r) in a DSR system with S open.

When switch S is closed across the secondary winding, leakage reactance of the STT is injected into the circuit. This mode of operation is modelled in MATLAB-SIMULINK and the current I_S in the system is determine. FIGURE 5.3 shows the simulation results of a DSR when switch S is closed.

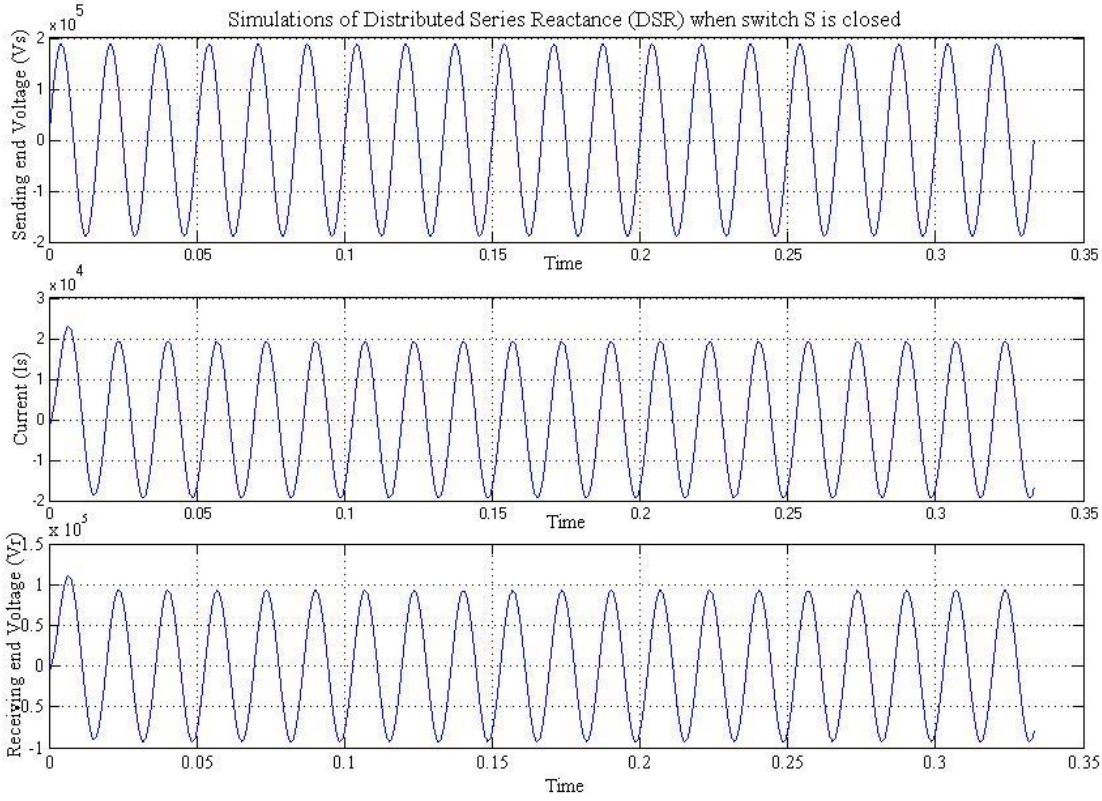

FIGURE 5.3: Sending Voltage (V_s), Line Current (I_s) and Receiving Voltage (V_r) in a DSR system with S closed.

Table 5.1 presents comparison of analytical and simulation results. FIGURE 5.2 and FIGURE 5.3 shows the waveforms for the cases when switch S is open and closed respectively. It is observed that the analytical results and simulated results are in agreement.

Table 5.1: Comparison of calculated and simulated parameters of single phase DSR system

S	Xeff	Calculated Current	Simulated Current
Open	170.6 Ω	550.40 A	570 A
Closed	8.49 Ω	1.11e4 A	1.43e4 A

5.4. Modeling of Distributed Series Impedance

The Distributed Series Reactance (DSI) system is modelled in MATLAB-Simulink software [21]. The schematic of the DSI model is shown in FIGURE 5.4. As explained in the earlier chapter, a DSI is an extension of a DSR by adding an L-C impedance network to the secondary side of the transformer. In addition to the series connected STT and its switch S on the secondary side, inductor L and capacitor C are inserted along with their switches S_L and S_C respectively.

A DSI operates in 3 modes of operation.

1) Inductance (L) mode: - When switch S is open and switch S_L is closed, injecting inductance L.
2) Capacitance (C) mode:-When switch S is open and switch S_C is closed, injecting capacitance C.
3) Impedance (Z) mode: - When switch S is open and both switches S_L and S_C are closed, injecting impedance.

Thus, controlling the effective impedance on the line. The simulation is performed in the MATLAB-Simulink software. The results obtained for different positions of the switch S are presented in the following Section 5.5.

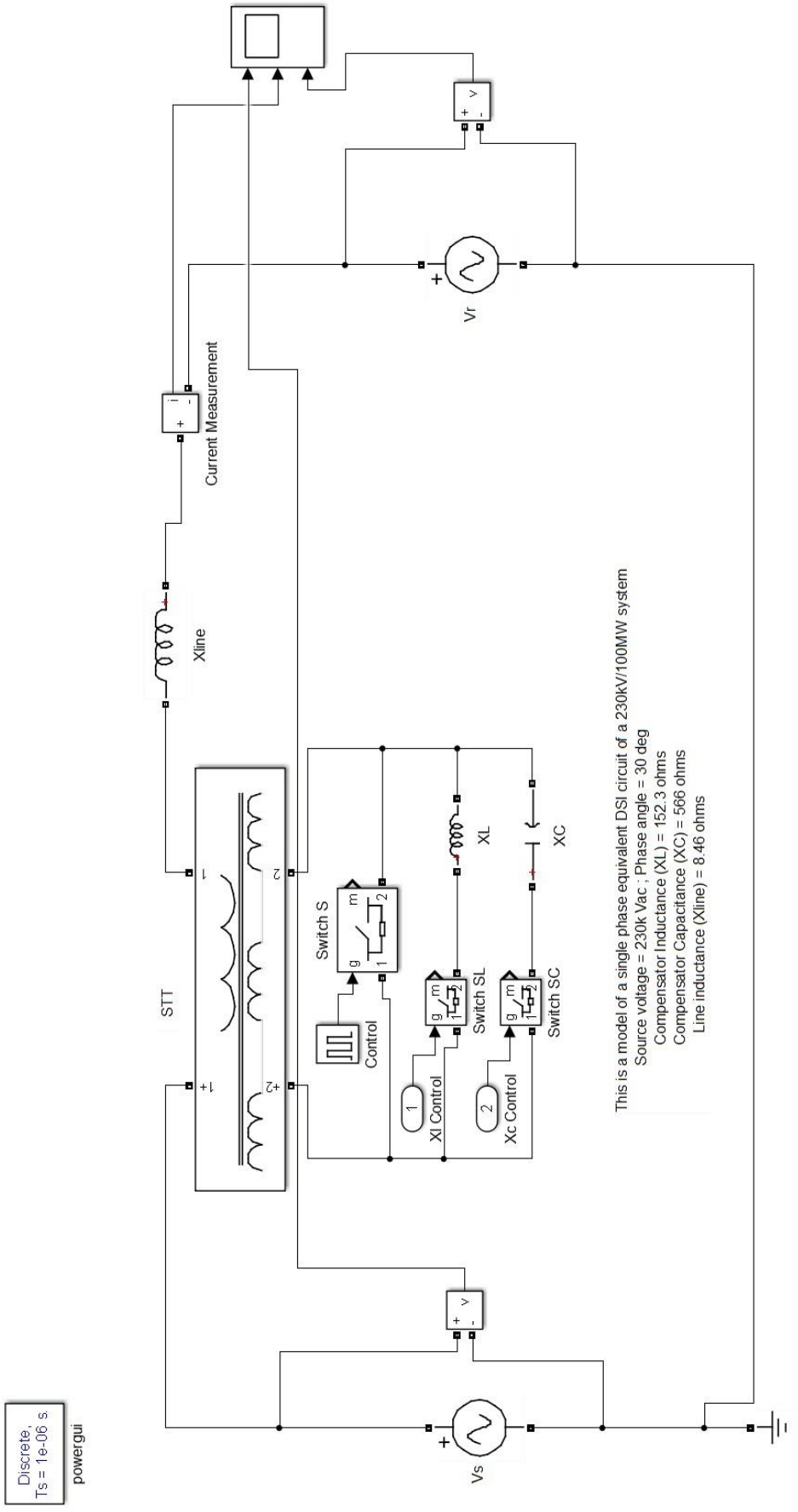

FIGURE 5.4: Simulation model of Distributed Series Impedance(DSI)

5.5. Simulation Results of Distributed Series Impedance

A single phase Distributed Series Impedance (DSI) circuit is modeled using Matlab-Simulink. The transmission system parameters: $V_r = V_s = 230kV_{L-L}$, S = 100 MVA, $\boldsymbol{\delta}$ = 30° lag, X_{line}= 8.46 Ω, X_{leak}= 0.033 Ω, X_{mag} = 162.11 Ω, X_L = 152.3 Ω, X_C = 566 Ω. From chapter 3 and FIGURE 3.9, it can be seen that DSI operates in three modes, depending upon the position of the switches S, S_L and S_C.

When switch S is open and switch S_L is closed, the DSI injects inductance L and operates in "inductance (L) mode". FIGURE 5.5 shows the simulation results of a DSI in inductance mode.

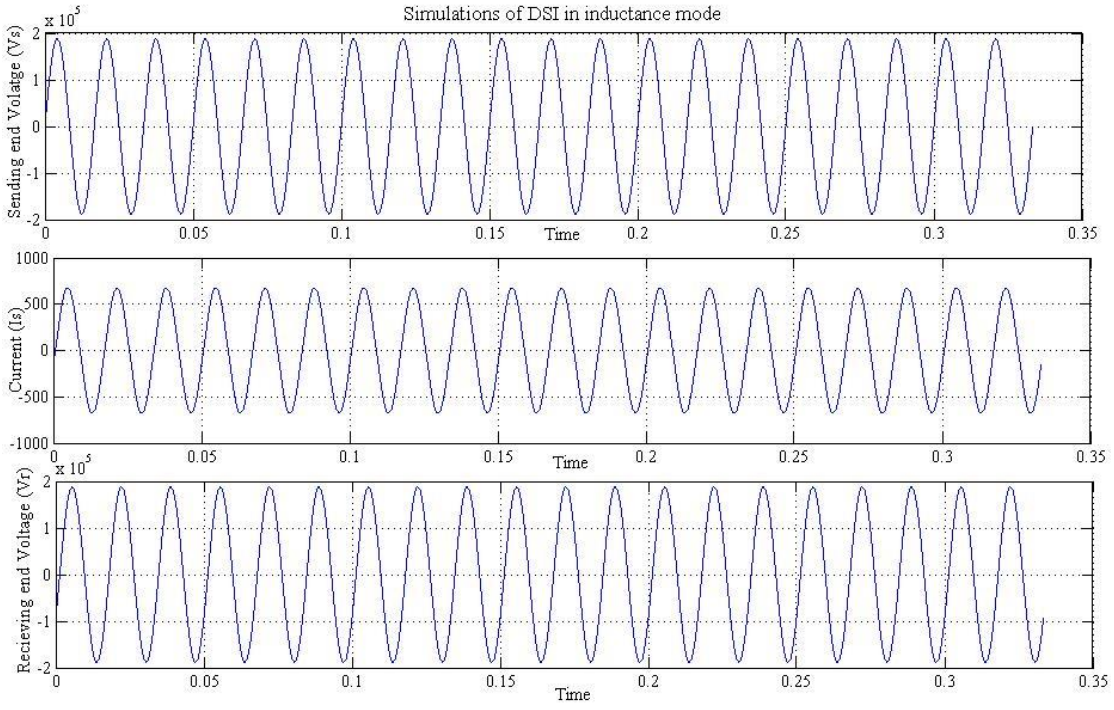

FIGURE 5.5: Sending Voltage (V_s), Line Current (I_s) and Receiving Voltage (V_r) in inductance-mode DSI system.

When switch S is open and switch S_C is closed, the DSI injects capacitance C and operates into "capacitance (C) mode". FIGURE 5.6 shows the simulation results of a DSI in capacitance mode.

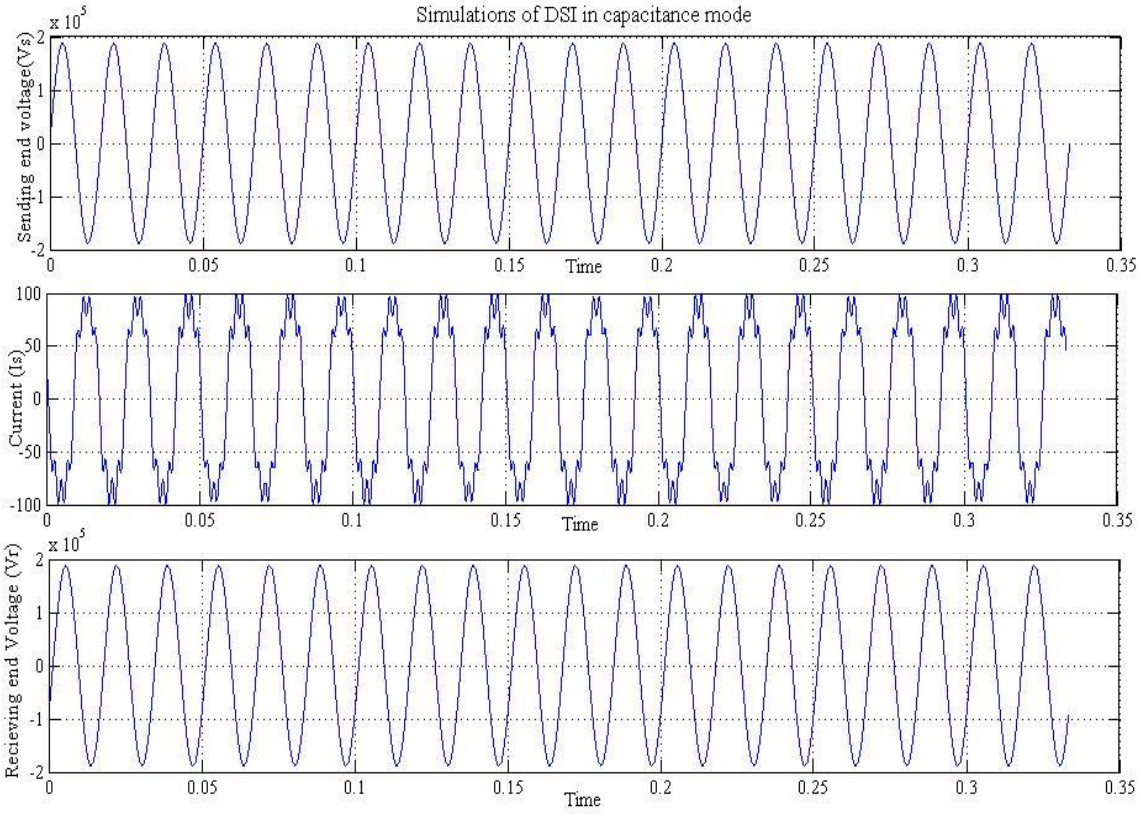

FIGURE 5.6: Sending Voltage (V_s), Line Current (I_s) and Receiving Voltage (V_r) in capacitance-mode DSI system.

When switch S is open and both switches S_L and S_C are closed, the DSI injects impedance and operates into "impedance (Z) mode".

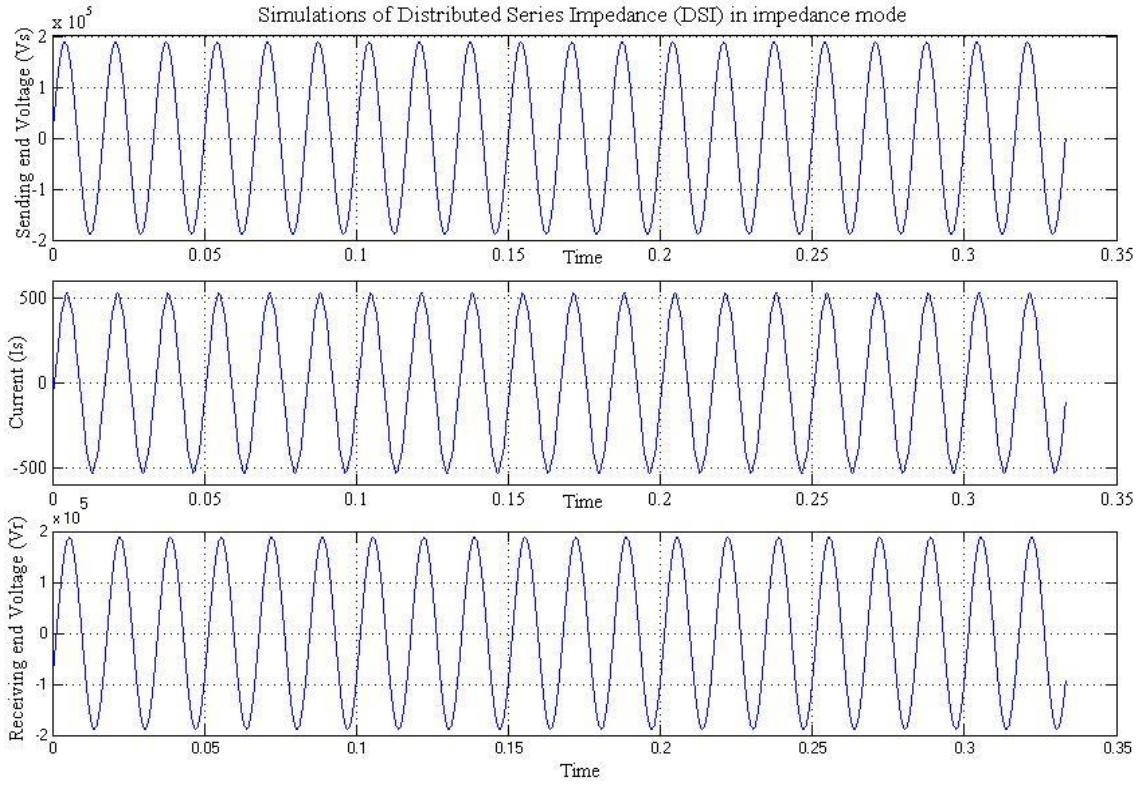

FIGURE 5.7: Sending Voltage (V_s), Line Current (I_s) and Receiving Voltage (V_r) in impedance -mode DSI system.

Table 5.2 presents comparison of analytical and simulation results. FIGURE 5.5, FIGURE 5.6. and FIGURE 5.7 show the waveforms for the inductance, capacitance and impedance modes respectively. It is observed that the simulation and analytical results are in agreement

Table 5.2: Comparison of calculated and simulated parameters of single phase DSI system

Mode	**X_{eff}**	**Calculated Current**	**Simulated Current**
Inductance	160.79 Ω	583.96 A	676.4 A
Capacitance	-557.50 Ω	168.42 A	97.02 A
Impedance	216.45 Ω	449.11 A	534.8 A

The proposed enhanced Power Flow Controller (ePFC) system is modelled in MATLAB-Simulink software [23]. The schematic of the ePFC model is shown in FIGURE 5.8.

As explained, an ePFC consists of a DSI with thyristor conduction angle control. The back to back thyristor switches operate on synthesized triggers, by the firing angle pulses with respect to the conduction angle (σ). The operation of these switches (in discrete steps), when connected to the compensator L and C, inserts a wide range of impedances in combination with the line inductance L_{line}. Therefore, the effective impedance on the line can be used effectively to control the power flow on the transmission system.

The model described in this chapter is used to simulate the enhanced Power Flow Controller (ePFC) system with impedance control strategy. The simulation is performed in MATLAB-Simulink software. The results obtained from these simulations are presented in the following section 5.7.

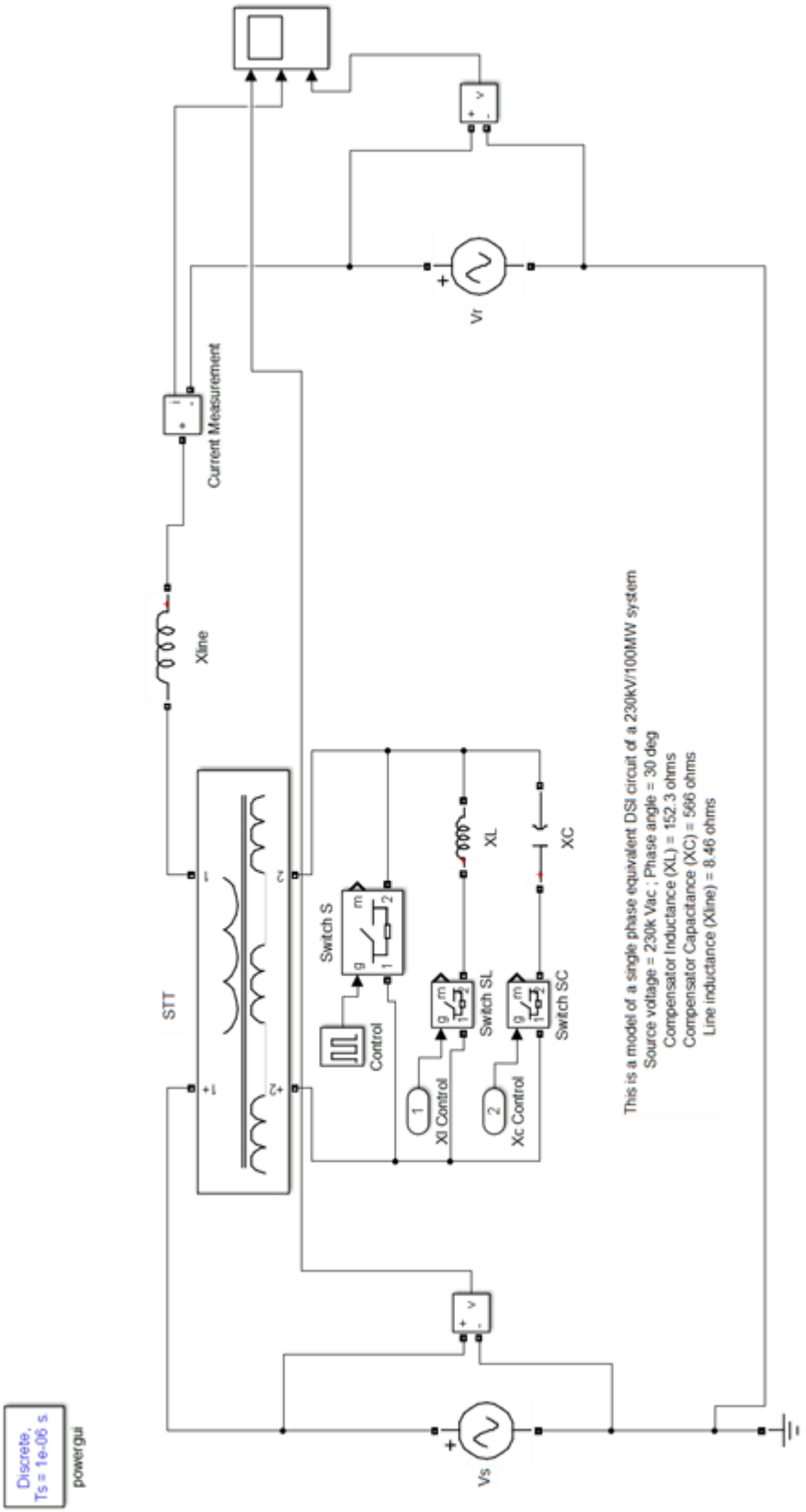

FIGURE 5.8: Simulation model of ePFC

5.7. Simulation Results of enhanced Power Flow Controllers

A single phase enhanced Power Flow Controller (ePFC) circuit is modeled using Matlab-Simulink. The transmission system parameters: $V_r = V_s = 230kV_{L-L}$, S = 100 MVA, $\boldsymbol{\delta} = 30°$ lag, $X_{line} = 8.46\ \Omega$, $X_{leak} = 0.033\ \Omega$, $X_{mag} = 162.11\ \Omega$, $X_L = 152.3\ \Omega$, $X_C = 566\ \Omega$. From chapter 4 and FIGURE 4.1, it can be seen that ePFC operates as a function of conduction angle (σ). Depending upon the angle of conduction in combination with X_C and X_{line}, ePFC primarily operates in 3 regions.

When conduction angle (σ) is operating before resonance. This mode of operation is modelled in MATLAB-SIMULINK and the current I_S in the system is determine. FIGURE 5.9 shows the simulation results of an ePFC in inductive region.

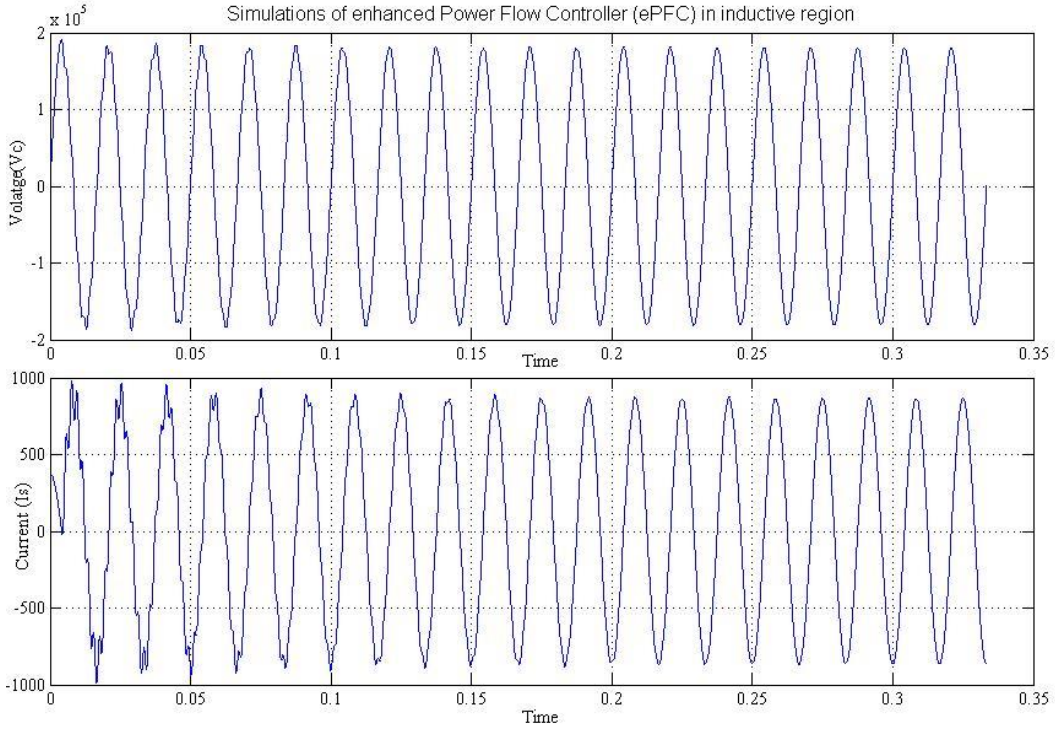

FIGURE 5.9: Capacitor Voltage (V_c), Line Current (I_s) in inductive-region ePFC system.

When conduction angle (σ) is operating after resonance. This mode of operation is modelled in MATLAB-SIMULINK and the current I_S in the system is determine. FIGURE 5.10 shows the simulation results of an ePFC in capacitive region.

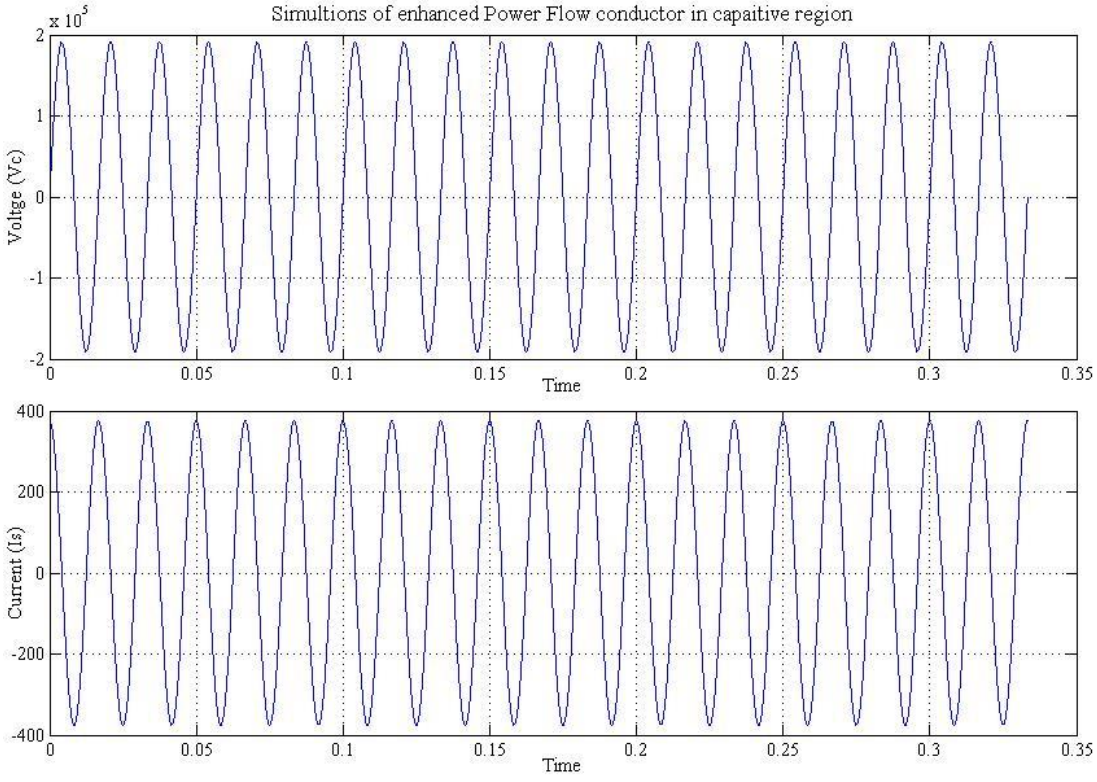

FIGURE 5.10: Capacitor Voltage (V_c), Line Current (I_s) in capacitive-region ePFC system.

When conduction angle (σ) is operating in resonance. This mode of operation is modelled in MATLAB-SIMULINK and the current I_S in the system is determine. FIGURE 5.11 shows the simulation results of an ePFC in resonance region.

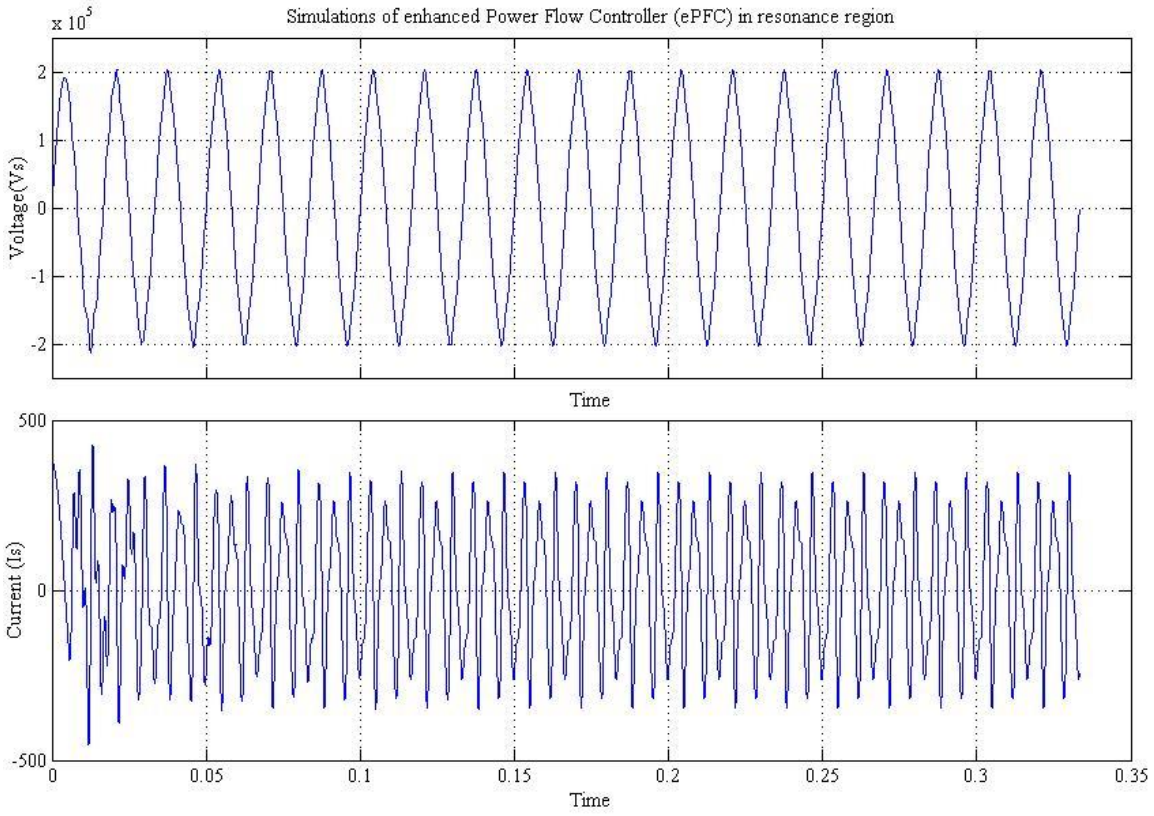

FIGURE 5.11: Capacitor Voltage (V_c), Line Current (I_s) in resonance-region ePFC system.

FIGURE 5.9, FIGURE 5.10 and FIGURE 5.11 show the waveforms for the inductive, capacitive and resonance regions respectively.

5.8. Block Diagram Representation of ePFC

As explained in the previous section, the proposed ePFC consist of a Distributed Series Impedance (DSI) with a thyristor based conduction angle (σ) control. The system primary functionality, to control the power flow is achieved by continuously varying the impedance on the transmission line. The functional block diagram is illustrated in FIGURE 5.12.

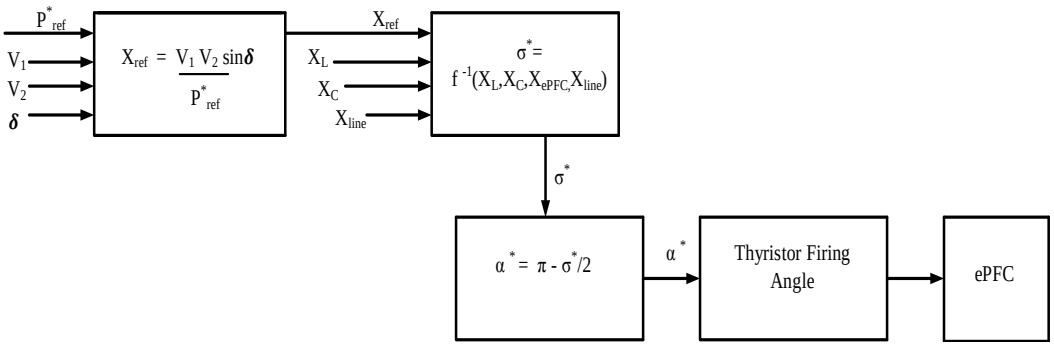

FIGURE 5.12: Functional block diagram of the proposed ePFC system

As depicted in the FIGURE 5.12, a control strategy to direct power flow is obtained by, measuring a reference power (P^*_{ref}) with respect to the bus voltages V_1, V_2 and phase angle ($\boldsymbol{\delta}$). The new effective impedance (X_{ref}) is calculated from the reference power (P^*_{ref}), bus voltages V_1, V_2 and phase angle ($\boldsymbol{\delta}$). Thus, the required conduction angle (σ^*) as a function of effective impedance (X_{ref}), compensator reactance (X_L), capacitance (X_C) and line inductance (X_{line}) is obtained from the look-up table. In turn, a required firing pulse is generated to trigger the switches of the ePFC system. This is accomplished by computing the firing angle (α^*) with the respective conduction angle (σ^*). Therefore by varying the firing angle of the thyristors, which in effect varies the equivalent impedance of the ePFC system and enables to control the power flow on the transmission line.

CHAPTER 6 : STABILITY ANALYSIS OF EPFC

6.1. Introduction

In this chapter, the aspect of stability in ideal enhanced Power Flow Controller (ePFC) is discussed. The chapter includes useful simplifications in computing stability of the nonlinear dynamical systems. Thyristors constrain their currents to zero when they are off. This important constraint is accounted for by changing the state space dimension as thyristors, switch on and off. The inhibition of thyristor turn on until a firing pulse is present has a significant effect on the system dynamics.

The stability of the ePFC system is determined using Poincaré map. The Poincaré map is a standard tool from dynamical systems theory to study the dynamics of periodic systems [23, 24]. In this case, the stability of the periodic orbit is usually determined by the Jacobian and particularly by the eigenvalues. If all the eigenvalues of lie inside the unit circle of the complex plane, then the periodic orbit is asymptotically stable. This stability result applies generally to conventional smooth nonlinear systems. Section 6.2 describes the ePFC system, followed by the determination of state equations and Poincaré Map in the subsequent sections. Finally, the stability of the proposed ePFC system is given by the eigen values of the Jacobian. The results are simulated.

6.2. System Description

A simplified schematic of an enhanced Power Flow Controller (ePFC) [25] is shown in FIGURE 6.1. This system consists of sending end voltage (V_{line}), receiving end voltage ($V_{line}\angle$-δ), line reactance (L_s) and compensation reactances L and C. The switching element of the ePFC consists of two back to back thyristors which conduct on alternate half cycles of the supply voltage. The thyristors are assumed to be ideal switches and any turn on/off time lags or switching losses are ignored. The firing pulses for both thyristors are assumed to be supplied periodically at their respective gates.

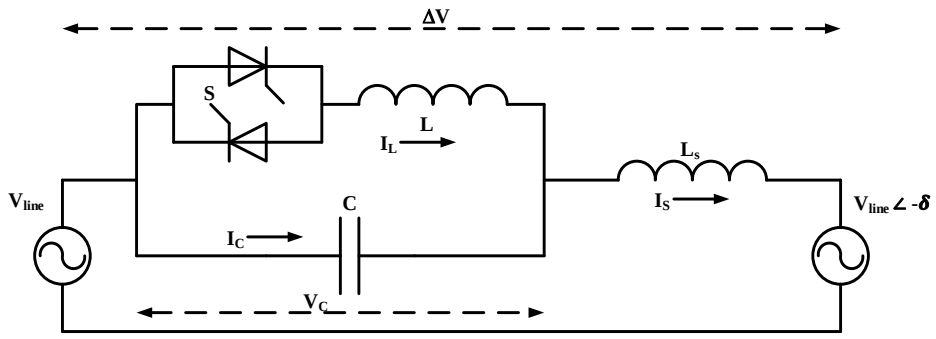

FIGURE 6.1: Simplified circuit schematic of the proposed enhanced Power Flow Controller (ePFC).

6.3. Dynamic State Equations

As may be seen from FIGURE 6.1, there are two modes of operation for the back-to-back connected thyristor switch, S, closed and open. Also, the number of states of the system is different in these two modes. Hence, we obtain two sets of state equations for the entire ePFC system.

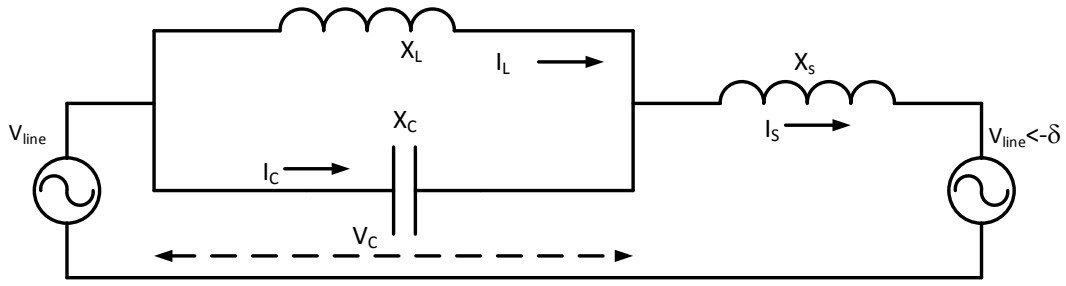

FIGURE 6.2: Simplified schematic of the equivalent ePFC system when back-to-back thyristor switch is closed.

First let us consider the case when the switch is closed. The equivalent ePFC system is as shown in FIGURE 6.2.

The state equations are

$$\frac{dI_L}{dt} = \frac{1}{L} V_C \tag{6.1}$$

$$\frac{dV_c}{dt} = \frac{1}{C} I_s - \frac{1}{C} I_L \tag{6.2}$$

$$\frac{dI_s}{dt} = \frac{1}{L_s} \Delta V - \frac{1}{L_s} V_c \tag{6.3}$$

where $$\Delta V = -2\, V_{line} \sin\frac{\delta}{2} \sin \omega t \tag{6.4}$$

This is of the form,

$$\frac{dx}{dt} = A_{closed} x + B_{closed} u \tag{6.5}$$

where, $$x = \begin{bmatrix} I_L \\ V_C \\ I_S \end{bmatrix} \tag{6.6}$$

$$A_{closed} = \begin{bmatrix} 0 & \frac{1}{L} & 0 \\ \frac{-1}{C} & 0 & \frac{1}{C} \\ 0 & \frac{-1}{L_S} & 0 \end{bmatrix} \tag{6.7}$$

$$B_{closed} = \begin{bmatrix} 0 \\ 0 \\ \frac{1}{L_S} \end{bmatrix} \tag{6.8}$$

and $$u = [\Delta V] \tag{6.9}$$

Similarly, when the thyristor switch, S, is open, ePFC system reduces to the circuit as shown in FIGURE 6.3. Now the state equations are,

$$\frac{dV_c}{dt} = \frac{I_S}{C} \tag{6.10}$$

$$\frac{dI_s}{dt} = \frac{1}{L_s}\Delta V - \frac{1}{L_s}V_c \tag{6.11}$$

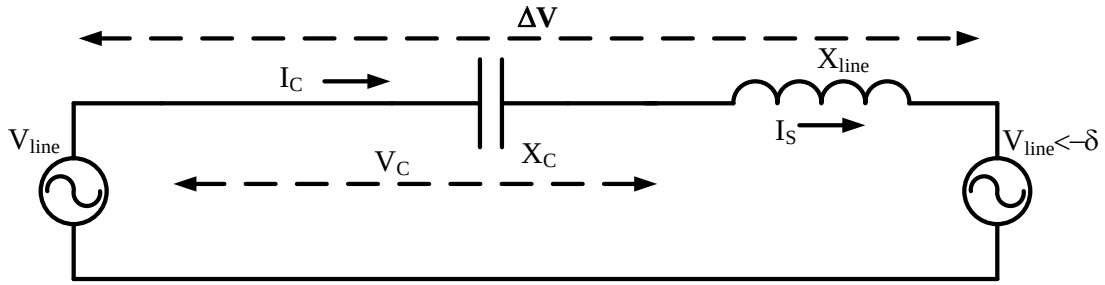

FIGURE 6.3: Simplified schematic of the equivalent ePFC system when back-to-back thyristor switch is open

This is of the form,

$$\frac{dy}{dt} = A_{open}y + B_{open}u \tag{6.12}$$

where, $$y = \begin{bmatrix} V_C \\ I_S \end{bmatrix} \tag{6.13}$$

$$A_{open} = \begin{bmatrix} 0 & \frac{1}{C} \\ \frac{-1}{L_S} & 0 \end{bmatrix} \tag{6.14}$$

$$B_{open} = \begin{bmatrix} 0 \\ \frac{1}{L_S} \end{bmatrix} \tag{6.15}$$

and $$u = [\Delta V] \tag{6.16}$$

6.4. Projection Matrix

Thus we have two sets of state equations as given in equations (6.5) and (6.12) and their solutions are interdependent. That means, the states for the case when the switch is closed are dependent on the states for the case when the switch is open and vice versa. Hence, in order to assist in the analysis, the states in these two cases are related by a matrix termed as projection matrix. The equation (6.12) can be expressed as

$$\frac{dy}{dt} = \pi A_{closed} \pi^T y + \pi B_{closed} u \tag{6.17}$$

where,
$$\pi = \begin{bmatrix} 0 & 1 & 0 \\ 0 & 0 & 1 \end{bmatrix} \tag{6.18}$$

This π is called the projection matrix.

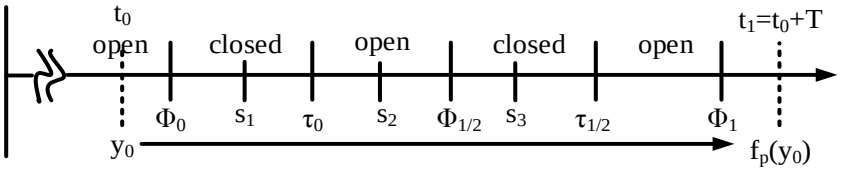

FIGURE 6.4: Poincaré map f_p

Table 6.1: State Description of ePFC

From	To	Switch 'S'	State	Matrices
Φ_0	τ_0	Closed	x	A_{closed}, B_{closed}
τ_0	$\Phi_{1/2}$	Open	y	$\pi A_{closed} \pi^T, \pi B_{closed}$
$\Phi_{1/2}$	$\tau_{1/2}$	Closed	x	A_{closed}, B_{closed}
$\tau_{1/2}$	Φ_1	Open	y	$\pi A_{closed} \pi^T, \pi B_{closed}$

As shown in Table 6.1, the system parameters at a particular instance of time can be described by the respective states in that particular time slot. The interdependence of the states can be expressed with the projection matrix as follows,

The state at the instance when switch S closes Φ_0,

$$x(\Phi_0) = \pi^T y(\Phi_0) \tag{6.19}$$

The state at the instance when switch S opens τ_0,

$$y(\tau_0) = \pi x(\tau_0) \tag{6.20}$$

6.5. Poincaré Mapping

The Poincaré mapping f_p is defined as,

$$f_p = f_p[\text{initial state}, t_{\text{initial}}, t_{\text{final}}] \tag{6.21}$$

Thus, required

$$y(\Phi_1) = f_p[y(\Phi_0), \Phi_0, \Phi_1] \tag{6.22}$$

Now, one can map the state parameters to the instance $\tau_0$with the knowledge of the state at Φ_0 using this kind of Poincaré mapping. From Table 6.1 and FIGURE 6.4, state x is given by

$$x(\tau_0) = f_{\text{closed}}[x(\Phi_0), \Phi_0, \tau_0] \tag{6.23}$$

Substituting for $x(\Phi_0)$ from equation (6.19)

$$x(\tau_0) = f_{\text{closed}}[\pi^T y(\Phi_0), \Phi_0, \tau_0] \tag{6.24}$$

Also, from FIGURE 6.4 and Table 6.1, state y is given by,

$$y(\Phi_{1/2}) = f_{\text{open}}[y(\tau_0), \tau_0, \Phi_{1/2}] \tag{6.25}$$

Substituting for $y(\tau_0)$ from equation (6.20)

$$y(\Phi_{1/2}) = f_{\text{open}}[\pi x(\tau_0), \tau_0, \Phi_{1/2}] \tag{6.26}$$

From equation (6.24), inserting value for $x(\tau_0)$

$$y(\Phi_{1/2}) = f_{open}[\pi f_{closed}[\pi^T y(\Phi_0), \Phi_0, \tau_0], \tau_0, \Phi_{1/2}] \quad (6.27)$$

Because it is half the period, $y(\Phi_{1/2})$ can also be denoted as

$$y(\Phi_{1/2}) = f_{p-half}[y(\Phi_0), \Phi_0, \Phi_{1/2}] \quad (6.28)$$

Hence, to map $y(\Phi_0)$ to $y(\Phi_{1/2})$, required Poincaré map for the half cycle, f_{p-half} is,

$$f_{p-half} = f_{open}\pi f_{closed}\pi^T \quad (6.29)$$

Now, to find (Φ_1),

$$y(\Phi_1) = f_p[y(\Phi_0), \Phi_0, \Phi_1] \quad (6.30)$$

$$y(\Phi_1) = f_{p-half}[y(\Phi_{1/2}), \Phi_{1/2}, \Phi_1] \quad (6.31)$$

From (6.28) and (6.29),

$$y(\Phi_1) = f_{p-half}[f_{open}[\pi f_{closed}[\pi^T y(\Phi_0), \Phi_0, \tau_0], \tau_0, \Phi_{1/2}], \Phi_{1/2}, \Phi_1] \quad (6.32)$$

$$y(\Phi_1) = f_{p-half}[f_{p-half}[y(\Phi_0), \Phi_{1/2}, \Phi_1]] \quad (6.33)$$

$$y(\Phi_1) = f_{open}\pi f_{closed}\pi^T f_{open}\pi f_{closed}\pi^T [y(\Phi_0), \Phi_{1/2}, \Phi_1] \quad (6.34)$$

Hence, to map $y(\Phi_0)$ to $y(\Phi_1)$, the required Poincaré map for the entire full cycle f_p is

$$f_p = f_{open}\pi f_{closed}\pi^T f_{open}\pi f_{closed}\pi^T \quad (6.35)$$

The physical equivalence of the Poincaré mapping can be described as sampling of the states after a definite period of time. So, if the system is periodic and has the time period T (as the ePFC system under consideration has), the Poincaré map would be a single point.

6.6. Stability Analysis

As described in the last section, the Poincaré map of a periodic system reduces to a point. So, the stability of such a system can be evaluated by analyzing the stability of that point. To determine this stability, the Jacobian of the Poincaré map with respect to the state is obtained and its Eigen values are inspected. If all the Eigen values fall within the unit circle on the complex plane, then the system is said to be asymptotically stable [15].

To derive the Jacobian of a periodic orbit, let us divide one period into subintervals. Each interval contains one thyristor switching which advances the state from the beginning to the end and then the chain rule is used to compute the Jacobian of the Poincaré map. It is assumed that there are no thyristor misfires, within the interval of interest.

For Interval containing a switch on, let $[s_2,s_3]$ be a time interval which includes a thyristor switch closing event at time $\phi_{1/2}$ and no other switching. Therefore the final state $x(s_3)$ from $y(s_2)$ is given by

$$x(s_3) = f_{s_3,s_2}(y(s_2)) \tag{6.36}$$

the thyristor switch S is open in $[s_2, \phi_{1/2}]$, which yields

$$y(\Phi_{1/2}) = f^{open}_{\Phi_{1/2},s_2}(y(s_2)) = e^{A_{open}(\Phi_{1/2}-s_2)}\,(y(s_2) + \int_{s_2}^{\Phi_{1/2}} e^{A_{open}(s_2-s)}B_{open}\,u(s))ds \tag{6.37}$$

the thyristor switch S is closed in $[\phi_{1/2}, s_3]$,

$$f_{s_3,s_2}(y(s_2)) = f^{closed}_{s_3,\Phi_{1/2}}\left(x\left(\Phi_{1/2}\right)\right) = e^{A_{closed}(s_2-\Phi_{1/2})}\,\pi^T y\left(\Phi_{1/2}\right) +$$

$$\int_{\Phi_{1/2}}^{s_3} e^{A_{closed}(s_3-s)} B_{closed}\,u(s)ds \tag{6.38}$$

Substituting (6.37) in (6.38), we get

$$f_{s_3,s_2}\left(y(s_2)\right) = g_{s_3,s_2}\left(y(s_2),\Phi_{1/2}\right) \tag{6.39}$$

$$= e^{A_{closed}(s_2-\Phi_{1/2})}\,\pi^T e^{A_{open}(\Phi_{1/2}-s_2)}\,(y(s_2) + \int_{s_2}^{\Phi_{1/2}} e^{A_{open}(s_2-s)} B_{open}\,u(s))ds +$$

$$\int_{\Phi_{1/2}}^{s_3} e^{A_{on}(s_3-s)} B_{closed}\,u(s)ds \tag{6.40}$$

Differentiating (49) with respect to $y(s_2)$ gives

$$Df_{s_3,s_2} = Dg_{s_3,s_2} + \frac{\partial g_{s_3,s_2}}{\partial \Phi_{1/2}} D\Phi_{1/2} \tag{6.41}$$

$D\Phi_{1/2}$ is the derivative of the switch off time with respect to $y(s_2)$. Since the thyristor is fired regularly, $\Phi_{1/2}$ is constant and hence $D\Phi_{1/2} = 0$

$$Df_{s_3,s_2} = Dg_{s_3,s_2} = e^{A_{closed}(s_2-\Phi_{1/2})}\,\pi^T e^{A_{open}(\Phi_{1/2}-s_2)} \tag{6.42}$$

Similarly, for the time interval $[s_1, s_2]$ containing an instance when the thyristor switch, S, is opened at time τ_0. The thyristor is on in $[s_1,\tau_0]$, which yields

$$x(\tau_0) = f^{closed}_{\tau_0,s_1}\left(x(s_1)\right) = e^{A_{closed}(\tau_0-s_1)}\,(x(s_1) + \int_{s_1}^{\tau_0} e^{A_{closed}(s_1-s)} B_{closed} u(s))ds \tag{6.43}$$

the thyristor switch S is open in $[\tau_0, s_2]$,

$$f_{s_2,s_1}\left(x(s_1)\right) = f^{open}_{s_2,\tau_0}\left(y(\tau_0)\right) = e^{A_{open}(s_2-\tau_0)}\,\pi x(\tau_0) + \int_{\tau_0}^{s_2} e^{A_{open}(s_2-s)} B_{open}\,u(s)ds$$

(6.44)

Substituting (6.43) in (6.44), we get

$$f_{s_2,s_1}(x(s_1)) = g_{s_2,s_1}(x(s_1),\tau_0) \tag{6.45}$$

$$= e^{A_{open}(s_2-\tau_0)}\, P e^{A_{closed}(\tau_0-s_1)}\,(x(s_1) + \int_{s_1}^{\tau_0} e^{A_{closed}(s_1-s)} B_{closed} u(s))ds +$$

$$\int_{\tau_0}^{s_2} e^{A_{open}(s_2-s)} B_{open}\, u(s)ds \tag{6.46}$$

Differentiating (6.46) with respect to $x(s_1)$ gives

$$Df_{s_2,s_1} = Dg_{s_2,s_1} + \frac{\partial g_{s_2,s_1}}{\partial \tau_0} D\tau_0 \tag{6.47}$$

Differentiating $\frac{\partial g_{s_2,s_1}}{\partial \tau_0}$, we get

$$\frac{\partial g_{s_2,s_1}}{\partial \tau_0} = e^{A_{open}(s_2-\tau_0)}\,(\pi A_{closed} - A_{open}\pi) e^{A_{closed}(\tau_0-s_1)}\,(x(s_1) +$$

$$\int_{s_1}^{\tau_{1/2}} e^{A_{closed}(s_1-s)} B_{closed} u(s))ds + e^{A_{open}(s_2-\tau_0)}(RB_{closed} - B_{open})u(\tau_0) \tag{6.48}$$

$$\frac{\partial g_{s_2,s_1}}{\partial \tau_0} = e^{A_{open}(s_2-\tau_0)}\,(\pi A_{closed} - A_{open}\pi)\, x(\tau_0) + e^{A_{open}(s_2-\tau_0)}(\pi B_{closed} -$$

$$B_{open})u(\tau_0) \tag{6.49}$$

Since $\pi B_{closed} = B_{open}$ (6.50)

and $A_{open} = \pi A_{closed}\pi^T.$ (6.51)

We get,

$$\frac{\partial g_{s_2,s_1}}{\partial \tau_0} = e^{A_{off}(s_2-\tau_0)}\pi A_{on}(I - \pi\pi^T)x(\tau_0) \tag{6.52}$$

Since $(I - \pi\pi^T) = c^T c$

where $c = (1 \quad 0 \quad 0)$ and I is an identity matrix.

$$\frac{\partial g_{s_2,s_1}}{\partial \tau_0} = e^{A_{open}(s_2-\tau_0)}\pi A_{closed} c^T c\, x(\tau_0) = 0 \tag{6.53}$$

Since the thyristor switch off condition is

$$0 = I_L(\tau_0) = (1 \quad 0 \quad 0)\, x(\tau_0) = c\, x(\tau_0) \tag{6.54}$$

Therefore,

$$Df_{s_2,s_1} = Dg_{s_2,s_1} = e^{A_{open}(s_2-\tau_0)}\, \pi e^{A_{closed}(\tau_0-s_1)} \tag{6.55}$$

Now, assembling the Jacobian from the Poincaré formula we get.

$$f_p(y_0) = f_{open}\pi f_{closed}\pi^T f_{open}\pi f_{closed}\pi^T f_{open}\, y_0 \tag{6.56}$$

Choose times s_3 in the interval $(\phi_{1/2}, \tau_{1/2})$, s_2 in the interval $(\tau_0, \phi_{1/2})$ and s_1 in (ϕ_0, τ_0).

Then

$$f_p(y_0) = f_{t_1 s_3} f_{s_3 s_2} f_{s_2 s_1} f_{s_1 t_0}\, y_0 \tag{6.57}$$

$$Df_p(y_0) = Df_{t_1 s_3} Df_{s_3 s_2} Df_{s_2 s_1} Df_{s_1 t_0} \tag{6.58}$$

$$Df_p(y_0) = (e^{A_{open}\left(t_1-\frac{\tau_1}{2}\right)}\, \pi e^{A_{on}\left(\frac{\tau_1}{2}-s_3\right)})(e^{A_{closed}\left(s_3-\frac{\phi_1}{2}\right)}\, \pi^T e^{A_{open}\left(\frac{\phi_1}{2}-s_2\right)})$$

$$(e^{A_{open}(s_2-\tau_0)}\, \pi e^{A_{closed}(\tau_0-s_1)})(e^{A_{closed}(s_1-\phi_0)}\, \pi^T e^{A_{open}(\phi_0-t_0)}) \tag{6.59}$$

$$= (e^{A_{open}\left(t_1-\frac{\tau_1}{2}\right)}\, \pi e^{A_{closed}\left(\frac{\tau_1}{2}-\frac{\phi_1}{2}\right)} \pi^T e^{A_{open}\left(\frac{\phi_1}{2}-\tau_0\right)}$$

$$e^{A_{closed}(\tau_0-\phi_0)}\pi^T e^{A_{open}(\phi_0-t_0)}) \tag{6.60}$$

When $t_0 = \phi_0$-, then the Jacobian becomes

$$Df_p(y_0) = e^{A_{open}(t_1-\tau_1)}\pi e^{A_{closed}(\tau_1-\phi_1)}\pi^T e^{A_{open}(\phi_1-\tau_0)}\pi e^{A_{closed}(\tau_0-\phi_0)}\pi^T \quad (6.61)$$

If the periodic orbit is assumed to be half wave symmetric, then $\phi_{1/2} = \phi_0 + \frac{T}{2}$ and $\tau_{1/2} = \tau_0 + \frac{T}{2}$ and (6.61) simplifies to,

$$Df_p(y_0) = \left(e^{A_{open}(\phi_1-\tau_0)}\pi e^{A_{closed}(\tau_0-\phi_0)}\pi^T\right)^2 \quad (6.62)$$

which can also be expressed in terms of the thyristor conduction time $\sigma = \tau_0 - \Phi_0$

$$Df_p(y_0) = \left(e^{A_{open}(\frac{T}{2}-\sigma)}\pi e^{A_{closed}\sigma}\pi^T\right)^2 \quad (6.63)$$

$$Df_p(y_0) = \left(\begin{bmatrix} 1 & e^{\frac{1}{C}(\frac{T}{2}-\sigma)} \\ e^{-\frac{1}{L_S}(\frac{T}{2}-\sigma)} & 1 \end{bmatrix}\begin{bmatrix}0 & 1 & 0\\ 0 & 0 & 1\end{bmatrix}\begin{bmatrix} 1 & e^{\frac{1}{L}\sigma} & 1 \\ e^{-\frac{1}{C}\sigma} & 1 & e^{\frac{1}{C}\sigma} \\ 1 & e^{-\frac{1}{L_S}\sigma} & 1 \end{bmatrix}\begin{bmatrix}0 & 0\\ 1 & 0\\ 0 & 1\end{bmatrix}\right)^2 \quad (6.64)$$

$$Df_p(y_0) = \left(\begin{bmatrix} 1 & e^{\frac{1}{C}(\frac{T}{2}-\sigma)} \\ e^{-\frac{1}{L_S}(\frac{T}{2}-\sigma)} & 1 \end{bmatrix}\begin{bmatrix}0 & 1 & 0\\ 0 & 0 & 1\end{bmatrix}\begin{bmatrix} 1 & e^{\frac{1}{L}\sigma} & 1 \\ e^{-\frac{1}{C}\sigma} & 1 & e^{\frac{1}{C}\sigma} \\ 1 & e^{-\frac{1}{L_S}\sigma} & 1 \end{bmatrix}\begin{bmatrix}0 & 0\\ 1 & 0\\ 0 & 1\end{bmatrix}\right)^2 \quad (6.65)$$

$$Df_p(y_0) = \left(\begin{bmatrix} 0 & 1 & e^{\frac{1}{C}(\frac{T}{2}-\sigma)} \\ 0 & e^{-\frac{1}{L_S}(\frac{T}{2}-\sigma)} & 1 \end{bmatrix}\begin{bmatrix} 1 & e^{\frac{1}{L}\sigma} & 1 \\ e^{-\frac{1}{C}\sigma} & 1 & e^{\frac{1}{C}\sigma} \\ 1 & e^{-\frac{1}{L_S}\sigma} & 1 \end{bmatrix}\begin{bmatrix}0 & 0\\ 1 & 0\\ 0 & 1\end{bmatrix}\right)^2 \quad (6.66)$$

$$Df_p(y_0) = \left(\begin{bmatrix} e^{\frac{1}{C}(\frac{T}{2}-\sigma)} + e^{-\frac{1}{C}\sigma} & 1 + e^{\frac{1}{C}(\frac{T}{2}-\sigma)}.e^{-\frac{1}{L_S}\sigma} & e^{\frac{1}{C}\sigma} + e^{\frac{1}{C}(\frac{T}{2}-\sigma)} \\ 1 + e^{-\frac{1}{L_S}(\frac{T}{2}-\sigma)}.e^{-\frac{1}{C}\sigma} & e^{-\frac{1}{L_S}(\frac{T}{2}-\sigma)} + e^{-\frac{1}{L_S}\sigma} & 1 + e^{\frac{1}{C}\sigma}.e^{-\frac{1}{L_S}(\frac{T}{2}-\sigma)} \end{bmatrix}\begin{bmatrix}0 & 0\\ 1 & 0\\ 0 & 1\end{bmatrix}\right)^2 \quad (6.67)$$

$$Df_p(y_0) = \left(\begin{bmatrix} 1 + e^{\frac{1}{C}\left(\frac{T}{2}-\sigma\right)}.e^{-\frac{1}{L_S}\sigma} & e^{\frac{1}{C}\sigma} + e^{\frac{1}{C}\left(\frac{T}{2}-\sigma\right)} \\ e^{-\frac{1}{L_S}\left(\frac{T}{2}-\sigma\right)} + e^{-\frac{1}{L_S}\sigma} & 1 + e^{\frac{1}{C}\sigma}.e^{-\frac{1}{L_S}\left(\frac{T}{2}-\sigma\right)} \end{bmatrix} \right)^2 \quad (6.68)$$

As may be observed, this Jacobian does not contain any term related to compensating reactance L. Only terms that appear in this Jacobian are compensating capacitance C and line reactance L_S. Thus, the eigen values can be calculated by

$$\left| \begin{bmatrix} 1 + e^{\frac{1}{C}\left(\frac{T}{2}-\sigma\right)}.e^{-\frac{1}{L_S}\sigma} & e^{\frac{1}{C}\sigma} + e^{\frac{1}{C}\left(\frac{T}{2}-\sigma\right)} \\ e^{-\frac{1}{L_S}\left(\frac{T}{2}-\sigma\right)} + e^{-\frac{1}{L_S}\sigma} & 1 + e^{\frac{1}{C}\sigma}.e^{-\frac{1}{L_S}\left(\frac{T}{2}-\sigma\right)} \end{bmatrix}^2 - \lambda \begin{bmatrix} 1 & 0 \\ 0 & 1 \end{bmatrix} \right| = 0 \quad (6.69)$$

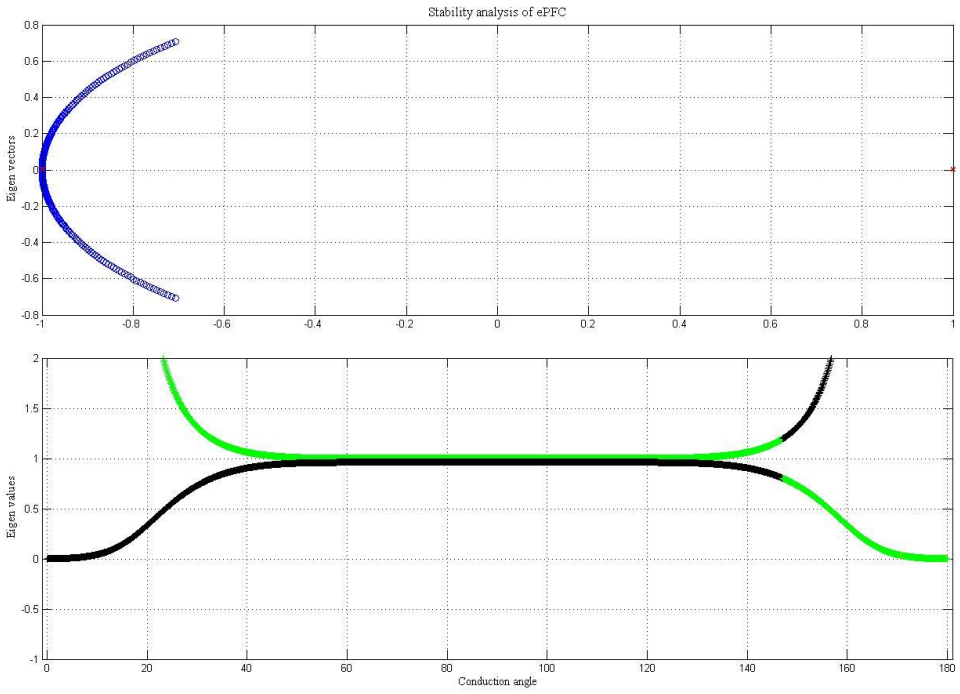

FIGURE 6.5. Eigen Values (as a function of σ) of the Jacobian of the Poincare map for the ePFC system

FIGURE 6.5 presents the eigen values of the Jacobian as a function of conduction angle (σ). As can be seen, the eigen vectors are in and on the unit circle, for sigma from 45° to 135° highlights the region of marginal stability.

CHAPTER 7 : CONCLUSIONS AND FUTURE SCOPE

7.1. Introduction

A methodology to accomplish smoother power flow control in a transmission line by employing enhanced Power Flow Controller (ePFC) is proposed. ePFC is an extension of D-FACTS devices recently presented in literature, however it offers superior performance attributes in terms of controllability and precision.

Extensive mathematical analysis is presented and a new expression is derived for effective fundamental impedance of a series connected L-C network where equivalent L is continuously varied through thyristor control.

The proposed treatment is based on the principle that only the end bus voltages are sinusoidal and all associated harmonics generated by series injection of ePFC are absorbed in the transmission line itself. To further explain, the majority of the harmonic voltage drop occurs in the line and that the source impedance behind the bus is very small compared to the line impedance and thus has small harmonic voltage drops. This approach further generalizes the state of the art (2^{nd} order approximation) model that has been employed to analyze series FACTS devices such as TCSC. The proposed ePFC analytical model is superior to the 2^{nd} order approximation in terms of predicting an additional resonance zone.

It is expected that when line reactance dominates, transmission line current can be treated as near sinusoidal (thus lacking harmonic content), and the expression for

effective fundamental impedance would degenerate into 2nd order approximation. The proposed model would further reduce into classical average inductance model (1st order approximation) when the compensating capacitance dominates, which makes voltage across this capacitance near sinusoidal and devoid of harmonics.

The stability of such an enhanced Power Flow Controller (ePFC) system is also presented. This particular type of network is challenging to analyze in power systems. The inherent non-linearity and discontinuity makes the system incomprehensible for standard mathematical tools like Lyapunov Stability Analysis etc. The study first describes the modeling of network which takes into account, the distortion across the capacitor voltage as well as the distortion line current. Then, an analytical study of the Poincare map is done on the system under consideration. This shows the regions of marginal stability for the ePFC system.

7.2. Contributions

The major contributions of this thesis are:

- Simulations of D-FACTS: Distributed Series Reactance (DSR) and Distributed Series Impedance (DSI).
- Mathematical analysis for effective fundamental impedance of a series connected L-C network where equivalent L is continuously varied through thyristor control using 1st order, 2nd order approximations and proposed enhanced Power Flow Controller (ePFC) model.
- Simulations of enhanced Power Flow Controller (ePFC).
- Stability of inherent non-linear and discontinuous L-C system.

- Effect of compensation reactance in determining stability of thyristor based L-C networks.

7.3. Recommendations for Future Work

The future work may account for the leakage reactance of the single turn transformer (STT) in modeling of enhanced Power Flow Controller (ePFC). Stability analysis work can be expanded to generalized thyristor switched L-C circuits. Experimental verification would help in providing the concepts which are explained and verified through simulations in this thesis.

BIBLIOGRAPHY

[1] S. Abraham, National Transmission Grid Study May 2002 Available:.eh.doe.gov/ntgs/, U.S. Dept. of Energy.

[2] D. Divan, W. Brumsickle, R. Schneider, B. Kranz, R. Gascoigne, D.Bradshaw, M. Ingram, and I. Grant, "Adistributed static series compensator system for realizing active power flow control on existing power lines," in *IEEE PSCE Conf. Records*, Oct. 2004.

[3] W. J. Museler, President and CEO of the New York Independent System Operator (NYISO), presentation May 22, 2003, New York City. Accessed April 2004 at retrieve.nyiso.com/topics/articles/news_releases/2003/pa3_presentation.pdf.

[4] N. Hingorani, "Flexible ac transmission," *IEEE Spectrum*, vol. 30, no.4, pp. 40–45, Apr. 1993

[5] N.G.etrie Hingorani and L. Gyugyi, *Understanding FACTS: Concepts and Technology of Flexible AC Transmission Systems*, Wiley-IEEE, 1999.

[6] D. Divan, H. Johal, "A smarter grid for improving system reliability and asset utilization," *IEEE-PEMC* 2006, pp. 1-7.

[7] D. Divan and H. Johal, "Distributed FACTS- A New Concept for Realizing Grid Power Flow Control," *IEEE Transactions on Power Electronics*, vol. 22, No. 6, Nov. 2007.

[8] Vaddiraj, A., & Manjrekar, M. (2014, July). Modeling and analysis of an ePFC (enhanced power flow controller) with conduction angle control. In *PES General Meeting| Conference & Exposition, 2014 IEEE* (pp. 1-5). IEEE.

[9] Thyristor Controlled Series Compensation, CIGRE Working Group 14.18.

[10] Paserba, J. J. (2003, September). How FACTS controllers-benefit AC transmission systems. In *Transmission and Distribution Conference and Exposition, 2003 IEEE PES* (Vol. 3, pp. 949-956). IEEE.

[11] retrieve.energy.siemens.com/hq/en/power-transmission/facts/series-compens.

[12] retrieve.energy.siemens.com/hq/en/power-transmission/facts/static-var-compensator-classic/.

[13] retrieve.energy.siemens.com/hq/en/power-transmission/facts/mechanical-switched-capacitor/.

[14] H. Johal, "Distributed Series Reactance: A new approach to realize grid power flow control," Ph.D. dissertation, School of. Electrical and Computer Engineering, Georgia Institute of Technology, Atlanta, GA, 2008.

[15] *FACTS Overview*, IEEE PES Special Publication 95-TP-108, 1995.

[16] E. Gholipour, S. Saadate, "Improving of transient stability of power systems using UPFC," *IEEE Transactions on Power Delivery*, vol. 20, no. 2, Apr. 2005, pp. 1677-1682.

[17] H. Johal, D. Divan, "Design considerations for series-connected distributed FACTS converters," *IEEE Transactions on Industry Applications*,vol. 43, no. 6, Nov./Dec. 2007, pp. 1609-1618.

[18] M. Eslami, H. Shareef, and A. Mohamed, "A survey on Flexible AC Transmission Systems (FACTS)," *Przeglad Elektrotechniczny (Electr. Rev.)*, 2012, pp. 1-11.

[19] S. Jalali, I. Dobson, R.H. Lasseter, G. Venkataramanan, "Switching Time Bifurcations in a Thyristor Controlled Reactor," *IEEE Transactions on Circuits and Systems – I: Fundamental Theory and Applications*, Vol. 43, No. 3, March 1996, pp 209-218.

[20] R. M. Mathur, R. K. Varma, *Thyristor-based FACTS controllers for electrical transmission systems*, John Wiley, 2002

[21] Lasseter, R. H., S. G. Jalali, and I. Dobson. "Dynamic response of a thyristor controlled switched capacitor." *IEEE Trans. Power Delivery* 9 (1994): 1609-1615.

[22] Dobson, Ian. "Stability and nonlinear dynamics in thyristor and diode circuits."*Nonlinear Phenomena in Power Electronic Circuits* (2001).

[23] A. Vaddiraj, M. D. Manjrekar, "Dynamic Analysis of an ePFC (enhanced Power Flow Controller) with Conduction Angle Control " *IEEE NAPS* , 2014.

[24] Grainger, J. J., & Stevenson, W. D. (1994). Power system analysis (Vol. 621). New York: McGraw-Hill.